DOT/FAA/CT-93/79
DOT-VNTSC-FAA-93-11

FAA Technical Center
Atlantic City International Airport,
N.J. 08405

Effects of Repair on Structural Integrity

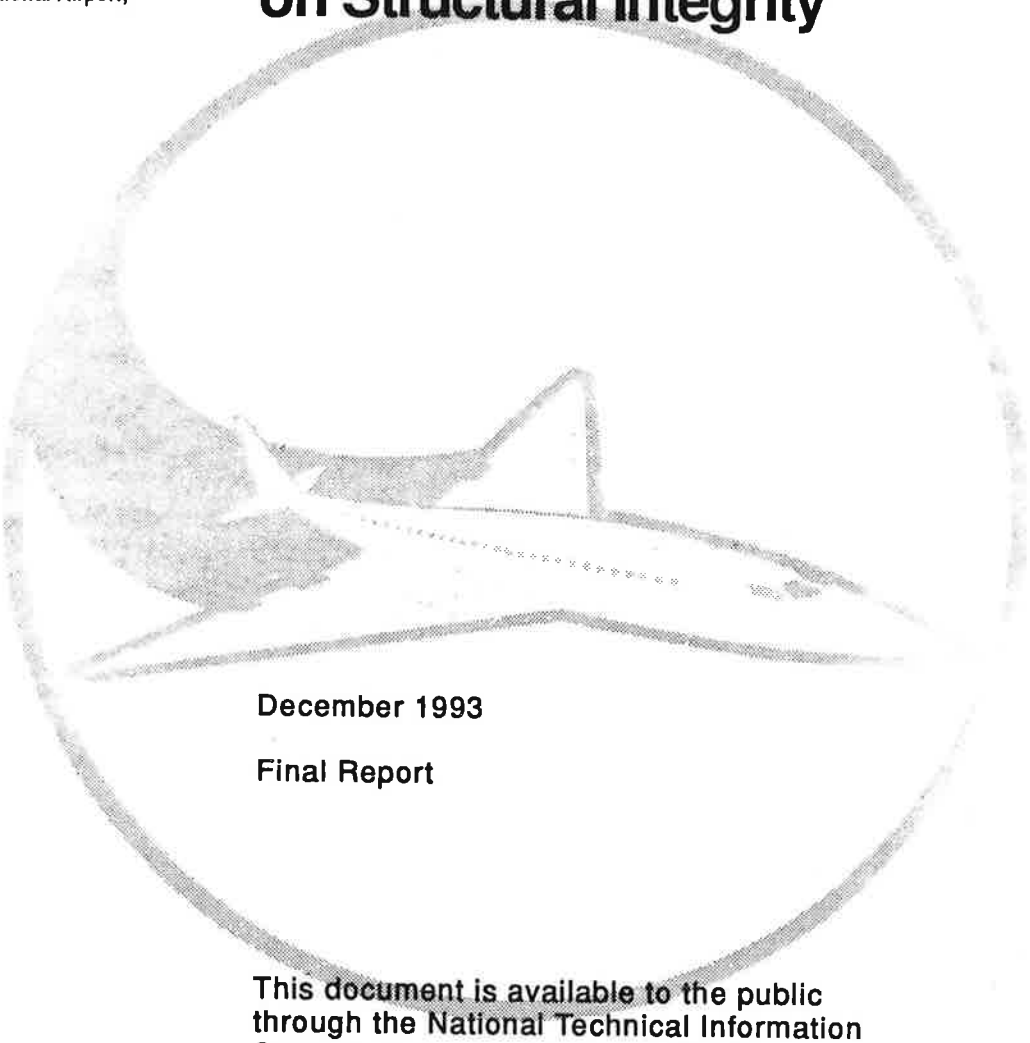

December 1993

Final Report

U.S. Department of Transportation
Federal Aviation Administration

REPORT DOCUMENTATION PAGE

Form Approved OMB No. 0704-0188

1. AGENCY USE ONLY (Leave blank)	2. REPORT DATE	3. REPORT TYPE AND DATES COVERED
	December 1993	Final Report January 1990-September 1992

4. TITLE AND SUBTITLE

Effects of Repair on Structural Integrity

5. FUNDING NUMBERS

FA3H2/A3128
DTRS-57-89-C-00006

6. AUTHOR(S)

R. Rice, R. Francini, S. Rahman, M. Rosenfeld, S. Rust, S. Smith, D. Broek

7. PERFORMING ORGANIZATION NAME(S) AND ADDRESS(ES)

BATTELLE*
505 King Avenue
Columbus, OH 43201

8. PERFORMING ORGANIZATION REPORT NUMBER

DOT-VNTSC-FAA-93-11

9. SPONSORING/MONITORING AGENCY NAME(S) AND ADDRESS(ES)

U.S. Department of Transportation
Federal Aviation Administration Technical Center
Atlantic City International Airport, NJ 08405

10. SPONSORING/MONITORING AGENCY REPORT NUMBER

DOT/FAA/CT-93/79

11. SUPPLEMENTARY NOTES

*Under Contract to: U.S. Department of Transportation
Volpe National Transportation Systems Center
Kendall Square
Cambridge, MA 02142

12a. DISTRIBUTION/AVAILABILITY STATEMENT

This document is available to the public through the National Technical Information Service, Springfield, VA 22161

12b. DISTRIBUTION CODE

13. ABSTRACT (Maximum 200 words)

FAA regulations require commercial aircraft operators to repair damaged aircraft structures. These repairs must be performed in a timely manner to reduce aircraft downtime and loss of revenue. A guiding principal for such repairs is to restore the structure to the original (or better) static strength and stiffness.

However, the repair must also be designed for adequate fatigue resistance, damage tolerance, and inspectability. Fatigue and damage tolerance (DT) analyses should be based on realistic stress histories which, in turn, should be derived from realist load spectra. Thus, an algorithm for the development of a stress history should be included in a comprehensive analysis of repairs.

Since many damage repair stations and airlines do have at least basic computer facilities that can be used for fatigue and damage tolerance analysis, one goal has been the development of a relatively simple, yet accurate analytical tool to design aircraft repairs more effectively.

Structural analysis and stress spectrum development procedures described in this report are approximate and , therefore, have certain limitations. These procedures might be used to qualitatively compare the quality of different repair options with the original structure.

14. SUBJECT TERMS	15. NUMBER OF PAGES
SKINFIX, load spectra, static strength, damage tolerance	154
	16. PRICE CODE

17. SECURITY CLASSIFICATION OF REPORT	18. SECURITY CLASSIFICATION OF THIS PAGE	19. SECURITY CLASSIFICATION OF ABSTRACT	20. LIMITATION OF ABSTRACT
Unclassified	Unclassified	Unclassified	

PREFACE

This report describes an effort undertaken by Battelle and funded by the FAA Technical Center via the Volpe National Transportation Systems Center (VNTSC) to address the influence of fuselage repairs on the structural integrity of todays aging commercial aircraft.

The authors wish to acknowledge the support of the following VNTSC staff members on this program — Dr. John Brewer[1], Dr. Sam Sampath[2], and Ms. Melanie Violette[3]. In addition, we acknowledge the efforts of the following Task 4 reviewers — Mr. Tom Swift, Los Angeles Aircraft Certification Office FAA, Long Beach, California; Dr. Jack Lincoln, ASD/ENFS, Wright Patterson AFB, Ohio; and Mr. Tom Disney, Marietta, Georgia.

The support of other capable Battelle staff members in the course of this program is also appreciated. In particular, we would like to acknowledge the efforts of Ms. Leota Alwine on Task 1, Mr. Ying-Liang Chou on Task 2, Mr. Nu Ghadiali on Task 3, and Messrs. Norm Frey, Michael Oliver, and David Utz on Task 5.

---

[1] Current VNTSC Technical Task Initiator.

[2] Former VNTSC TTI, currently Director, National Aging Aircraft Research Program, FAA Technical Center, Atlantic City, New Jersey.

[3] Former VNTSC TTI, currently working toward PhD at RPI.

METRIC/ENGLISH CONVERSION FACTORS

ENGLISH TO METRIC

LENGTH (APPROXIMATE)

1 inch (in.) = 2.5 centimeters (cm)
1 foot (ft) = 30 centimeters (cm)
1 yard (yd) = 0.9 meter (m)
1 mile (mi) = 1.6 kilometers (km)

AREA (APPROXIMATE)

1 square inch (sq in, in^2) = 6.5 square centimeters (cm^2)
1 square foot (sq ft, ft^2) = 0.09 square meter (m^2)
1 square yard (sq yd, yd^2) = 0.8 square meter (m^2)
1 square mile (sq mi, mi^2) = 2.6 square kilometers (km^2)
1 acre = 0.4 hectares (he) = 4,000 square meters (m^2)

MASS - WEIGHT (APPROXIMATE)

1 ounce (oz) = 28 grams (gr)
1 pound (lb) = .43 kilogram (kg)
1 short ton = 2,000 pounds (lb) = 0.9 tonne (t)

VOLUME (APPROXIMATE)

1 teaspoon (tsp) = 5 milliliters (ml)
1 tablespoon (tbsp) = 15 milliliters (ml)
1 fluid ounce (fl oz) = 30 milliliters (ml)
1 cup (c) = 0.24 liter (l)
1 pint (pt) = 0.47 liter (l)
1 quart (qt) = 0.96 liter (l)
1 gallon (gal) = 3.8 liters (l)
1 cubic foot (cu ft, ft^3) = 0.03 cubic meter (m^3)
1 cubic yard (cu yd, yd^3) = 0.76 cubic meter (m^3)

TEMPERATURE (EXACT)

[(x - 32) (5/9)] °F = y°C

METRIC TO ENGLISH

LENGTH (APPROXIMATE)

1 millimeter (mm) = 0.04 inch (in)
1 centimeter (cm) = 0.4 inch (in)
1 meter (m) = 3.3 feet (ft)
1 meter (m) = 1.1 yards (yd)
1 kilometer (km) = 0.6 mile (mi)

AREA (APPROXIMATE)

1 square centimeter (cm^2) = 0.16 square inch (sq in, in^2)
1 square meter (m^2) = 1.2 square yards (sq yd, yd^2)
1 square kilometer (km^2) = 0.4 square mile (sq mi, mi^2)
1 hectare (he) = 10,000 square meters (m^2) = 2.5 acres

MASS - WEIGHT (APPROXIMATE)

1 gram (gr) = 0.036 ounce (oz)
1 kilogram (kg) = 2.2 pounds (lb)
1 tonne (t) = 1,000 kilograms (kg) = 1.1 short tons

VOLUME (APPROXIMATE)

1 milliliter (ml) = 0.03 fluid ounce (fl oz)
1 liter (l) = 2.1 pints (pt)
1 liter (l) = 1.06 quarts (qt)
1 liter (l) = 0.26 gallon (gal)
1 cubic meter (m^3) = 36 cubic feet (cu ft, ft^3)
1 cubic meter (m^3) = 1.3 cubic yards (cu yd, yd^3)

TEMPERATURE (EXACT)

[(9/5) y + 32] °C = x °F

QUICK INCH-CENTIMETER LENGTH CONVERSION

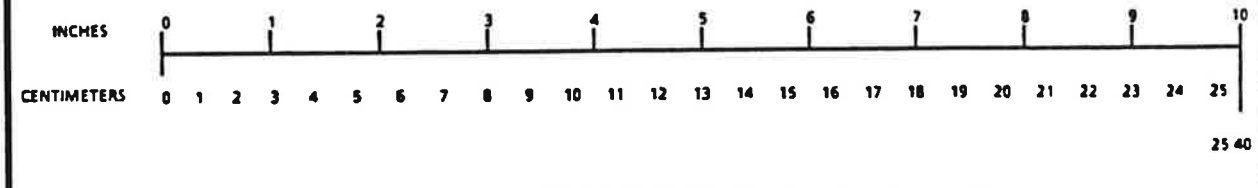

QUICK FAHRENHEIT-CELSIUS TEMPERATURE CONVERSION

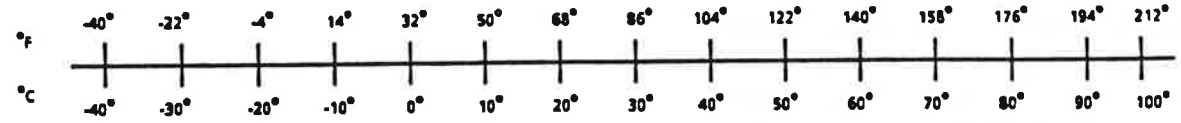

For more exact and or other conversion factors, see NBS Miscellaneous Publication 286, Units of Weights and Measures. Price $2.50. SD Catalog No. C13 10286.

TABLE OF CONTENTS

TABLE OF CONTENTS (Continued)

LIST OF FIGURES

LIST OF FIGURES (Continued)

LIST OF TABLES

LIST OF ABBREVIATIONS

AATF	Aging Aircraft Task Force (a.k.a Airworthiness Assurance Task Force)
ACO	Aircraft Certification Office
AD	Airworthiness Directive
ARS	Aviation Research & Support
ASIP	Aircraft Structural Integrity Program
AWACS	Airborne Warning and Control System
CDA	Compatible Displacement Analysis
COD	Crack Opening Displacement
CPOD	Cumulative Probability of Detection
CPU	Central Processing Units (Seconds)
DER	Designated Engineering Representative
DOT	Department of Transportation
DT	Damage Tolerance
FAA	Federal Aviation Administration
FEA	Finite Element Analysis (a.k.a FEM)
FEM	Finite Element Method (a.k.a. FEA)
FORM	First Order Reliability Method
GAG	Ground-Air-Ground
MCS	Monte Carlo Simulation
MSD	Multiple Site Damage
NACA	National Advisory Committee for Aeronautics
NASA	National Aeronautics and Space Administration
NDI	Nondestructive Inspection
NLP	Nonlinear Programming
NLR	National Aerospace Laboratory (Netherlands)
OEM	Original Equipment Manufacturer
POD	Probability of Detection
PRA	Probabilistic Risk Assessment
SDR	Service Difficulty Report
SORM	Second Order Reliability Method
STC	Supplemental Type Certificate
TTI	Technical Task Initiator (at VNTSC)
TOGAA	Technical Oversight Group for Aging Aircraft
TWA	Trans World Airlines
TWIST	Standardized Spectrum for Transport Aircraft Wing Structures
VGH	Velocity, Acceleration of Gravity and Altitude
VNTSC	Volpe National Transportation Systems Center

LIST OF SYMBOLS

a,b	Parameters used in CDA analysis, material dependent
a_{eff}	Effective crack length
a_p	Permissible crack size
A	Effective strip area in CDA analysis
$\overline{A}$, $\overline{\overline{A}}$	Parameters, dependent on aircraft type
$A_{c,s,d}$	Effective element areas used in computation of CDA element stiffnesses
A_{st}	Area of tear strap
C	Coefficient
c	Element chord length
cg	Center of gravity
C_L	Three dimensional lift coefficient
D and D_s	Fastener shank diameter
D_h	Fastener head diameter
d	Element diagonal length
$dC_L/d\alpha$	Slope of C_L vs. α curve
$E[N_0]$	Mathematical expectation operator representing the expected mean value of the random initiation life N_0
$E_{f,s,r}$	Elastic moduli of fastener, sheet and reinforcement material
E	Material modulus
$f_A(a)$	Probability density after inspection and repair at N_1 cycles
F_B	Cumulative distribution function
g, G	Acceleration of gravity
g(X)	Performance function in reliability analysis
G_{al}	Gust alleviation factor
h	Element thickness
$I_{c,s,d}$	Element moments of inertia
K_A, K_B	Stress intensity factors corresponding to specific loading environments
k	Number of stringers
k_f	Fastener stiffness
L	Lift load (force), also fastener spacing transverse to loading direction
m	Mass
M_b	Bending moment
M_t	Torsional moment
n_z	Vertical acceleration load factor
N	Number of cycles
N_0	Number of cycles to crack initiation
p	Fuselage pressure level
P	Fastener load
P_F	Probability of failure
r	Radius of curvature
R	Fuselage radius
S	Wing area
S_{eq}	Equivalent stress
$S_{x,y}$	Average CDA element stresses in x and y directions

LIST OF SYMBOLS (Continued)

s	Element side length, also fastener spacing
T_{xy}	CDA element shear stress
t	Fuselage skin thickness
$t_{s,r}$	Thickness of sheet and reinforcement
T	Tail load (force)
v	Gust velocity
V	Airspeed
V_p	Coefficient of variation of fuselage pressure
V_t	Density of air
w	Angular velocity
W	Weight
W_{eff}	Effective panel width
z	Z-direction distance
α	Angle of attack
α_1	Constant dependent on stiffening ratio
$\Delta\alpha$	Increment of α
$\Delta\sigma_{bl}$	Range of bending stress
ΔK	Stress Intensity Range
ΔL	Incremental lift
ρ	Density of air
σ_1	Cyclic stress
σ_{bl}	Local bending stress
$\sigma_{bl\text{-}1g}$	1g bending stress
σ_{LL}	Limit load stress
σ_m	Mean stress, membrane stress
σ_{max}	Maximum stress
σ_p	Circumferential pressurization stress (hoop stress)
σ_{pl}	Longitudinal pressurization stress
σ,σ_t	Total stress
σ_{1g}	One g stationary stress
ν	Poisson's ratio
τ_t	Shear stress
θ	Angle of vector

EXECUTIVE SUMMARY

Commercial aircraft operators are required by FAA regulations to repair damaged aircraft structures. These repairs must be performed in a timely manner to reduce aircraft downtime and loss of revenue. A guiding principle that has been used for many aircraft structural repairs is to simply restore the structure to its original (or better) static strength and stiffness.

However, fuselage repairs must withstand significant fatigue loadings and be damage tolerant if cracks do form in them. It must be understood where cracks are most likely to form so appropriate inspection procedures can be instituted.

This report describes an effort undertaken by Battelle and funded by the FAA Technical Center via the Volpe National Transportation Systems Center (VNTSC) to address these issues. Since many repair stations and airlines do have at least basic computer facilities that can be used for fatigue and damage tolerance analysis, one goal has been the development of a relatively simple, yet accurate analytical tool to design aircraft repairs more effectively.

The following significant accomplishments resulted from this study:

- A two dimensional compatible displacement analysis program (SKINFIX) was developed. It calculates skin and doubler stresses as well as rivet displacements within 5 percent accuracy in regions of modest load transfer. This approach was found to be less precise (although generally within 15 percent accuracy) in regions of high load transfer or significant out-of-plane bending.
- Fatigue tests on strain-gaged Type III repair panels were performed, including precise measurements of rivet displacements under load. Deformation and stress redistribution behavior in simulated fuselage doublers were determined. Such data do not exist elsewhere in the public domain.
- SKINFIX can be used to analyze a wide range of typical fuselage skin repairs and produce realistic estimates of rivet loads. These rivet loads can be used to estimate fatigue quality and crack growth behavior.
- A methodology to obtain an approximate stress history for specific locations in an aircraft fuselage was developed. Two methods for estimating nominal fuselage skin stresses were also constructed. The first method was based on static equilibrium requirements and the second was based on a limit load analysis.
- The service difficulty reporting (SDR) database was merged with the Aircraft Utilisation Database. The result was previously unavailable information regarding the service history of particular Boeing 737 aircraft at points in their history when repairs were made.
- A methodology for probabilistic modeling of aged aircraft subject to variable loading conditions, periodic inspection and repair was formulated. One of the first practical problems addressed with this model was the potentially adverse effects of multiple site cracks in a fuselage lap joint.

1.0 INTRODUCTION

Commercial aircraft operators are required by FAA regulations to repair damaged aircraft structure. These repairs must be performed in a timely manner to reduce aircraft downtime and loss of revenue.

A guiding principle for many aircraft structural repairs has been to restore the structure to its original (or better) static strength and stiffness. However, the repair must also be designed for adequate fatigue resistance, damage tolerance and inspectability.

Fatigue and damage tolerance (DT) analyses should be based on realistic stress histories which, in turn, should be derived from realistic load spectra. Therefore, an algorithm for the development of a stress history should be included in a comprehensive analysis of repairs. Finally, the ramifications of missed cracks during inspection and repair quality on an aircraft's reliability should be examined.

This research program was initiated with these requirements in mind.

This study of the Effects of Repair on Structural Integrity, as defined by VNTSC and the FAA Technical Center, included six tasks. These tasks and their major objectives are listed in Table 1-1.

TABLE 1-1. TASKS AND OBJECTIVES

Task	Major Objective(s)
Planning and Industry Coordination	First, identify aircraft industry concerns regarding aircraft repairs; then communicate results to the industry.
Repair Database Assessment	Identify whether existing databases could be used to identify specific repairs that required frequent re-repair; isolate overall trends in aircraft repairs as aircraft age.
Compatible Displacement Analysis	Develop a simple, accurate analytical tool for estimating local stresses in fuselage skin repairs.
Standardized Load Spectra	Develop a methodology for developing realistic stress histories at specific locations in typical commercial aircraft fuselages.
Repaired Panel Testing	Develop laboratory data on, flat-panel simulated fuselage repairs to assess the accuracy of the compatible displacement analysis procedure.
Reliability Assessment	Develop an analytical tool that may eventually assess the ramifications of variable inspection accuracy and repair quality on the reliability of a commercial aircraft.

The major activities in each of these tasks are discussed in this report. Overall conclusions and recommendations are also provided.

The structural analysis and stress spectrum development procedures described in this report are approximate and, therefore, have certain limitations. These methods might be used to qualitatively compare the quality of different repair options with the original structure. If more precise quantitative analyses are required, more detailed structural analysis and stress results for specific locations in the aircraft should either be obtained from the origin equipment manufacturer (OEM) or calculated through the use of sophisticated structural analysis codes such as three dimensional finite element methods.

2.0 PLANNING AND INDUSTRY COORDINATION

At the beginning of this program it was understood that the analysis of aircraft repairs was both complex and controversial. Because of this, considerable effort was expended to make aircraft industry representatives aware of this research effort and to solicit their inputs regarding the best directions for the program.

The major coordination activities undertaken in the course of this program are listed in Table 2-1 below.

TABLE 2-1. COORDINATION ACTIVITIES

Date	Principal Individual or Group	Purpose of Visit and/or Presentation
2/2/90	Mr. Tom Swift, FAA National Resource Specialist for Fracture Mechanics and Metallurgy	Define principal elements of analytical and experimental effort
3/20-22/90	International Symposium on Structural Integrity of Aging Airplanes	Review program plans with industry and government to obtain feedback regarding planned analytical and experimental efforts
5/8/90	Aging Aircraft Repairs Program Representatives	Discuss plans for the FAA/VNTSC repair program; learn more about the large aircraft manufacturers initiative to review and update aircraft repairs
8/8/90	Technical Oversight Group for Aging Aircraft (TOGAA)	Present initial program results and near-term program plans to ensure the practical utility of work undertaken
12/4/90	Various airlines and repair stations	Review initial results from the SKINFIX analysis program and illustrate (through a computer demonstration) the potential utility of this program for analysis of fuselage repairs
1/22-23/91	Aging Aircraft Task Force (AATF)	Review the derivation of the SKINFIX analysis procedure and discuss the current attributes and limitations of the method; compare predicted repair stresses and displacements with laboratory data

2.1 Initial Meetings and Presentations

The initial coordination visit to Long Beach, California to meet with Mr. Tom Swift, the FAA National Resource Specialist for Fracture Mechanics and Metallurgy was useful in defining specific

research objectives. It was agreed that the initial focus would be on fuselage skin repairs and that an extension of the traditional compatible displacement analysis procedure held promise as a simple, yet accurate repair analysis tool.

Battelle researchers prepared an overview presentation for the 1990 International Symposium on Structural Integrity of Aging Airplanes in Atlanta, Georgia. The presentation addressed the scope of this study and included a discussion of the role of repairs in aging aircraft. A program overview including program schedule and critical milestones was provided, including a discussion of plans and issues related to each task. Comments and inputs from industry representatives were requested.

2.2 Aging Aircraft Repairs Program Meeting

After the Atlanta presentation, a follow-up meeting was scheduled with several large aircraft manufacturers. This meeting was held in May, 1990, in Long Beach, California. Representatives from Douglas Aircraft Company, Boeing Commercial Aircraft, and Lockheed, the FAA Aircraft Certification Office in Long Beach, the FAA Technical Center and VNTSC attended.

The airframe manufacturers presented an overview of their Aircraft Repairs Program and defined a timetable for completion of their efforts. They indicated that their efforts had been underway on an industry-coordinated basis since 1986. Their proposal can be summarized as follows:

- Develop operator usable system to evaluate repairs on aircraft.
- System would establish appropriate course of action for each repair evaluated, including
  - Inspection program requirements
  - Normal maintenance
  - NDI inspection thresholds/repetition rate
  - Removal limits (if required)
- Evaluation process would not be under an airworthiness directive (AD) — but would involve all aircraft repairs.
- Time frame for completion of evaluation would be under an AD.
- Regulator penalties for substandard repairs or repairs lacking documentation would not be assessed.

Following this presentation, Battelle presented an overview of its repairs program (VNTSC OMNI Task VA-0013). In regard to the repair database assessment, it was disclosed that Battelle was using the Service Difficulty Reporting (SDR) System in conjunction with the Aircraft Utilisation Database (maintained by Aviation Research & Support Limited in Warks, England) as a means to determine the location of repeat repairs and potentially troublesome types of repairs. Many factors influence whether a report is made to the SDR System and the level of detail of the data. Nonetheless, it was explained that findings from such a database interrogation might well provide useful indications of trends.

Battelle indicated that the primary focus was on smaller aircraft but that this program might be applicable to the industry in general. Since manufacturers of large transport aircraft already had a common repairs evaluation program underway, it was suggested that Battelle consider investigating commuter aircraft along the same lines to further the concept of an industry common approach.

To aid in the fuselage stress spectra development effort, Battelle also requested data on fuselage skin stresses from the large transport manufacturers represented at the meeting. Similar inquiries had already been made to the National Aeronautic Laboratory of the Netherlands (NLR) and to Deutsche Airbus. This information was requested to help develop several generic fuselage spectra for testing simulated aircraft repairs in the laboratory. The industry representatives were reluctant to provide such information because of the substantial range of fuselage pressurization stresses, variations of design life goals and other model specific differences, as well as the problems related to releasing such proprietary data. As a result, Battelle took the initiative to develop an alternative procedure for estimating fuselage stress spectra (see Section 5 of this report.)

Several suggestions were made concerning panel testing for repairs. A minimum width of 15 inches was suggested for damage tolerance testing. This recommendation was accepted in developing the final specimen design for laboratory testing in this program, as discussed in Section 6 of this report.

2.3 TOGAA Meeting

Since its inception the Technical Oversight Group for Aging Aircraft (TOGAA) has met at regular intervals to review pertinent research activities and offer recommendations for further work. In August, 1990, TOGAA met at the FAA Technical Center in Atlantic City, New Jersey. Participants in various aging aircraft research programs, including Battelle, were invited to present progress reports.

At the time of this meeting, the specimen design for fatigue testing of repairs had just been decided, so no laboratory fatigue data were available. However, virtually all of the work associated with the repair database assessment was completed. The results of this effort were reviewed. Considerable progress had also been made on the formulation of the compatible displacement analysis methodology, so an overview of this work was also presented. An overview of plans for the remainder of the program was offered.

2.4 Damage Tolerance Conference

In October 1990, Battelle was contacted by the New York City Certification Office of the FAA. Several individuals within that office were interested in learning more about this program and its potential long range utility to airlines and repair stations. Arrangements were made to hold a workshop at Kennedy Airport on December 4, 1990. The workshop evolved into a one day Damage Tolerance Symposium with 29 participants.

Presentations were made by Messrs. Tom Swift and Dick Johnson of the FAA, Dr. Pin Tong of VNTSC, Messrs. Walter Winkler and Paul Sawhny of Pan Am, Mr. Michael Lai of Federal Express, and Mr. Richard Rice of Battelle. The presentation by Battelle on the Effects of Repair on Structural Integrity was the central presentation of the symposium.

2.5 Airworthiness Assurance Task Force Meeting

Shortly after the Aloha B737 incident in April, 1988, the Airworthiness Assurance Task Force (also known as the Aging Aircraft Task Force) was set up by the Air Transport Association of America and the Aerospace Industries Association. Various technical experts representing airlines, aircraft manufacturers, international organizations and regulatory bodies comprise this group. Members of the steering committee agreed to periodic meetings to review aircraft airworthiness issues and research. One of those meetings was scheduled at VNTSC for January 22 - 23, 1991. Battelle gave a presentation on the work accomplished on the Structural Integrity of Repairs Program.

With the exception of the reliability assessment work, which was initiated later in 1991, the majority of the significant, approved technical activity on this program was accomplished by the time of this meeting. The first generation of the new compatible displacement analysis model was completed, all of the laboratory testing was finished, and all of the repair database assessment work was done. A detailed presentation of the overall program was made.

3.0 REPAIR DATABASE ASSESSMENT

The primary objective of this task was to identify whether certain types of repairs were more likely to require subsequent re-repair than others. A secondary objective was to identify significant trends within the commercial aging aircraft fleet regarding the incidence of fatigue and corrosion damage.

Representative findings from key database searches are included in the following paragraphs. Complete copies of the mini-databases that were generated were previously supplied to VNTSC[1][1]. The entire SDR database (over 200 megabytes of information on three magnetic tapes representing over 150,000 SDR reports) was also provided.

3.1 Acquisition and Setup of the SDR and ARS Databases

At the beginning of February 1990, Sam Smith and Richard Rice of Battelle visited the Aviation Standards National Field Office in Oklahoma City, Oklahoma along with Dr. Sam Sampath. The following individuals from the FRA discussed the attributes of the service difficulty reporting (SDR) system:

Cheryl Walker, AVN-121B	Jean Fossett, AVN-121B
Jack Price, AVN-124	Oscar Ball, AVN-112
Jim McLean, AVN-143	Donald Schein, AVN-124.

After this meeting, Dr. Sam Sampath of VNTSC sent a letter to Mr. Mark Rosenthal, APR-300 at the Federal Aviation Administration Headquarters in Washington, D.C. requesting release of the complete SDR database to Battelle. Several weeks later Battelle received the complete database from Boeing Computer Services on three magnetic tapes.

These tapes were referred to as follows:

- On-line: Data which is currently on-line in the SDR system
- History: Data which is stored off-line but is in the same format as the "on-line" data

---

1 Numbers in brackets refer to References listed at the end of this report.

- Old History: Data which is stored off-line and has a slightly different format from the "on-line" data.

TABLE 3-1. SDR DATA TAPE INFORMATION

Tape Name	Time Period	Number of Reports	Total Megabytes of Data	Reduced Megabytes of Data
On-line	1984-1990	83,918	116	42
History	1980-83	30,377	45	15
Old History	1973-79	41,093	39	13
TOTAL	1973-1990	155,388	200	70

The information contained on the tapes is described in Table 3-1. The "total megabytes" column gives the approximate storage requirements for the entire set of 92 SDR variables.

The SDR variable list was examined to determine which of the 92 variables were essential to this study. It was determined that 33 of the SDR variables were necessary. The remaining 59 variables could be derived from these 33 accessed or through the use of look-up tables. The "reduced megabytes" column of Table 3-1 gives the approximate storage requirements for the essential set of 33 SDR variables.

The next step in the database assessment process was to break down the SDR data into individual datasets for particular aircraft models. Initially, this process was completed for a single aircraft model, the Boeing 737, in order to create a dataset for exploratory analyses. Table 3-2 is a summary description of the B737 dataset.

TABLE 3-2. SDR DATA FOR 737 AIRCRAFT

Tape Name	Time Period	Number of Reports	Total Megabytes of Data	Reduced Megabytes of Data
On-line	1984-1990	9,533	13.2	4.5
History	1980-1983	3,663	5.4	1.8
Old History	1973-1979	2,241	2.1	0.7
TOTAL	1973-1990	15,437	20.7	7.0

On April 9, 1990, VNTSC sent to Battelle a copy of the Aircraft Utilisation Database developed and maintained by Aviation Research & Support in Warks, England. The Department of Transportation purchased a license to this database and loaned the manuals and database to Battelle for use on this task. In April the SDR and ARS databases were loaded onto one of Battelle's VAX computers and several different merges of these databases were accomplished.

Appendix A of Reference [1] provided a sampling of selected fields from the SDR database for several B727 aircraft. These records included only skin-related SDR incidents where the part condition was identified as either corroded or cracked. It was obvious from this sampling that individual aircraft were tracked principally by tail number and aircraft model. Inconsistencies in the part location description hampered attempts to perform automated searches for problems at specific part locations within a given aircraft make and model. Similar samplings were provided in Appendices B through D of Reference [1] for B737, B747, and DC-9 aircraft.

Appendix E of Reference [1] provided a sampling from the ARS database. This database provided more information than the SDR database concerning operator and service history.

3.2 Analysis of SDR and ARS Data

Several examples of output that were generated from these databases are included here to help illustrate the information available within them. Tables 3-3(a) through (d) show summary statistics of

TABLE 3-3(a). BREAKDOWN OF SDR'S FOR BOEING 727 AIRCRAFT

Time Period	Total SDR'S	Fraction of SDR's Involving Structural Elements		Fraction of SDR's Involving Either	
		Skin	Other	Corrosion	Cracking
1985-1990	20,540	13.0%	4.7% (Stringers)	15.5%	30.6%
1979-1984	7,082	4.9%	4.8% (Fittings)	6.3%	30.6%
1973-1978	8,693	3.2%		5.6%	31.4%
TOTAL	36,315	9.1%		11.4%	30.8%

service difficulty reports for structural parts from Boeing 727, 737, 747, and McDonnell-Douglas DC-9 aircraft. A number of observations were made from these tables, including the following:

TABLE 3-3(b). BREAKDOWN OF SDR'S FOR BOEING 737 AIRCRAFT

Time Period	Total SDR'S	Fraction of SDR's Involving Structural Elements		Fraction of SDR's Involving Either	
		Skin	Other	Corrosion	Cracking
1985-1990	9,533	17.1%		14.2%	35.5%
1979-1984	3,663	9.8%	4.3% (Frames) 3% (Fittings)	20.2%	39.0%
1973-1978	2,241	3.4%	3% (Doors) 2.5% (Frames)	7.4%	31.0%
TOTAL	15,437	13.4%		14.7%	35.7%

TABLE 3-3(c). BREAKDOWN OF SDR'S FOR BOEING 747 AIRCRAFT

Time Period	Total SDR'S	Fraction of SDR's Involving Structural Elements		Fraction of SDR's Involving Either	
		Skin	Other	Corrosion	Cracking
1985-1990	20,540	13.0%	4.7% (Stringers)	15.5%	30.6%
1985-1990	4,110	8.8%	7.1% (Fittings)	16.5%	37.5%
1979-1984	1,411	9.4%	6% (Fittings)	7.6%	45.4%
1973-1978	1,415	3.5%	5.2% (Fittings)	5.0%	21.6%
TOTAL	6,936	7.8%		12.4%	35.9%

- The total number of SDR citations have increased in all cases in recent years. This is partially attributable to a larger number of aircraft in each category, but may also be a reflection of effects of their increasing age.

- The percentage of SDR incidents that are fuselage skin-related have increased in recent years.

- The number and percentage of structural parts suffering from corrosion-related damage have increased substantially in recent years.

- The percentage of structural parts causing an SDR report because of cracking incidents has been substantial for years. The percentages shown in Tables 3-3(a) through (d) under part condition are for all parts, not just structural parts.

- The percentage of frame and longeron related incidents relative to skin incidents tends to be higher for aircraft that have lower skin stresses due to pressurization.

Table 3-4 provides an example of an SDR/ARS merge in which SDR data (first 6 columns) were combined with ARS derived information (last 4 columns). Output such as this could not be produced by interrogating either database independently. With this merged database it was possible to

TABLE 3-3(d). BREAKDOWN OF SDR'S FOR MCDONNELL-DOUGLAS DC-9 AIRCRAFT

Time Period	Total SDR'S	Fraction of SDR's Involving Structural Elements		Fraction of SDR's Involving Either	
		Skin	Other	Corrosion	Cracking
1985-1990	13,945	7.1%	6.4% (Longerons)	8.7%	31.9%
1979-1984	5,637	4.9%	3.7% (Frames) 5.7% (Fittings) (Fittings)	5.2%	48.4%
1973-1978	6,546	4.1%	3.0% (Frames) 6.8% (Fittings) 4.0% (Longerons)	7.6%	48.1%
TOTAL	26,128	5.9%		7.7%	39.5%

TABLE 3-4. DC-9 AIRCRAFT WITH SKIN CORROSION OR CRACKING PROBLEMS, MERGED SDR AND ARS DATABASE INFORMATION

Aircraft Serial Number	Aircraft Model	SDR Date	Part Name	Part Location	Part Condition	Operator Code	Estimated Age	Estimated Flight HPS	Estimated Landings
	DC914	80-01-14	Skin	STA 555	Cracked	EALA	•	•	•
	DC915	82-06-21	Skin	FSTA 884	Cracked	EMAA	•	•	•
		87-08-14	Skin	STA 756-776	Corroded	TWAA	•	•	•
	DC931	84-11-13	Skin	Right Wing	Cracked	OZAA	•	•	•
17316	DC931	89-12-22	Skin	Station 756	Cracked	CALA	•	•	•
19674	DC932	89-05-19	Skin	Above Pylon	Cracked	TWAA	•	•	•
45316	DC931	80-06-30	Skin	STA 756	Corrosion	TXIA	•	•	•
45695	DC914	74-11-04	Skin	STA 738 and 718	Corroded	TXI	9	22720	27698
		75-03-12	Skin	Station 200	Corroded	TXI	10	23532	28687
		77-04-05	Skin	Station 859	Cracked	TXI	12	28319	34524
		79-06-14	Skin	S25L STA 817	Corrosion	TXI	14	33392	40708
		80-02-22	Skin	Station 817	Corrosion	TXI	15	34997	42664
		81-12-22	Skin Panel	STA 170 DR Frame	Cracked	TXIA	16	39239	47835
		82-06-29	Skin	STA 755 766	Corroded	TXIA	17	40437	49296
		88-11-25	Skin	FS 710	Cracked	SWXA	23	55282	67393
45696	DC914	87-02-02	Skin	STA 817	Corroded	MWEA	20	45680	49189
		87-02-02	Skin	STA 439	Corroded	MWEA	20	45680	49189
		87-02-02	Skin	STA 766-801	Corroded	MWEA	20	45680	49189
		89-05-26	Skin	Stations 177-184	Cracked	MWEA	22	50819	54722
		89-05-26	Skin	Station 106	Cracked	MWEA	22	40819	54722
		89-08-25	Skin	WS XRS 215	Cracked	MWEA	23	51373	55319
		89-08-25	Skin		Cracked	MWEA	23	51373	55319

make meaningful comparisons between SDR trends and aircraft service history. This capability to link service history and owner history directly with incidents of service difficulty is believed to have been unique at the time.

Initial SDR analysis results were presented at a meeting in Long Beach on May 8, 1990. At this meeting it was generally agreed that many factors have influenced whether an SDR report was made and its level of detail. Nonetheless, findings from such a database interrogation can provide useful indicators of trends.

Based on this meeting, a decision was made to perform a survey of the SDR database to get a better idea of what aircraft were represented and to better identify which ones showed substantial SDR activity, especially in terms of skin-related problems. This information is summarized in Table 3-5.

As a rudimentary method of sorting the various makes and models of aircraft in terms of their SDR "criticality", two criteria were developed and all aircraft categories were compared against these two criteria. The first criterion was based on the ratio of total SDR reports compared with the number of aircraft within a category. Criterion 1 was set at a ratio of 10 or greater. A brief scan of Table 3-5 reveals that relatively few aircraft show an average of more than 10 SDR reports per aircraft.

The second criterion was based on the percentage of SDR incidents that involved skin damage, suggesting the need for doubler repairs like those addressed in this program. Criterion 2 was set at 5 percent or greater. Again, relatively few aircraft showed a high percentage of skin-related problems. Many of these aircraft types were also the ones that satisfied Criterion 1.

Overall, the aircraft models that appeared to represent the highest level of SDR criticality were those that represented the mainline, older commercial transport aircraft models. This finding was not particularly surprising considering that the evaluation criteria did not take into account aircraft age or size, both of which could reasonably be expected to influence the average number and type of SDR incidents.

Table 3-6 shows the cross-section of active aircraft within the commercial fleet among the older McDonnell Douglas and Boeing aircraft models. Of the six models included, approximately 70 percent of these aircraft are flown by the top ten operators. If DC-8's are excluded, the percentage of the remaining five aircraft models flown by the top ten operators moves up to almost 75 percent.

TABLE 3-5. SUMMARY OF SIGNIFICANT SDR CITATIONS BY AIRCRAFT MAKE AND MODEL

		All types of Damage		Skin Related Damage			
Aircraft Make Code	Aircraft Model	Number of Different Aircraft	Number of SDR's	Number of Different Aircraft	Number of SDR's	Exceeds Criteria 1[1]	2[2]
AEROSP	262NORD	60	402	1	1		
	ATR42	81	245	1	1		
AIRBUS	A300	195	974	12	13		
	A310	30	66	0	0		
	A320	11	26	0	0		
AMD	FALCON 10	83	199	1	1		
	FALCON 20	202	1007	12	12		
	FALCON 50	45	72	1	1		
BAC	111	166	2074	50	172	*	*
	146	71	450	4	7		
BAG	BAE146	53	261	7	11	*	
	JETSTM	160	1837	0	0		
BEECH	1900	131	1302	8	10	*	
	300	52	535	7	8	*	
BELL	214	38	315	1	2		
BOEING	707	542	6813	163	453	*	*
	720	70	454	13	18		
	727	2364	36315	774	3294	*	*
	737	1097	15437	257	2069	*	*
	747	381	6935	134	543	*	*
	757	130	667	16	16		
	767	123	635	7	9		
BRAERO	DH125	200	427	5	5		
CASA	C212	55	326	2	2		
CESSNA	650	94	245	1	1		
CNDAIR	CL44	10	97	0	0		
	CL600	85	417	1	2		
CURTIS	C46	58	139	0	0		

[1] Ratio of SDR's to number of aircraft exceeds 10 for all types of damage.
[2] More than 5 percent of all SDR's are related to skin damage.

TABLE 3-5. SUMMARY OF SIGNIFICANT SDR CITATIONS BY AIRCRAFT MAKE AND MODEL (CONTINUED)

		All types of Damage		Skin Related Damage			
Aircraft Make Code	Aircraft Model	Number of Different Aircraft	Number of SDR's	Number of Different Aircraft	Number of SDR's	Exceeds Criteria 1[1]	2[2]
CVAC	22	11	15	1	1		
	240	30	64	0	0		
	30	21	158	3	4		
	340	56	166	6	7		
	440	46	236	6	9		
	580	174	5387	99	437	*	*
	600	37	606	15	25	*	
	640	46	470	8	16	*	
DHAV	DHC7	1167	1167	11	26	*	
	DHC8	806	806	13	28		
DORNER	DO228	48	185	1	1		
DOUG	DC3	209	376	5	7		
	DC4	20	26	0	0		
	DC6	141	607	16	31		*
	DC7	15	26	1	1		
	DC8	704	6785	180	402		*
	DC9	1465	26174	493	1532	*	*
	DC10	337	4423	83	152	*	
EMB	120	174	1075	1	1		
FOKKER	F27	76	881	9	33	*	
	F28	72	868	32	70	*	*
FRCHLD	F27	114	886	10	13		
	FH227	74	1075	4	4	*	
GRUMAN	SA16	9	15	0	0		
GRUMAV	G159	21	22	0	0		
GULSTM	G1159	432	1669	13	13		
HAMFLU	HFB320	12	21	1	1		
HWKSLY	DH125	82	146	3	5		

[1] Ratio of SDR's to number of aircraft exceeds 10 for all types of damage.
[2] More than 5 percent of all SDR's are related to skin damage.

TABLE 3-5. SUMMARY OF SIGNIFICANT SDR CITATIONS BY AIRCRAFT MAKE AND MODEL (CONCLUDED)

		All types of Damage		Skin Related Damage			
Aircraft Make Code	Aircraft Model	Number of Different Aircraft	Number of SDR's	Number of Different Aircraft	Number of SDR's	Exceeds Criteria 1[1]	2[2]
ISRAEL	1121	108	1245	11	11	*	
	1123	25	75	0	0		
	1124	116	409	3	4		
KAWSKI	KV107	11	57	0	0		
LEAR	24	260	554	8	11		
	25	312	756	5	6		
	35	381	893	3	3		
	55	64	140	17	21		*
LKHEED	1011	344	4203	74	133	*	
	1329	121	289	4	4		
	188	222	2916	26	46	*	
	382	96	2190	10	27	*	
MARTIN	404	28	104	1	1		
MTSBSI	MU300	44	66	0	0		
NIHON	YS11	97	708	4	5		
RKWELL	NA265	384	2411	17	43		
SAAB	SF340	147	757	1	1		
SKRSKY	S58	24	39	1	1		
	S58T	30	10	1	2		
	S61	30	221	1	1		
SNIAS	SA330	17	144	0	0		
STBROS	SD3	281	3179	9	11	*	
VICKER	745	17	71	0	0		

[1] Ratio of SDR's to number of aircraft exceeds 10 for all types of damage.
[2] More than 5 percent of all SDR's are related to skin damage.

Figures 3-1(a) and (b) show when these aircraft models were introduced into service. This figure rather dramatically illustrates the large percentage of B727 and DC-9 aircraft between 20 and 25 years old and the great percentage of B747 and DC-10 aircraft between 15 and 20 years old.

Two additional issues were also explored in the SDR database. First, an attempt was made to find evidence within the SDR database that repairs were being made in accordance with specific SRM

TABLE 3-6. NUMBER OF AIRCRAFT FOR MAJOR UNITED STATES AIRLINES

OP(OPERATOR)	TYPE (MODEL)						
Frequency	B727	B737	B747	DC10	DC8	DC9	Total
UNITED	144	148	33	55	27	0	407
USAIR	44	208	0	0	0	74	326
NORTHWEST	71	0	45	20	0	140	276
CONTINENTAL	94	97	8	15	0	40	254
DELTA	130	74	0	0	0	36	240
AMERICAN	164	12	2	59	0	0	237
FEDERAL EXP	114	0	0	25	6	0	145
TWA	69	0	19	0	0	48	136
PAN AM	89	5	37	0	0	0	131
EASTERN	55	0	0	2	0	73	130
OTHERS	259	261	43	69	178	175	985
Total	1233	805	187	245	211	586	3267

SOURCE: AIRCRAFT UTILISATION DATABASE, AVIATION RESEARCH & SUPPORT, ENGLAND

recommendations. Second, the SDR database was examined to determine whether there was any evidence of the need for additional repairs in the vicinity of these repairs, or the need for re-repair of these "sanctioned" repairs.

It was found in general that SRM's were cited in an SDR report in the comment fields, if at all. Rather than attempting text-string searches for specific SRM designations, partial listings of the comment fields were developed for DC-9 and B737 aircraft (as shown in Appendices F and G of Reference [1], respectively). Based on a review of comment fields for about 50 DC-9 aircraft (out of 493 represented in the database) and 50 B737 aircraft (out of 257) the following observations were made:

- A number of cases where the same SDR is cited twice for the same aircraft represents a single repair. In these cases the first entry is simply a notice of observed damage. The second entry (which usually occurs days later) is a recording of the actual repair.

- Within our limited sampling, some type of repair designation was given about 1/4 of the time for DC-9 aircraft and about 1/2 of the time for B737 aircraft. All other cases did not provide a reference number that might provide further details on the nature of the

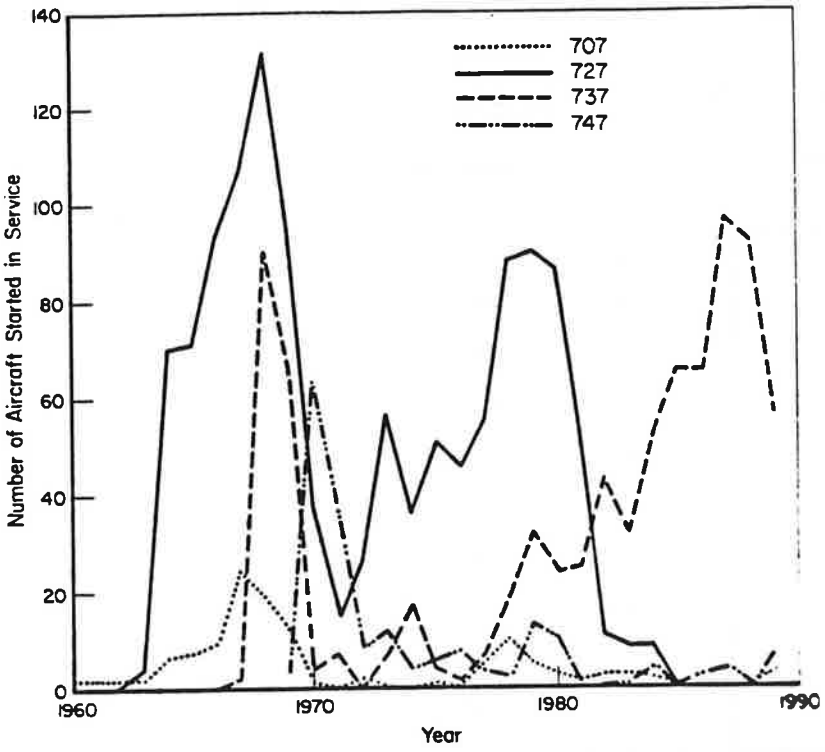

SOURCE: AIRCRAFT UTILISATION DATABASE

(a) Boeing Aircraft

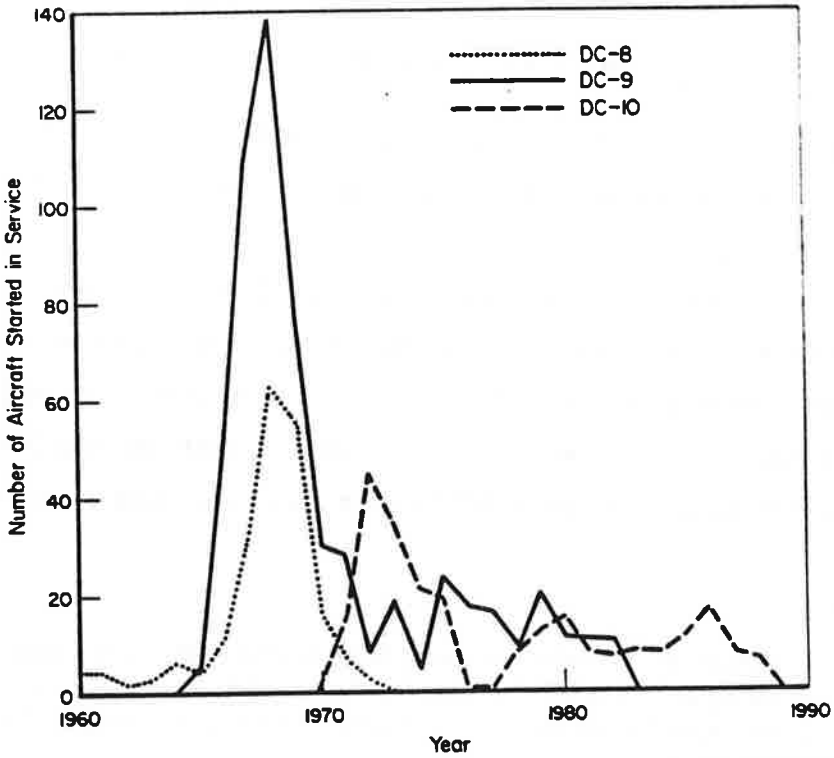

SOURCE: AIRCRAFT UTILISATION DATABASE

(b) McDonnell-Douglas Aircraft

FIGURE 3-1. NUMBER OF AIRCRAFT STARTED INTO SERVICE SINCE 1960

repair. In general, the exact type of repair made is not stated explicitly within the comment field.

- In about 15 percent of the cases where an SRM number is cited, the repair is described specifically by including a page number or figure number along with the SRM number. In all other cases the SRM number that is specified only identifies a general class of repairs.

- Other numbering systems appear in the comment fields, which apparently represent repairs from other manuals or simply orders for repairs.

- In most cases, the location of the repair is defined only by the fuselage station. In less than half of these cases the location is further specified by longeron number.

Although the information provided in the SDR database alone may have limited usefulness in identifying problematic repairs or trouble spots in aircraft, it can provide meaningful global trends concerning the incidence of aircraft structural problems and associated repairs when combined with the Aircraft Utilisation Database. For example, a simple interrogation of the SDR database in combination with the Aircraft Utilisation Database allowed the development of Figures 3-2 through 3.4 for three airlines flying DC-9 aircraft. In these figures, the relationship between aircraft age, flight hours and aircraft landings with the number of cracking and/or corrosion-related SDR's is evident: Each data point represents the total number to date of SDR's of a certain type for a single aircraft as of the last update of the database. In any case, little SDR activity would be expected until an aircraft is at least 10 years old. After the aircraft reaches an age of about 20 years, the number of cracking and corrosion incidents could be expected to go up rather dramatically. The number of incidents of corrosion is less well correlated with flight hours, and even more poorly correlated with aircraft landings. An examination of these trends against specific airlines did not reveal significantly different trends.

These results show a dramatic increase in the number of repair incidents as an aircraft's age exceeds 15 to 20 years. An obvious conclusion is that repairs to aging aircraft will likely increase in the U.S. commercial fleet unless a large percentage of these older aircraft are retired in the next few years.

The utility of the SDR system could be enhanced by introducing greater standardization in reporting requirements and introducing more required fields, especially fields that would specify the exact type and location of damage and the specific type of repair.

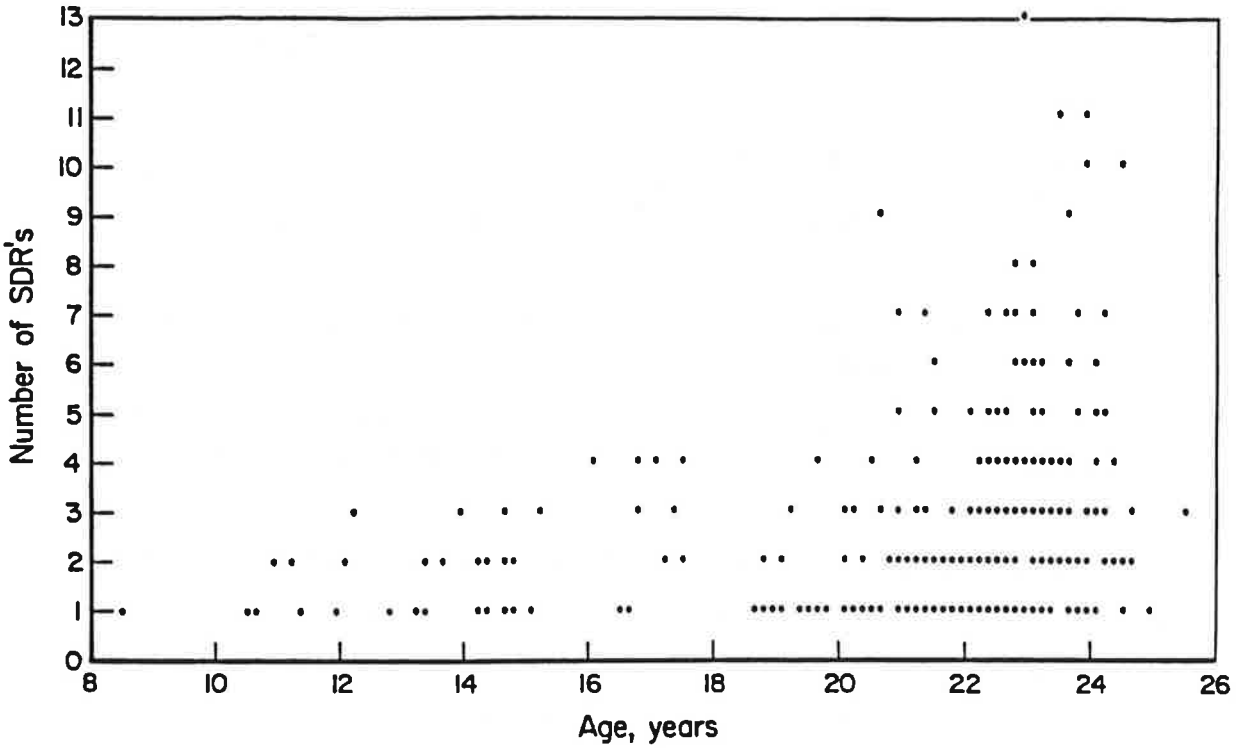

a. Cracking Incidents

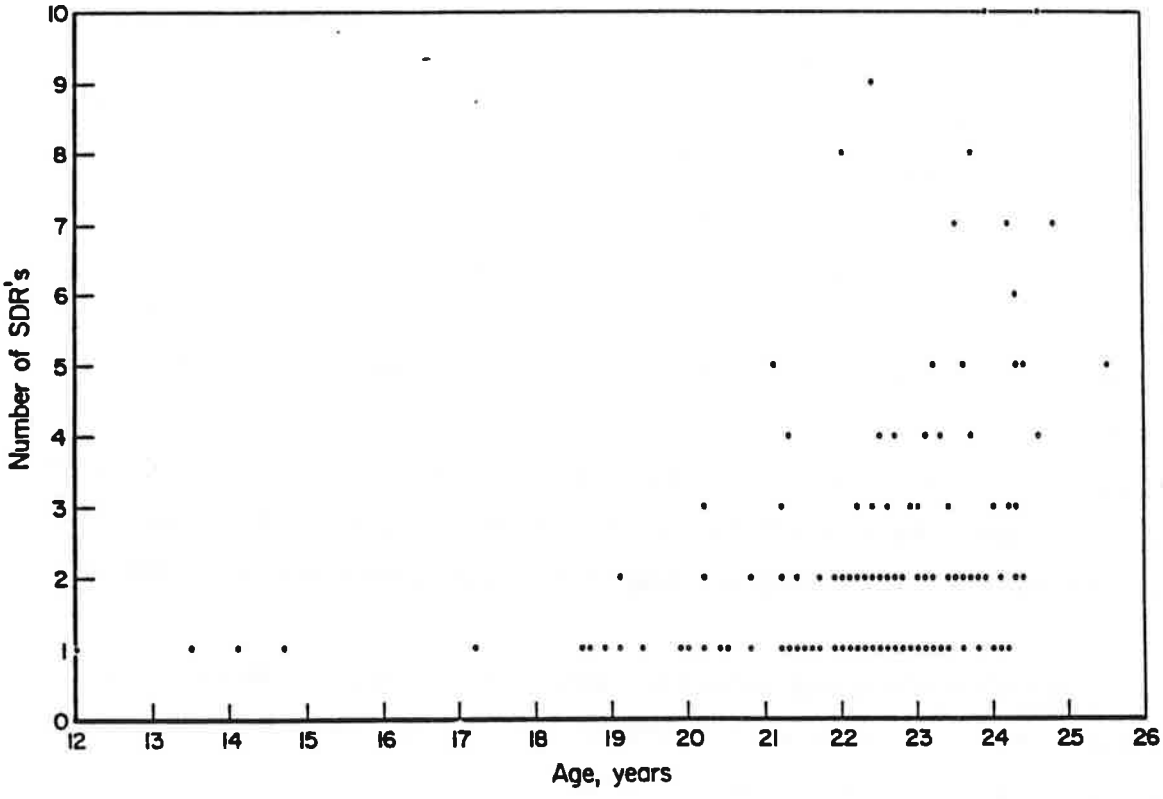

b. Corrosion Incidents

FIGURE 3-2. NUMBER OF SDR'S VERSUS AIRPLANE AGE

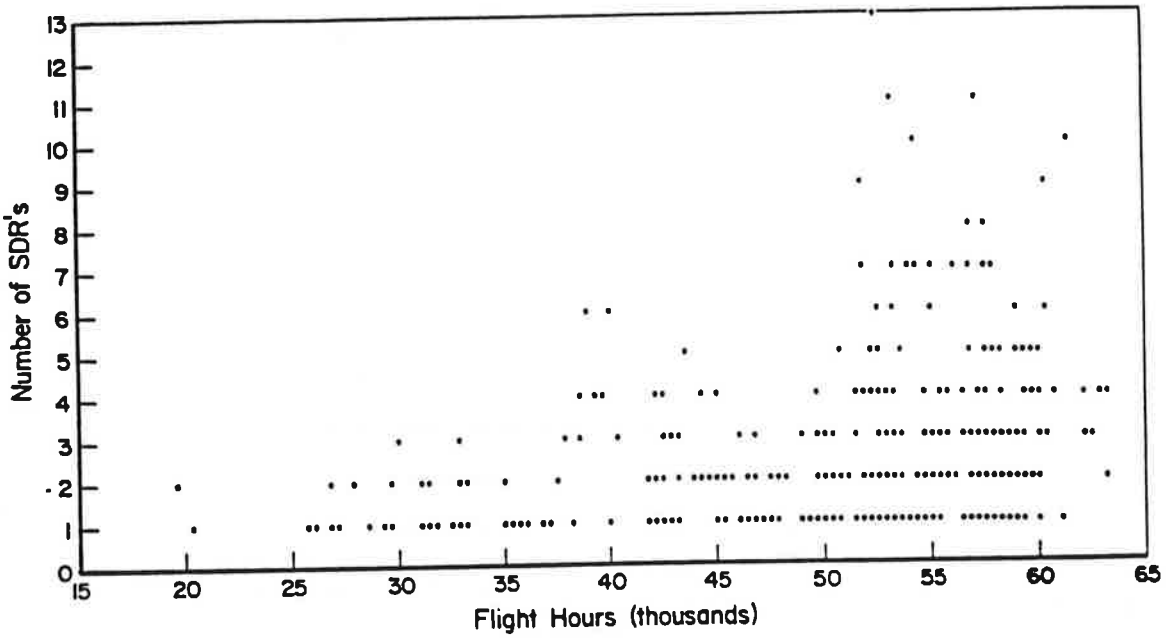

a. Cracking Incidents

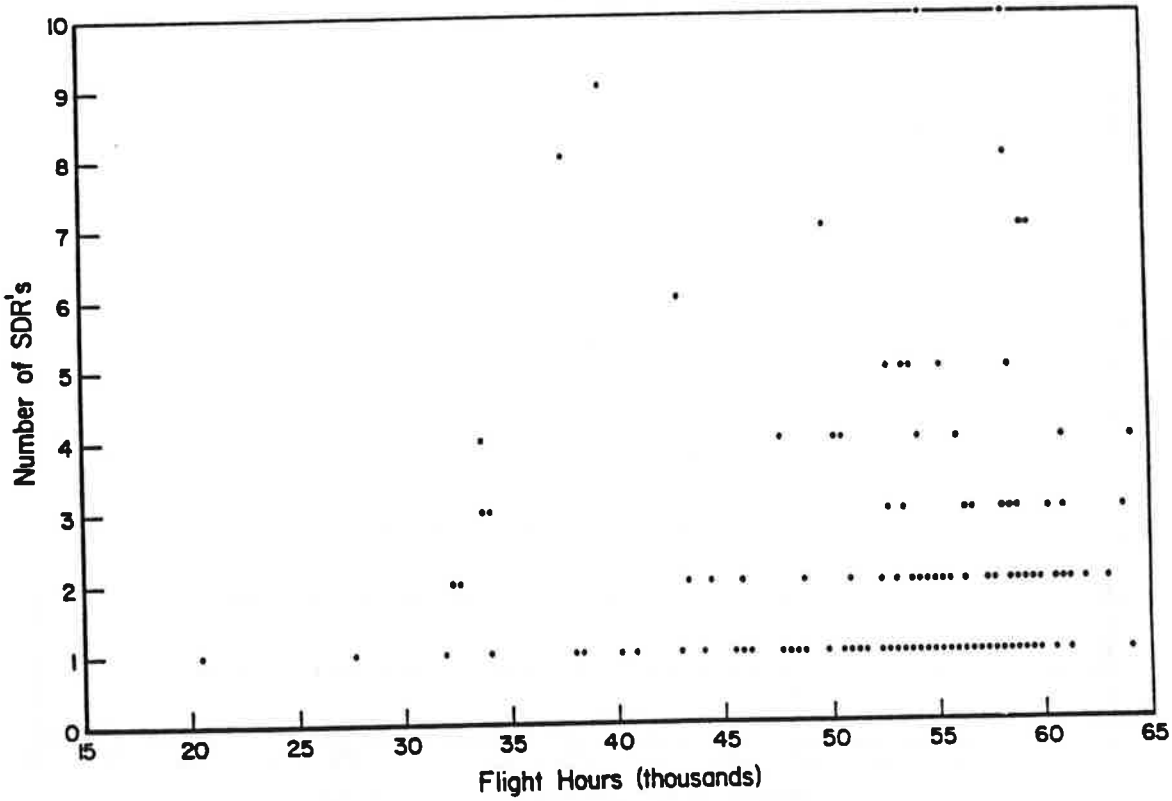

b. Corrosion Incidents

FIGURE 3-3. NUMBER OF SDR'S VERSUS FLIGHT HOURS

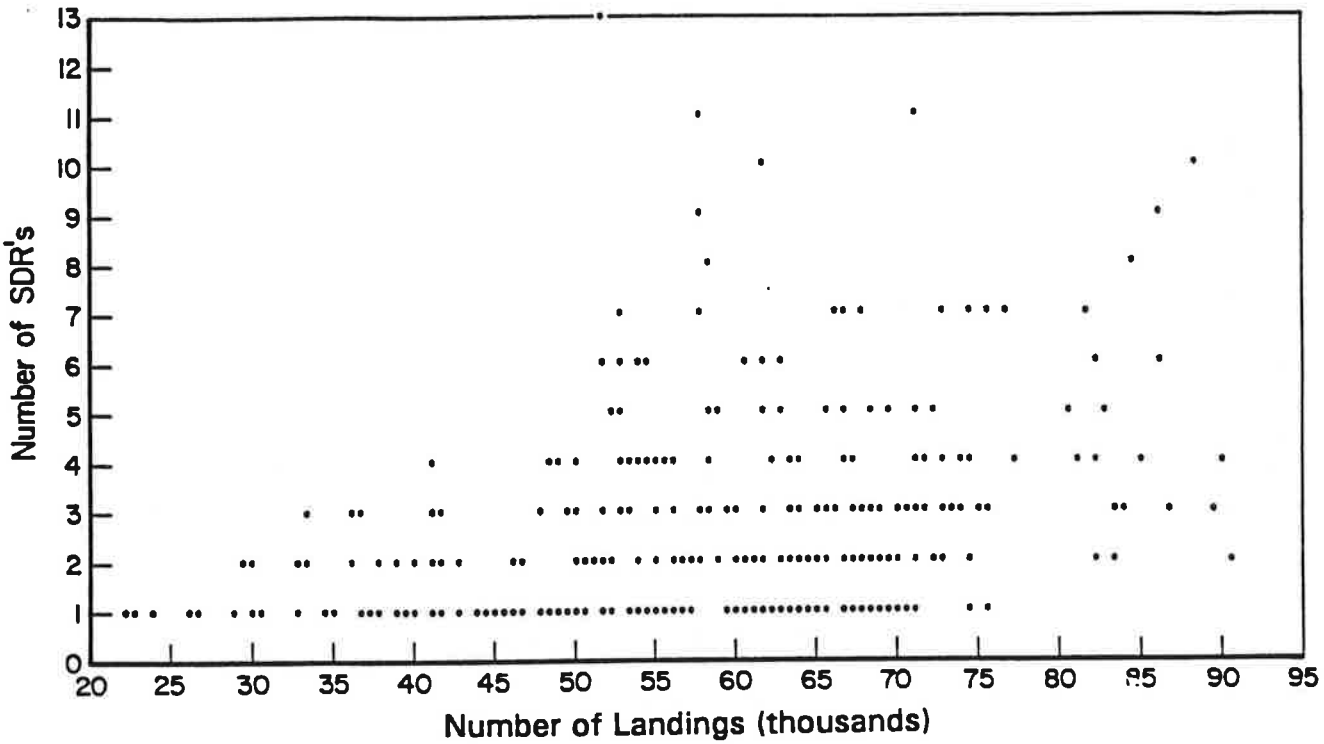

a. Cracking Incidents

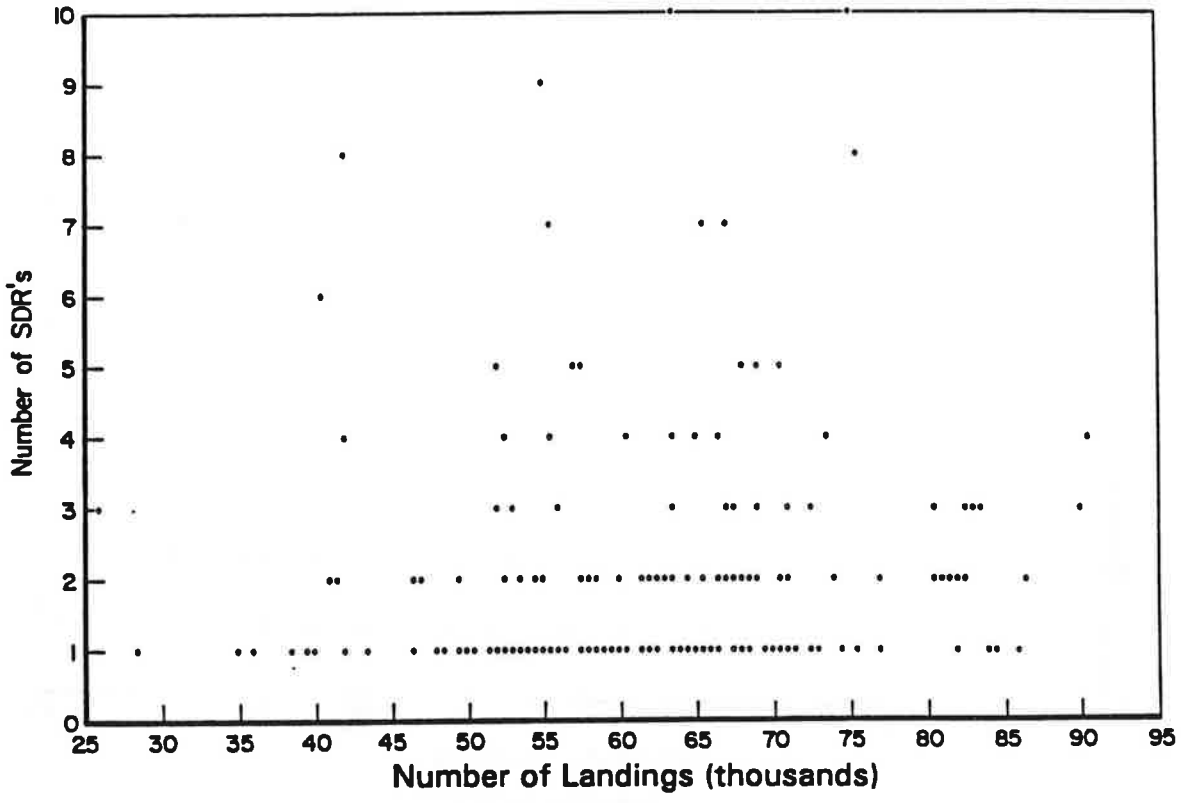

b. Corrosion Incidents

FIGURE 3-4. NUMBER OF SDR'S VERSUS NUMBER OF LANDINGS

4.0 COMPATIBLE DISPLACEMENT ANALYSIS

At present, aircraft repairs are often designed on the basis of static strength. In order to assure a damage-tolerant repair, it is necessary to perform engineering calculations at a sufficient level of detail to identify the most fatigue-critical locations in a proposed repair and evaluate its effect on structural fatigue life. Accurate fatigue life estimates require calculating the fastener loads and skin or reinforcement member stresses in a highly redundant structure. One means of accomplishing this is to perform finite element analysis (FEA) of the repair. FEA requires sufficiently capable commercial software, supporting hardware, and knowledgeable staff to correctly implement and interpret the analyses. These facilities and skills may not be available at small aircraft repair facilities. An alternative approach is to perform a "displacement-compatibility" analysis, in which equations are written for the displacements of the loaded sheet and doubler elements and made "compatible" by accounting for fastener displacements. This still results in a matrix of linear equations, which must be solved numerically (on a computer), but this approach potentially requires less sophisticated computational resources than a typical FEA analysis. One relatively sophisticated approach to compatible-displacement analysis was explored in this program[2].

4.1 Methods of Compatible-Displacement Analysis

Compatible-displacement analysis (CDA) involves writing equations for the displacements of the skin, all reinforcing members (in this context, one or more thin plates), which are mechanically fastened to the skin, and the fasteners, in terms of the unknown fastener loads. This system of equations is solved to obtain the unknown fastener loads and displacements and, subsequently, stresses in the repaired skin and reinforcement. The process of writing and solving equations for displacements in terms of forces is also inherent in finite element analysis. FEA differs from CDA, however, in that the behavior of the continuous structure is modeled with an assembly of discrete elements, the fundamental behavior of which are chosen such that the behavior of the actual structure is approached as the elements are reduced in size and increased in number. Hence, solution accuracy is dependent upon mesh refinement relative to stress gradients and the numerical integration order of the element formulation. CDA relies on the explicit expression of the structure's behavior or, at the very least, on a discrete element behavior that is representative of the macroresponse of the structure.

Vlieger and Sanderse[3] developed a computer code to evaluate the residual strength of a uniformly loaded continuous sheet, reinforced with fastened stringers oriented in the direction of loading and containing a central crack. Equations for sheet displacement at the fastener locations were written from elasticity solutions for uniformly stressed and point-loaded membranes, and then fastener loads were determined by equating the sheet displacements to the stiffener displacements. The fasteners were considered rigid, although they could also have been treated as flexible. Vlieger and Sanderse's method represented a sophisticated approach with the advantage of accounting for local sheet displacements around fasteners and cracks. However, the approach did not appear to be readily implementable to general repair configurations which might include arbitrary openings in the skin, complex reinforcement geometries, and nonuniform loading.

At the opposite end of the spectrum of technical rigor, Swift[4] developed a highly simplified approach in which the sheet and reinforcement was reduced to a uniaxial extensional strip

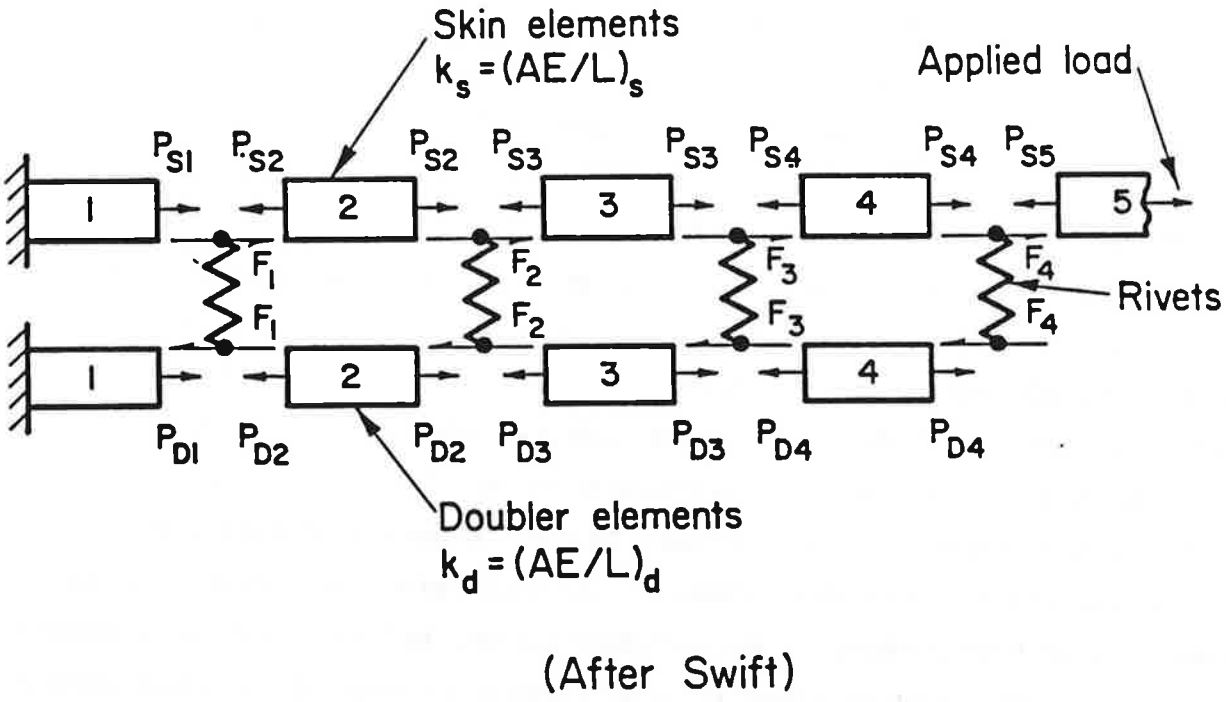

FIGURE 4-1. SWIFT CDA MODEL

equal in width to the fastener spacing transverse to the direction of loading, as in Figure 4-1. The sheet and reinforcement(s) were individually modeled as discrete axial spring members with stiffness

expressed as AE/L, where A was the product of width and thickness of the strip of sheet or reinforcement, E was the material modulus, and L was the fastener spacing in the direction of loading. The fasteners were modeled as shear springs connecting the sheet and reinforcements. The fastener stiffness values were estimated empirically from double-lap shear tests[5]. This scheme has the advantages of simplicity and of empirically accounting for local fastener-plate interactions. However, it does not adequately address the in-plane shear load transfer and biaxial stresses that result in and around a wide sheet having a finite-width reinforcement.

It was decided (within the constraints of the repairs program scope and with the concurrence of the VNTSC TTI), that the best approach would be to apply the Swift model, expanded as a bidirectional spring member, thereby simultaneously improving the CDA element's accuracy and general applicability.

4.2 The Bidirectional CDA Element

Expanding Swift's approach to two dimensions resulted in spring-like discrete members connecting fasteners in both principal axes, each with axial and shear stiffness terms. However, to adequately model the membrane behavior of a plate, in-plane diagonal coupling between fasteners was also required, as defined in Figure 4-2. In this application, the side and chord members possess both axial and bending properties and the diagonals are trusses (with axial properties only). For an isotropic rectangular plate element of thickness h, side length s, chord length c, diagonal length d, and Poisson's ratio ν[6],

$$A_c = \frac{h(s^2 - \nu c^2)}{2s\,(1 - \nu^2)} \tag{4-1a}$$

$$A_s = \frac{h(c^2 - \nu s^2)}{2c(1 - \nu^2)} \tag{4-1b}$$

$$A_d = \frac{hd^3\,\nu}{2sc(1 - \nu^2)} \tag{4-1c}$$

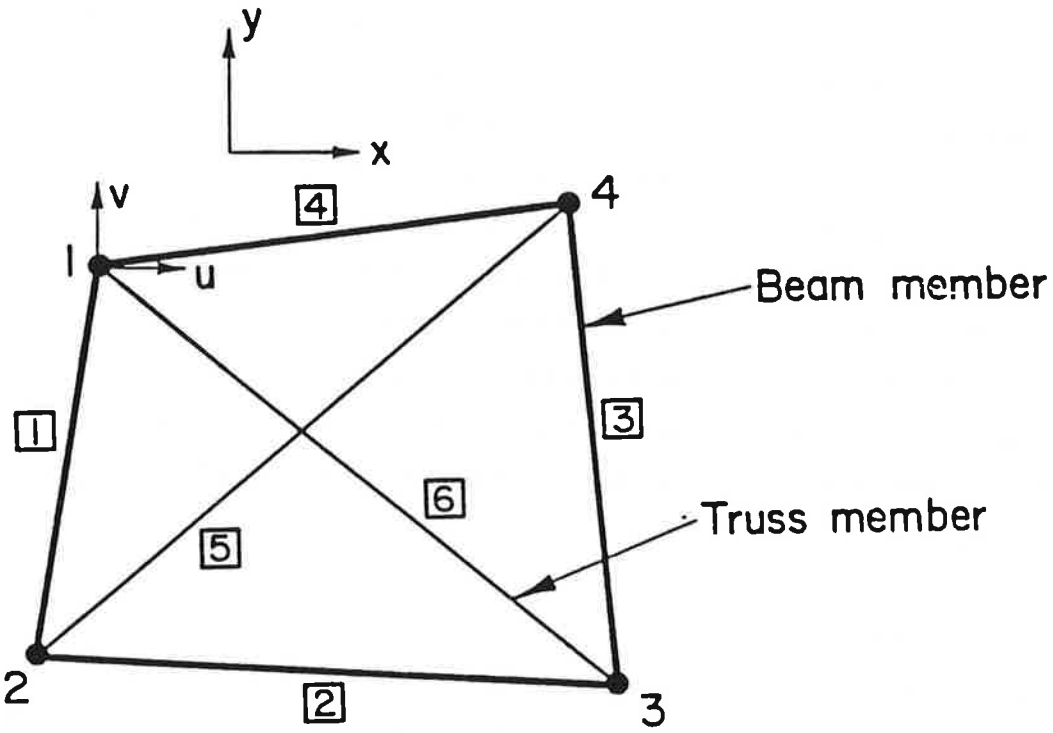

FIGURE 4-2. BIDIRECTIONAL CDA ELEMENT

$$I_c = \frac{\left(\frac{hsc^2}{24}\right)(1 - 3v)}{1 - v^2} \tag{4-2a}$$

$$I_s = \frac{\left(\frac{hcs^2}{24}\right)(1 - 3v)}{1 - v^2} \tag{4-2b}$$

$$I_d = 0 \tag{4-2c}$$

The axial stiffness of each member is then AE/L, and the in-plane bending stiffness is $12EI/L^3$. The member properties of an irregular quadrilateral can be approximated, within undefined limits, with averaged side and chord dimensions. Since modeling each segment of the sheet and reinforcement between individual groups of fasteners, or between fasteners and member boundaries by six individual members would be a serious nuisance, a stiffness matrix representing the combined stiffness of all six members is automatically assembled by the program.

The fastener stiffness is an empirical expression derived from double-lap shear tests[5],

$$\frac{1}{k_f} = \frac{a}{E_f D} + b\left(\frac{1}{E_s t_s} + \frac{1}{E_r t_r}\right) , \qquad (4\text{-}3)$$

where

k_f = fastener stiffness,

D = fastener diameter,

$E_{f,s,r}$ = elastic moduli of fastener, sheet, and reinforcement material,

$t_{s,r}$ = thickness of sheet and reinforcement,

and a and b are parameters which depend on the fastener material. For steel, a = 1.667 and b = 0.86; for aluminum, a = 3.125 and b = 0.82; and for titanium, a = 5.0 and b = 0.80. This relationship implicitly accounts for local plate deformations and fastener rotations. There may be limits to the range of other parameters such as fastener diameter, plate thickness, and fastener spacing for which this relationship remains valid. These limits, which must be explored experimentally, have not been addressed in the literature or by Battelle. Other fastener flexibility models that were examined and compared with Swift's model for one specific case were found to be at variance (both indicating lower stiffness) by factors of 2 and 10. Although there is no consensus on fastener flexibility, Swift's estimates appeared to be widely accepted. Furthermore, estimating a higher fastener stiffness would tend to result in higher estimates of bearing loads, which would generally be conservative in the repair context.

The stiffness matrix of the entire structure was assembled from the plate and fastener member stiffnesses. The solution for unknown displacements, reactions, and internal forces was then accomplished through a straight-forward matrix structural analysis procedure[7].

Once displacements were known at the vertices of each bi-directional element, an average stress, equal to the "bypass" stress, was calculated as:

$$S_x = \frac{E\left[(u_1+u_2-u_3-u_4)s/c + \nu(v_1-v_2-v_3+v_4)\right]}{2s(1-\nu^2)} \qquad (4\text{-}4a)$$

$$S_y = \frac{E\left[(v_1 - v_2 - v_3 + v_4) + \nu(u_1 + u_2 - u_3 - u_4)s/c\right]}{2s(1-\nu^2)} \qquad (4\text{-}4b)$$

$$T_{xy} = \frac{E\left[(u_1 - u_2 + u_3 + u_4)s/c + (v_1 + v_2 - v_3 - v_4)\right]}{4s(1-\nu^2)} \qquad (4\text{-}4c)$$

Direct bearing stresses and the distribution of stresses moving away from the hole were obtained after the fastener loads were calculated. Average (bypass) stresses of distorted elements were likewise calculated using averaged side and chord dimensions, which were reasonable approximations for small element distortions. The limits of distortion for acceptable approximation were not explored.

4.3 CDA Program SKINFIX

The CDA analysis program, SKINFIX, is written in FORTRAN and was driven by menus in a main menu routine, which calls the appropriate subroutines based on user input. This structure is shown in Figure 4-3. The menu is self-explanatory. On first use, the menu requests instruction from the user as to which set of input data is to be provided, or whether to go to the solution and assembly phase or stress output phase. Based on user response, the appropriate subroutine is called For example, if the user responds with "N", for node input, subroutine GEOMETRY is called GEOMETRY will ask for the form of input data (single node entry, node generation, or external data file), will call the appropriate subroutine, and then return to the main menu. At this time, only the file input-mode (as opposed to the interactive mode) is operational. This is a programming matter that is not of technical importance. A similar procedure applies to input for elements, materials, forces, and boundary conditions. Element and node numbers in the model need not be consecutive.

It is not necessary to provide the problem input in any particular order (i.e., nodes before elements), except that all such input must be made available before entering the assembly and solution phase. This phase is called by entering "A" from the main menu, which then calls the subroutine SOLVE. SOLVE is the largest single subroutine in the program. It automatically assembles plate elements from the constituent beam-truss members, and then assembles a global stiffness matrix from plate and fastener stiffness matrices. It also identifies degrees of freedom associated with prescribed displacements and known forces. The global stiffness matrix is partitioned accordingly:

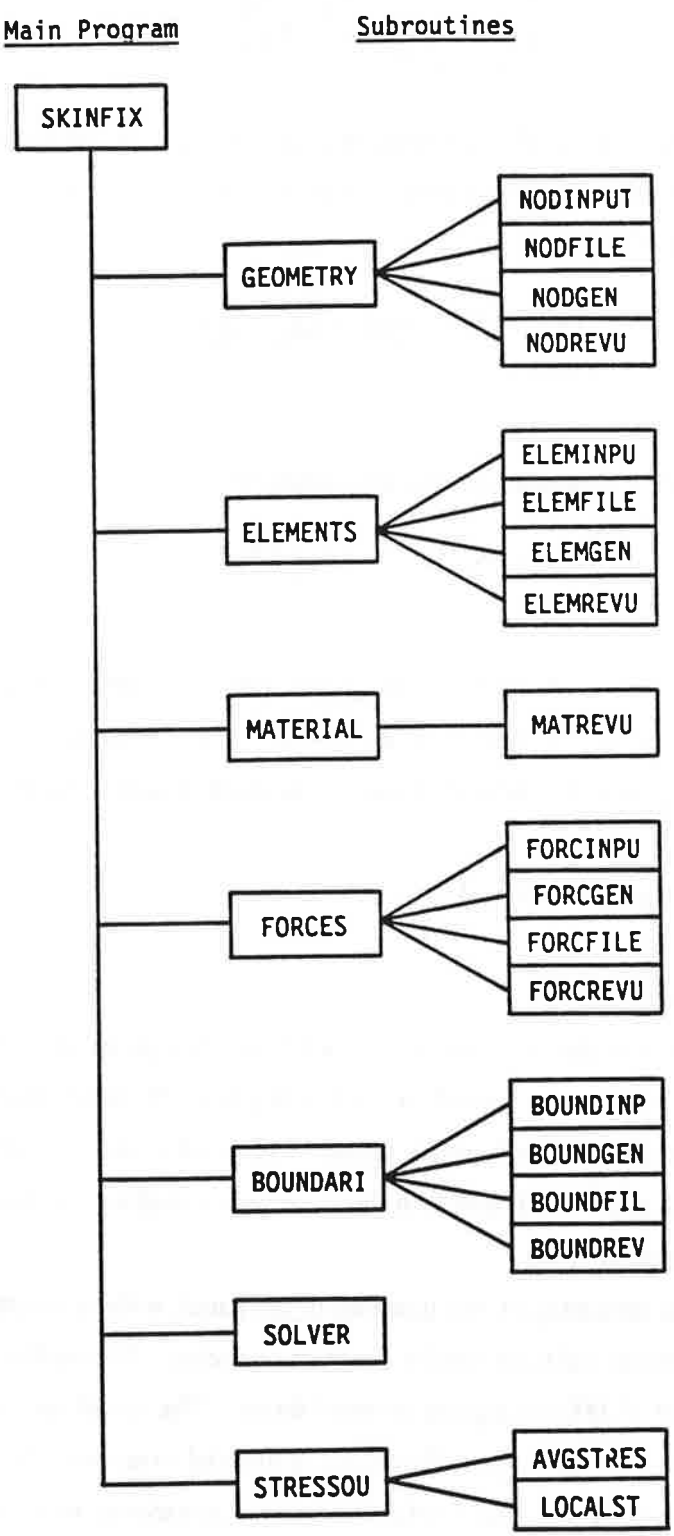

FIGURE 4-3. SKINFIX PROGRAM STRUCTURE

$$\begin{Bmatrix} P_f \\ P_s \end{Bmatrix} = \left[\begin{array}{c|c} K_{ff} & K_{fs} \\ \hline K_{sf} & K_{ss} \end{array}\right] \begin{Bmatrix} d_f \\ d_s \end{Bmatrix} \tag{4-5}$$

where $\{P_f\}$ are known external forces, $\{P_s\}$ are unknown reactions, $\{d_f\}$ are unknown displacements, and $\{d_s\}$ are prescribed displacements. The unknown displacements are solved for by performing Gaussian reduction in-core on $[K_{ff}]$

$$\{d_f\} = [K_{ff}]^{-1} \{\{p_f\} - [K_{fs}] \{d_s\}\} \tag{4-6}$$

The unknown reactions are then obtained from the displacements

$$\{P_s\} = [K_{sf}] \{d_f\} + [K_{ss}] \{d_s\} \quad . \tag{4-7}$$

This particular solution scheme was chosen for convenience, but it is a limiting factor in the size of the problem that can be solved on a PC operating under DOS. This limit is around 150 degrees of freedom. Implementing a segmented solution scheme would enable much larger problems to be solved on a PC.

A complete program listing was provided in Reference [2].

4.4 Analysis of Test Specimen

A highly instrumented test specimen was used to fulfill dual purposes of program verification and physical study. This specimen consisted of an aluminum panel, 20 inches wide, 30 inches long, and 0.039 inch thick, with a central 2-inch square cutout. The panel was reinforced with an aluminum doubler, 7 inches square and 0.039 inch thick. A repair doubler was fastened to the panel over the cutout with 66 aluminum rivets.

An initial CD analysis consisting of one quadrant of the panel, without a central cutout or reinforcement, was performed to verify successful program operation. The model was subjected to a uniaxial tension equivalent of 10,000 psi applied as nodal forces. The model returned uniform average stresses in the direction of loading of 10,000 psi, a uniaxial extension of 0.009435 inch, and a Poisson contraction of 0.00311 inch. The displacements were at variance from what was calculated

theoretically by about 5 percent. However, this analysis confirmed that the program was executing correctly and returning a solution of acceptable accuracy.

A quadrant of the test panel was then modeled with the cut-out, reinforcement, fasteners, and appropriate boundary conditions on lines of symmetry. A schematic of the model is shown in

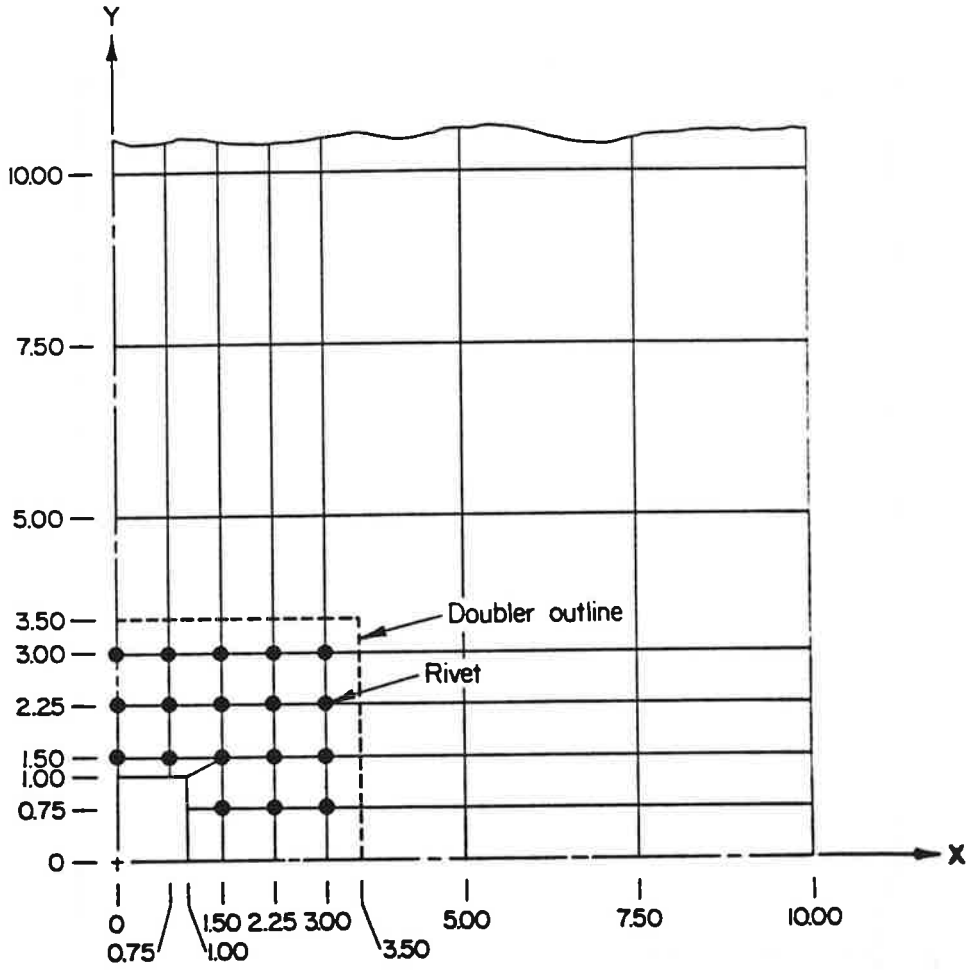

FIGURE 4-4. COMPATIBLE DISPLACEMENT ANALYSIS MODEL OF TEST SPECIMEN NO. 25

Figure 4-4. The test specimen is shown in Figure 4-5. Listings of the input data required to run this model were provided in Appendix B of Reference [2]. The model required 101 nodes, 74 plate elements, and 18 fasteners. The output listing was provided in Appendix C of Reference [2]. The panel was modeled to a dimension of y = 10 inches, which corresponds to a panel length of only 20 inches, to save modeling effort.

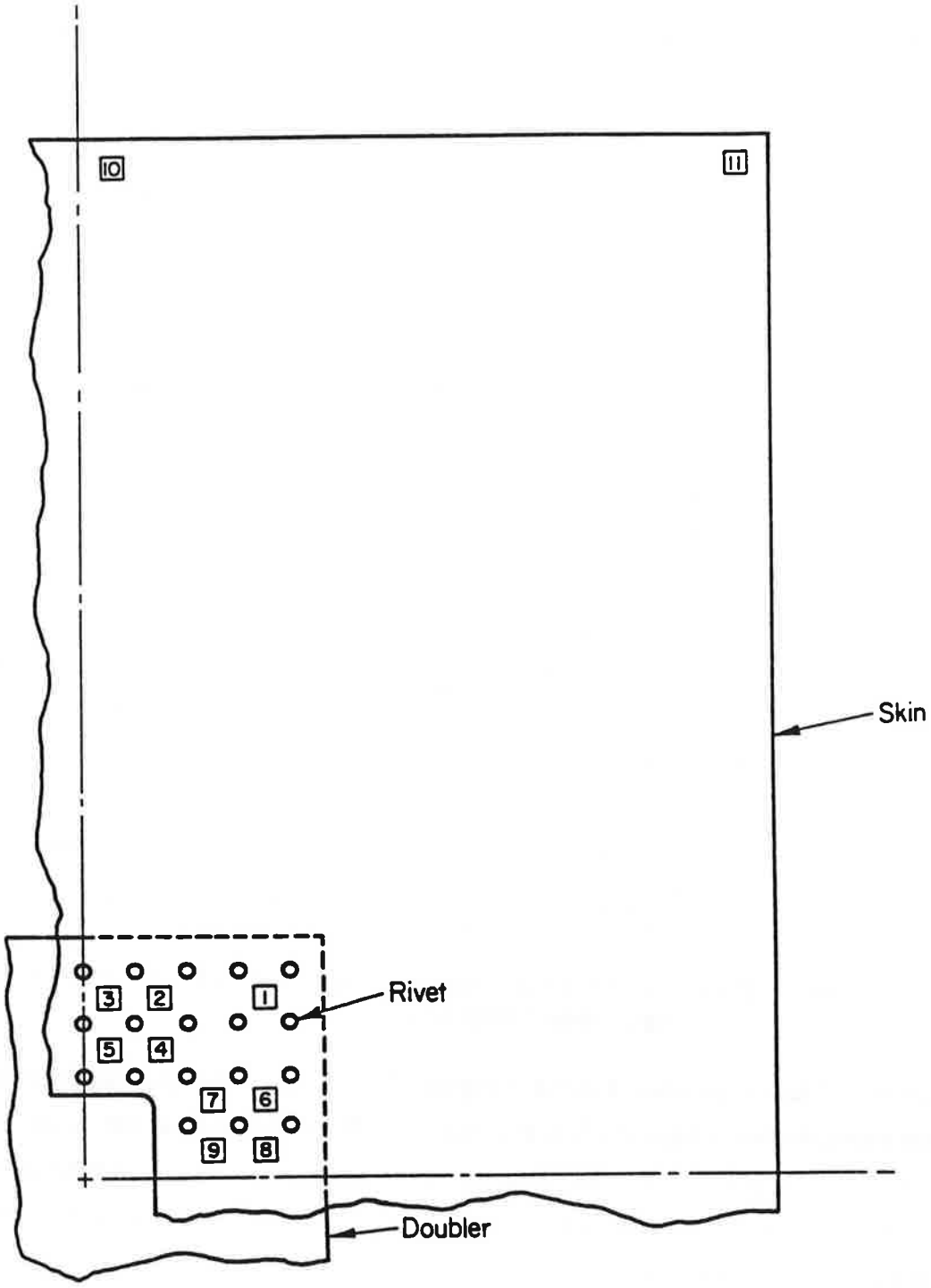

FIGURE 4-5. STRAIN GAGE LOCATIONS (SPECIMEN NO. 25)

Two boundary conditions at the point of loading were evaluated for the test specimen. One condition was a uniform applied load corresponding to a test panel load of 7,000 pounds (3,500 pounds for a quadrant), the other was a uniform applied displacement. The applied displacement was taken as the average displacement across the top of the panel for the uniform load case, which was 0.085 inch. This resulted in an effective panel load of 7,322.3 pounds (3661.2 pounds for a quadrant), so all results were adjusted linearly to compare to a panel load of 7,000 pounds. The better results (as determined by a match against strain-gage data near the top of the specimen) were obtained from the uniform displacement case, adjusted for the equivalent load by multiplying the results by 7000/7322 = 0.956. The method of far-field loading had little influence on stress estimates in the reinforced region. The output listings were presented in Appendix C of Reference [2] for the uniform load and displacement cases, respectively. The necessary input files were also provided with self-explanatory file names (i.e., NODES03 for nodal data).

The fasteners were represented in accordance with Swift. For the fasteners on the vertical line of symmetry, it was necessary to specify a reduced fastener diameter equal to about 30 percent of the nominal diameter, to produce approximately half the overall fastener stiffness. This effective diameter was calculated from Swift's formula and the desired stiffness value. It was then also necessary to make adjustments to calculated fastener and bearing stresses attributed to those fasteners because they were calculated by the program using the reduced diameter. If this technique was not employed, the program would have indicated excess load transfer at those fasteners. This technique would not have been required if the entire width of the panel were modelled. Thus, some engineering judgement was required to achieve correct results. With a more automated approach to modelling, the need for user judgement could be reduced.

It should be noted that the doubler material outside the fastener pattern envelope was specifically included in the model. This material performs an important load transfer function through compression and shear. A more complex reinforcement, such as a fingered plate or a rolled-shape stiffener, could also be modeled.

Results of the above analysis are summarized in Table 4-1 and Figures 4-6 through 4.12. It can be seen that bypass stresses are in good agreement with strain-gage data except in the areas of high bearing-to-bypass stress ratios. These locations, at Strain Gages 1, 2, and 5, occur in first and last rivet rows adjacent to free edges transverse to the direction of loading. Unfortunately, Location 1 is the most fatigue critical. Figures 4-6 and 4-7 also indicate some nonlinearity with load level in the experimental data.

TABLE 4-1. RATIO OF CALCULATED TO MEASURED STRESSES

Strain Gage Location	Skin		Doubler	
	7000 #	14000 #	7000 #	14000 #
1	0.86	0.81	1.24	1.44
2	0.95	0.85	0.97	1.24
3	1.05	0.88	0.82	0.98
4	1.02	0.88	0.85	0.87
5	1.48	1.21	0.72	0.76
6	0.95	0.92	0.96	1.00
7	0.98	0.96	1.03	1.04
8	1.00	0.98	1.02	1.05
9	1.05	0.98	1.04	1.07
10	1.04	1.03	—	—
11	1.10	1.03	—	—

Two causes for the variance between the analyses and test results have been postulated. One is that local (out-of-plane) bending occurs as a result of the asymmetry of the repair with respect to the applied load. The current CDA model does not account for out-of-plane bending, although the necessary degrees of freedom could be added. To investigate this further, a coarse finite element analysis of the same configuration was performed using ANSYS. When the panel was constrained to in-plane degrees of freedom, its results were in good agreement with the model. When the panel was allowed to displace out of plane, the overall quality of the results with respect to the actual measurements degraded significantly. These results did not support the argument for bending effects, although they do not necessarily refute it, either, since the FEA was based on linear small-displacement theory.

Examining the test data at the locations of greatest disagreement with the CD analysis showed that large stresses were measured at the same locations as small differential fastener displacements, and vice-versa. Furthermore, the pattern of differential displacements indicated that the assembly bulged at its center with the doubler on the concave side, and that the curvature was reversed in the vicinity of the first two horizontal rows of rivets. Finally, the displacements were used to estimate

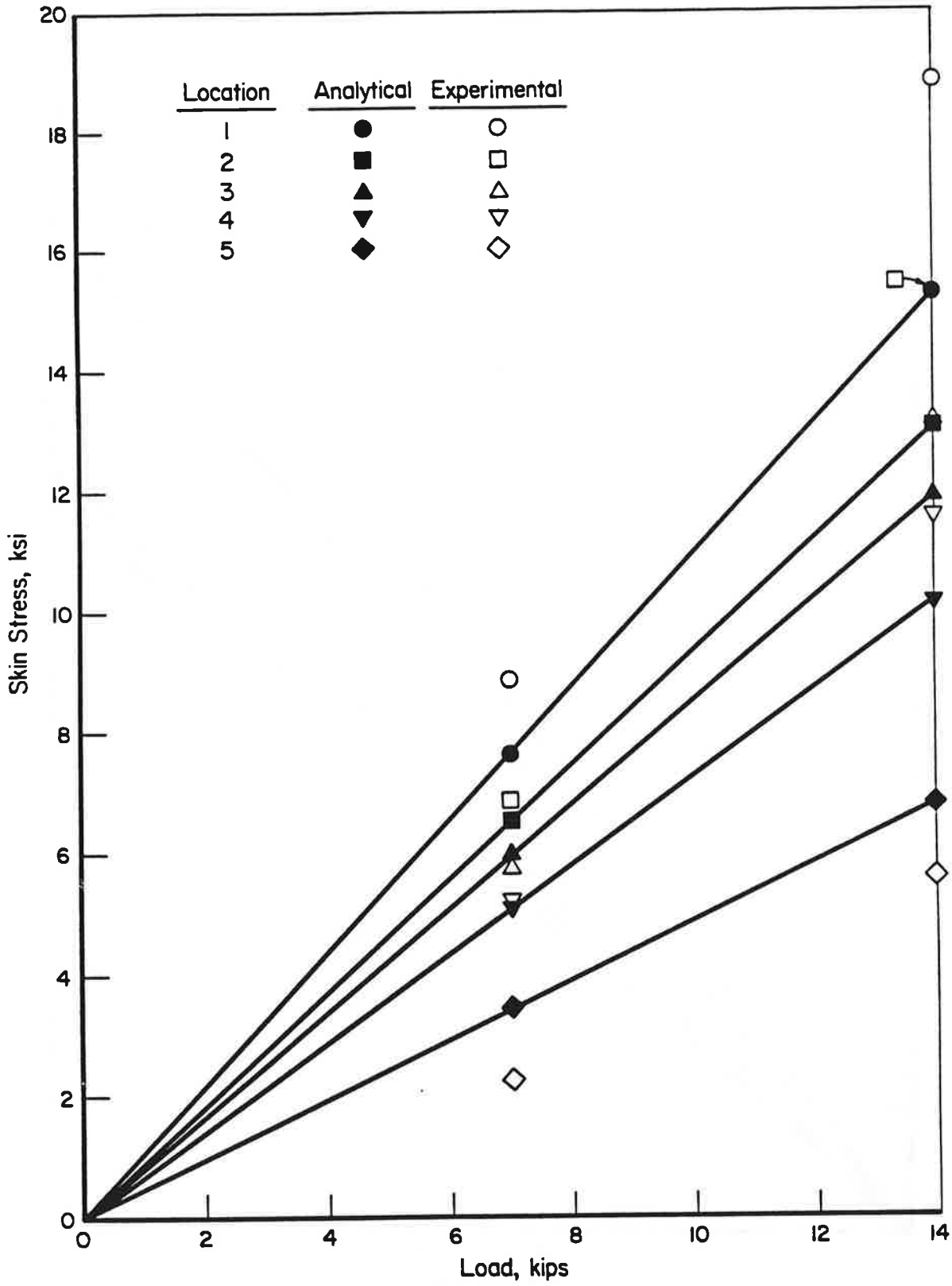

FIGURE 4-6. SKIN STRESSES (SPECIMEN NO. 25)

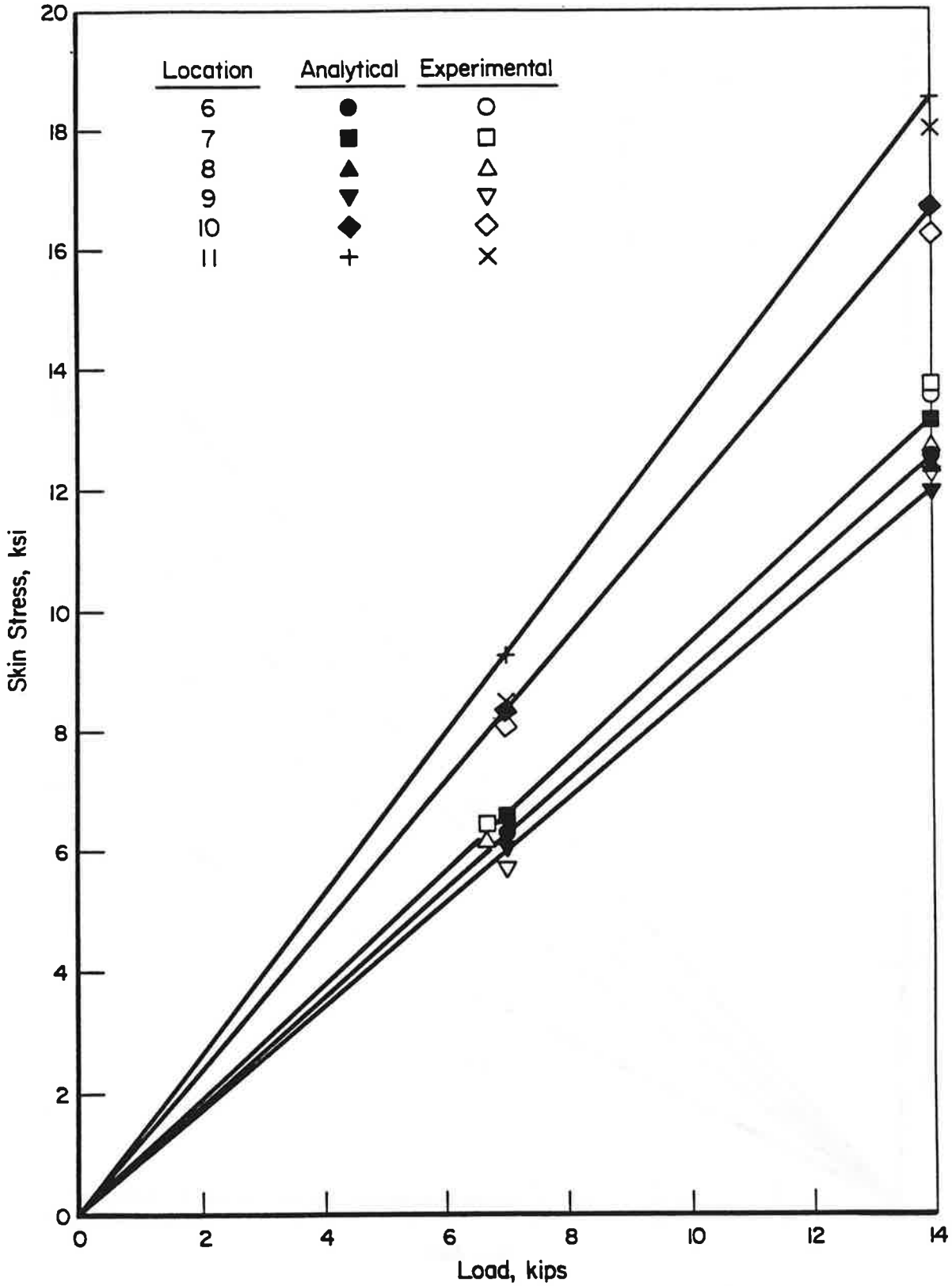

FIGURE 4-6. SKIN STRESSES (SPECIMEN NO. 25) (CONCLUDED)

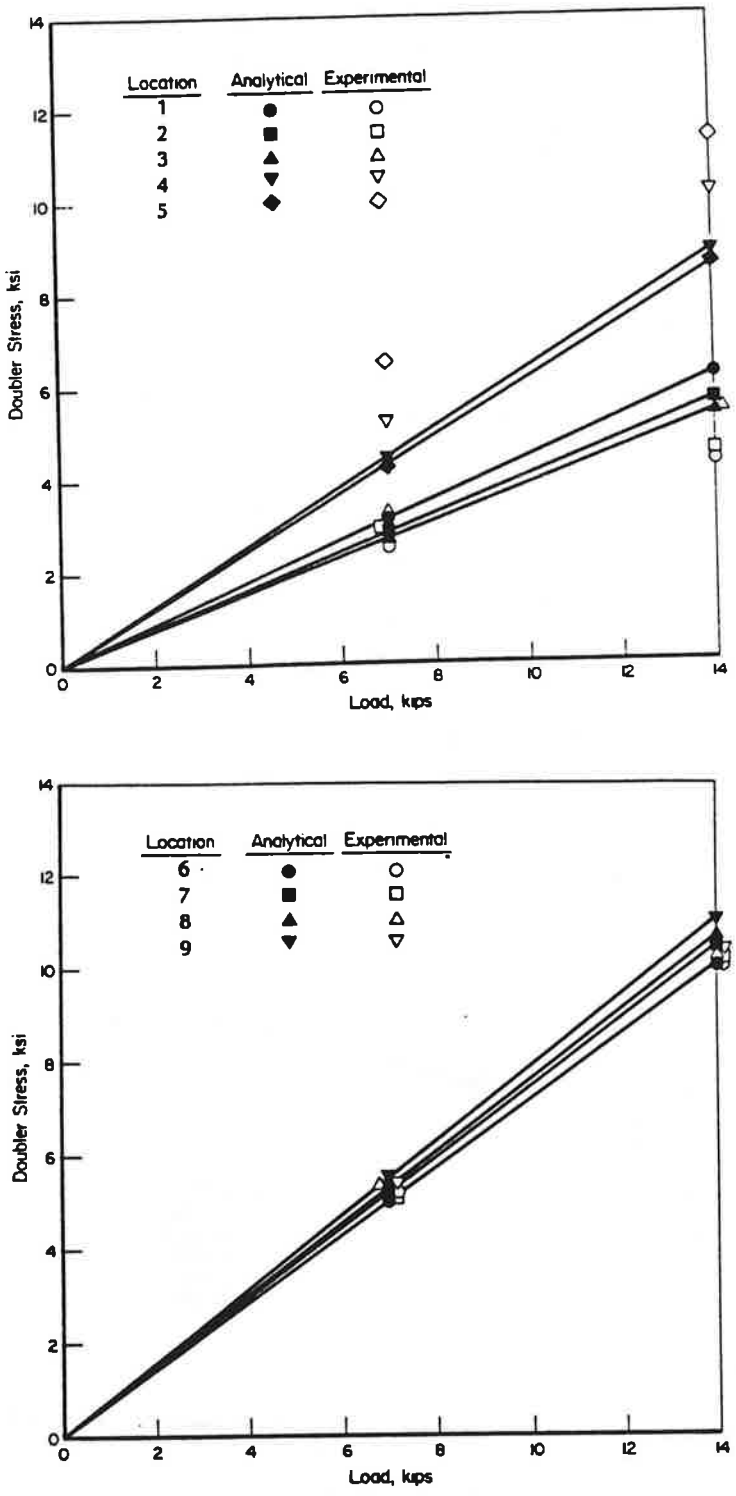

FIGURE 4-7. DOUBLER STRESSES (SPECIMEN NO. 25)

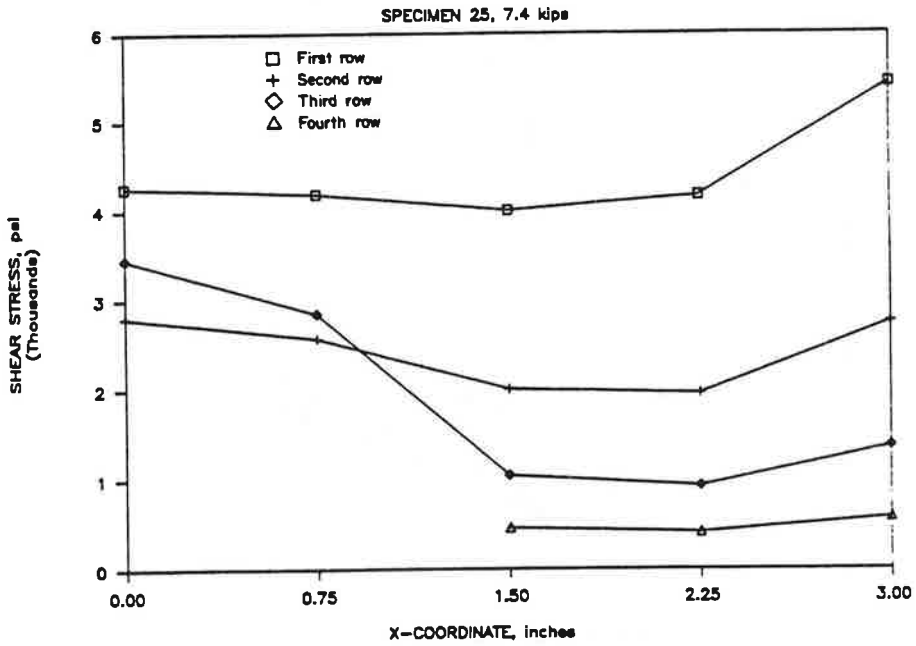

FIGURE 4-8. FASTENER SHEAR STRESSES

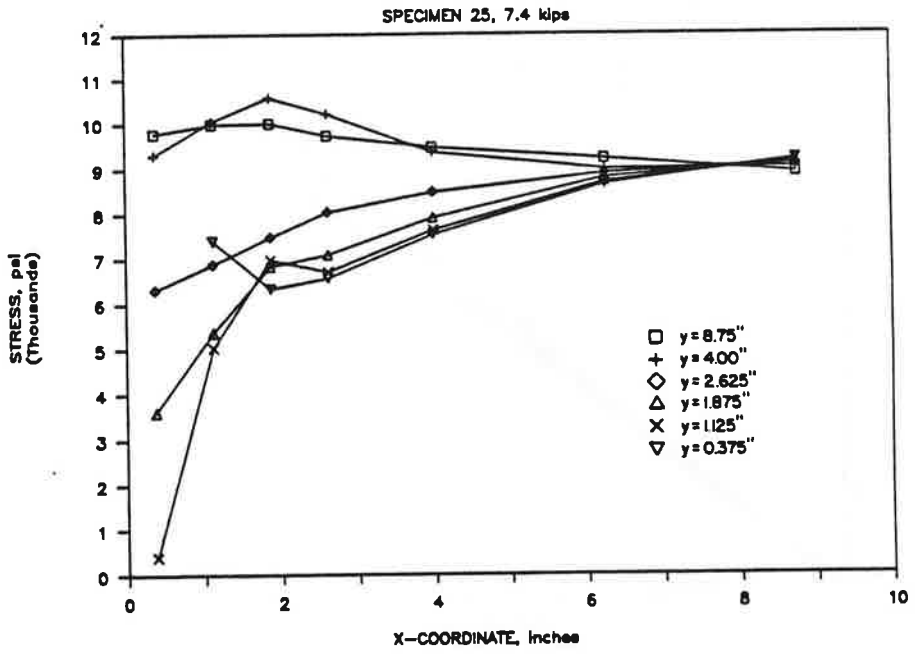

FIGURE 4-9. SKIN STRESSES

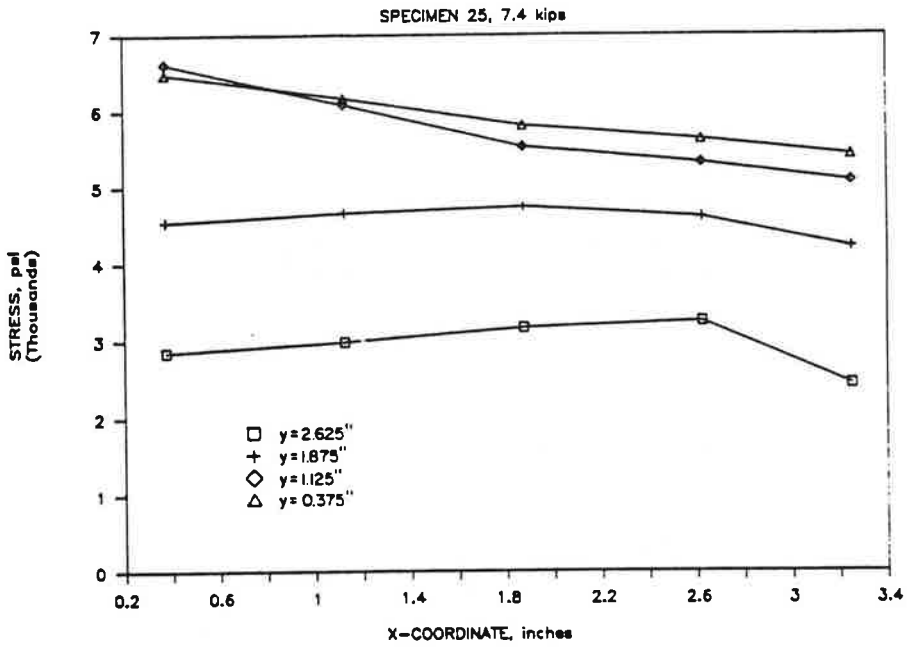

FIGURE 4-10. DOUBLER STRESSES

stresses and were found to agree with the strain gage data. These factors could only be rationalized by concluding that local bending was affecting the stresses.

The other possible cause of the error is that the local fastener-plate interaction may not be correctly accounted for by SKINFIX when bearing-to-bypass stress ratios are very high. Inherent in the CDA approach used in SKINFIX is the assumption that the gross load-displacement response of the assembly is dominated by plate-like membrane behavior, and that local effects are accounted for in the fastener flexibility. Gross response is what determines load transfer. However, if bearing loads are high in a region of low bypass stresses, the local loading effects dominate the gross load-displacement response. It has been assumed that Swift's fastener model is sufficient to account for the local effects. However, its validity may be limited to some range in physical parameters beyond the test configurations from which it was derived. Thus, if Swift's fastener model does not apply, then the gross response and resultant load transfer will not be correct.

Two different solutions for deformations in elastic membranes due to point loadings were examined[3,8]. They were not in agreement as to the relative displacement of the load points with respect to the displacement of a uniformly loaded membrane. According to Reference [8], the

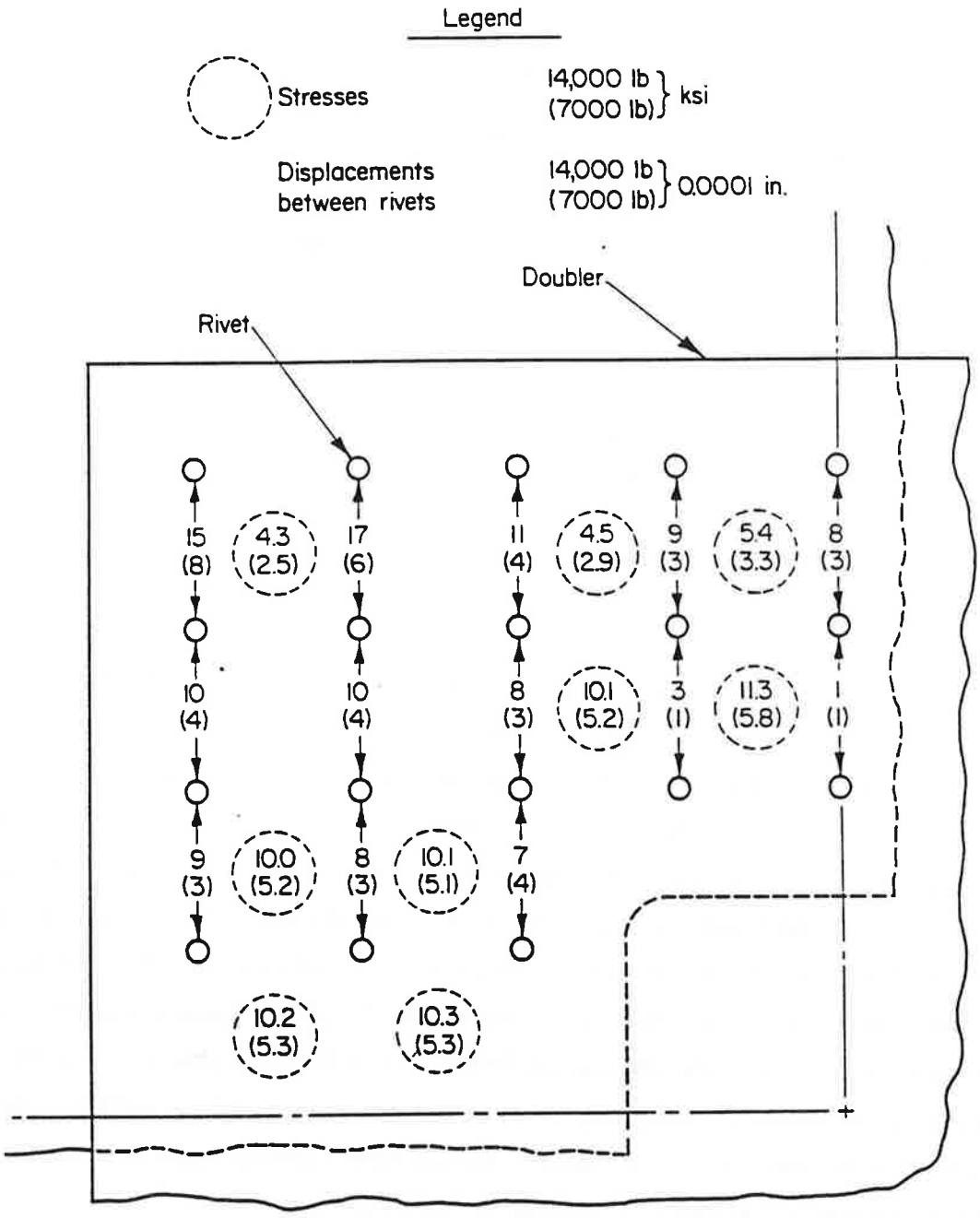

0.039 Panel with 0.039 patch
Specimen No. 25 (with cutout)

FIGURE 4-11. DOUBLER STRESSES AND RIVET DISPLACEMENTS

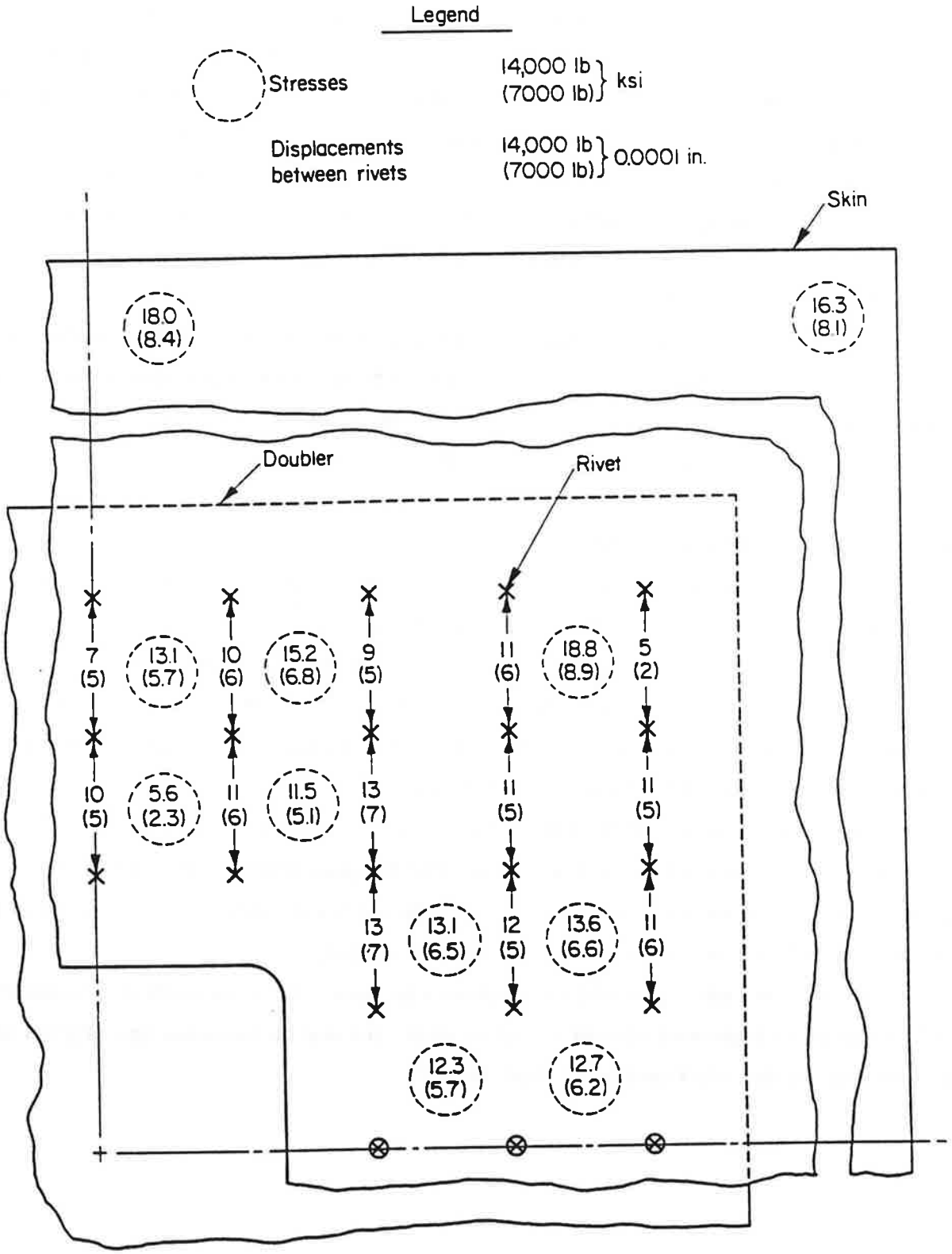

FIGURE 4-12. SKIN STRESSES AND RIVET DISPLACEMENTS (SPECIMEN NO. 25)

relative displacement approaches a limiting value of 32 percent of the uniformly loaded case as the ratio of fastener diameter to fastener spacing decreases. The result is that the point-loaded membrane is stiffer than the uniformly loaded membrane. If this is the case, the situation of high bearing-low bypass loading would result in greater local load transfer through the fasteners than would be estimated by SKINFIX. Except at the first/last rows of fasteners, the uniformly loaded behavior dominates as evidenced by the pattern of agreement between analysis and test specimens. An iterative solution, in which the plate element stiffness is adjusted based on bearing-bypass stresses would be required to obtain better results.

To test sensitivity to fastener stiffness, the flexibility coefficients were altered to produce a ± 50 percent variation in fastener stiffness. The estimated bypass stresses in the sheet at the location corresponding to SG-1 shifted only ± 2.5 percent. The bearing stresses, which are proportional to fastener load shifted by -20/+12 percent. These effects are shown in Figures 4-13 and 4-14.

4.5 Cracked Panel Strain Contours

During the course of the CDA model development Battelle was requested by VNTSC to undertake another related analytical effort under Task 3. The objective of this analysis was to obtain strain contour plots for a test panel under tension loading. The analytical results were then compared by VNTSC with shearography results. The test panel consisted of a single rivet hole with two different length cracks emanating from it. The dimensions of the panel are shown in Figure 4-15. The panel was analyzed using the finite element method.

A two dimensional finite element model was prepared using the IDEAS software[9]. The model is shown in Figure 4-16. The model consisted of 480 plane stress elements and 1590 grid points. A uniform tensile stress of 1000 psi and appropriate boundary conditions were applied to the model. The analysis was conducted using the ABAQUS code[10].

Several strain contour plots of the entire panel were made. The strain levels of the contours and the number of levels were adjusted to obtain a clearer plot near the two crack tips. Typical strain contour plots are shown in Figures 4-17, 4-18, and 4-19.

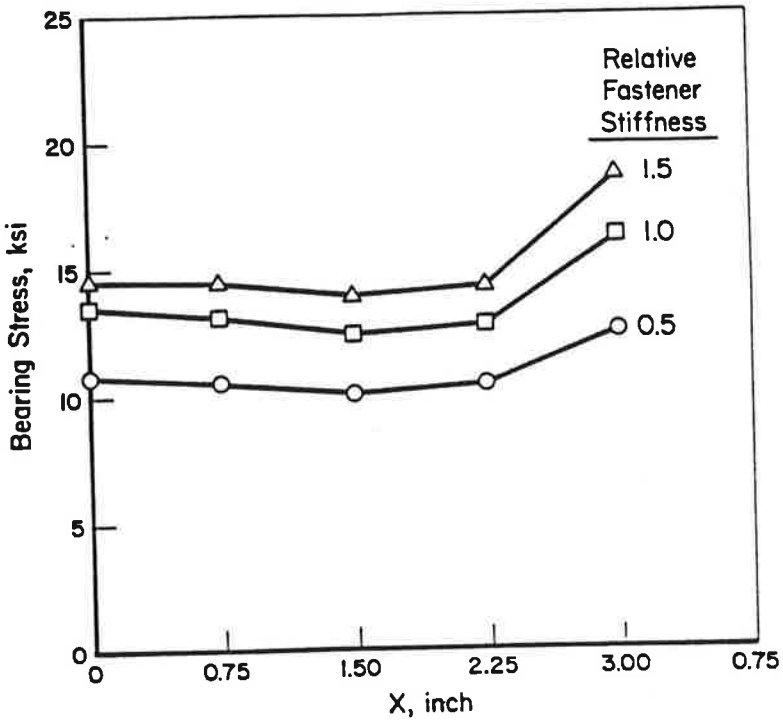

FIGURE 4-13. EFFECT OF RELATIVE FASTENER STIFFNESS ON FIRST ROW BEARING STRESSES

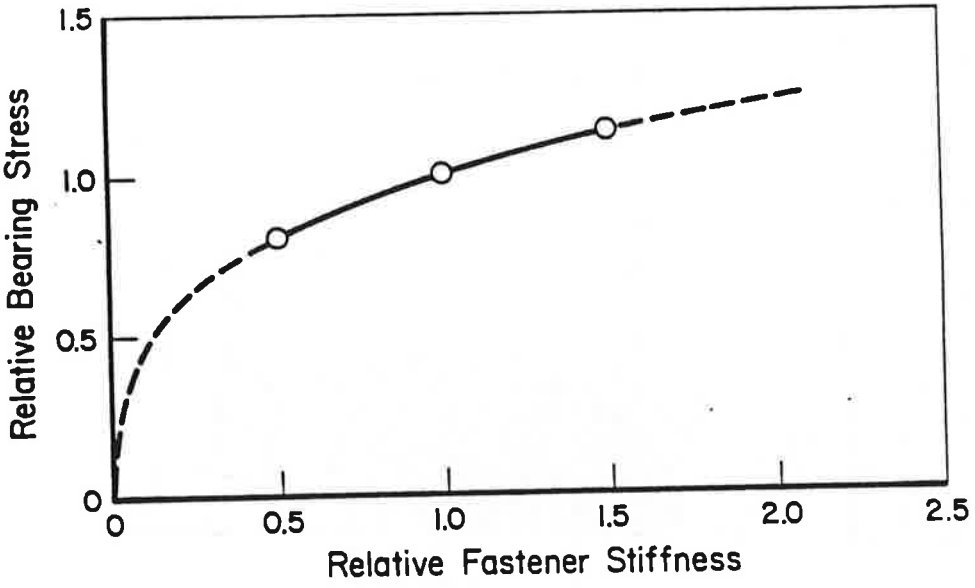

FIGURE 4-14. EFFECT OF RELATIVE FASTENER STIFFNESS ON MAXIMUM BEARING STRESSES

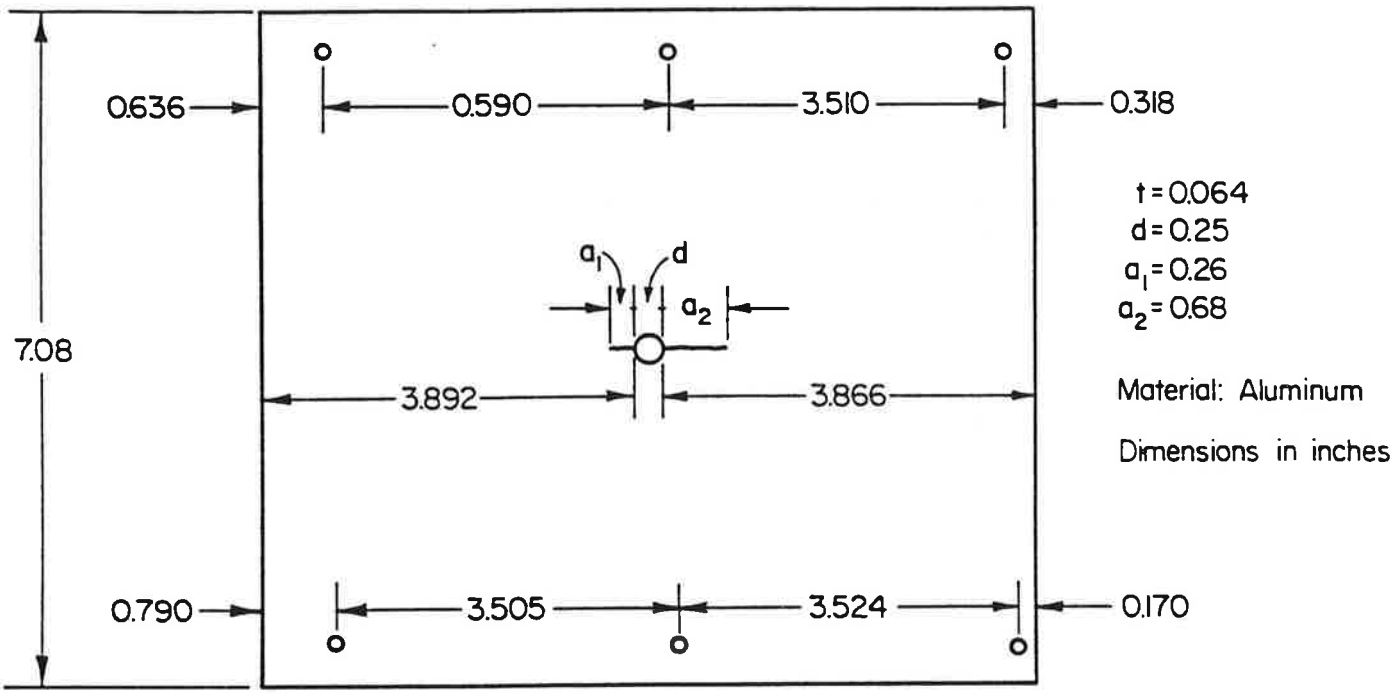

FIGURE 4-15. TEST PANEL GEOMETRY

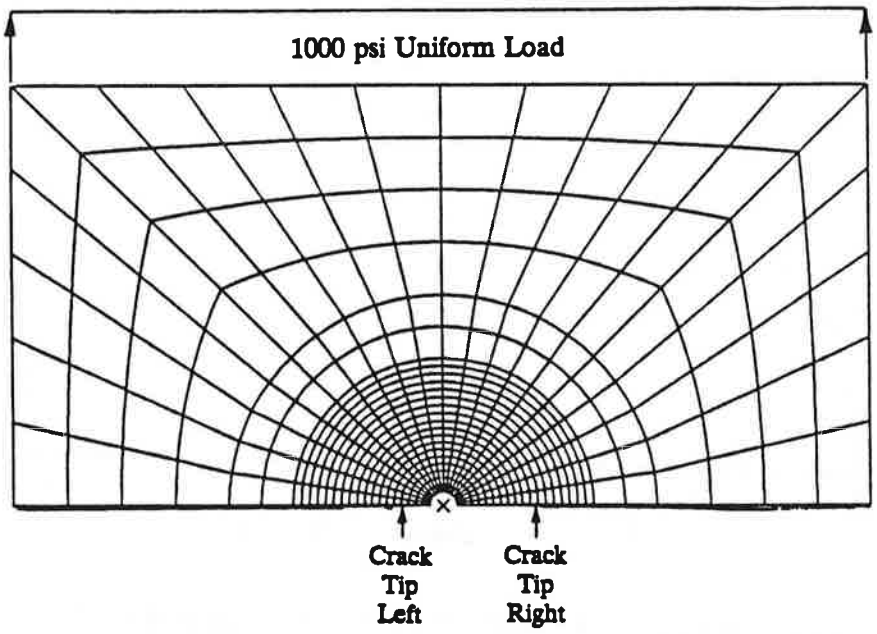

FIGURE 4-16. FINITE ELEMENT MODEL OF TEST PANEL

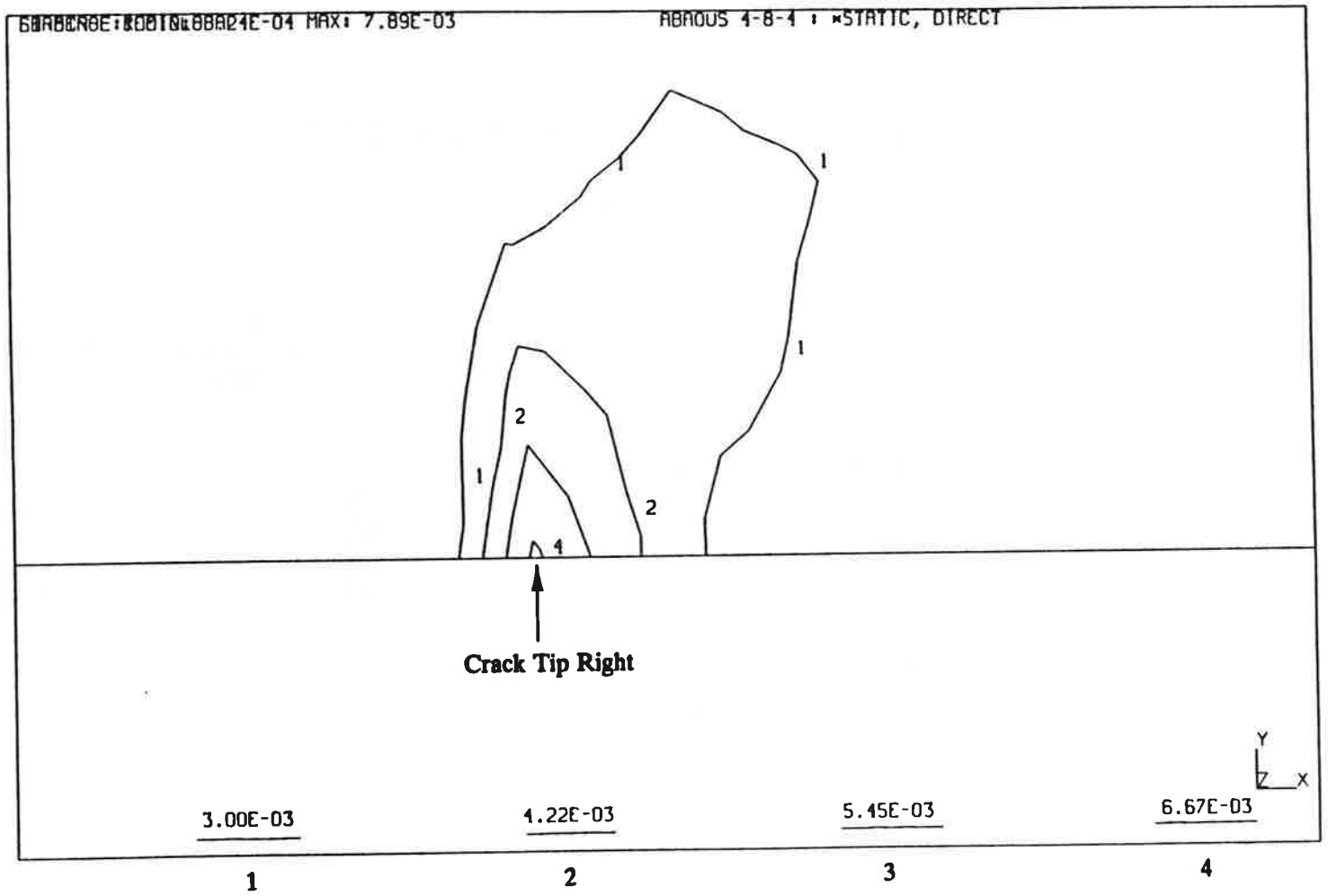

Eyy Contours - 4 Levels
Right Area Enlarged
Uniform Loading

FIGURE 4-17. STRAIN CONTOURS FOR LONGER CRACK

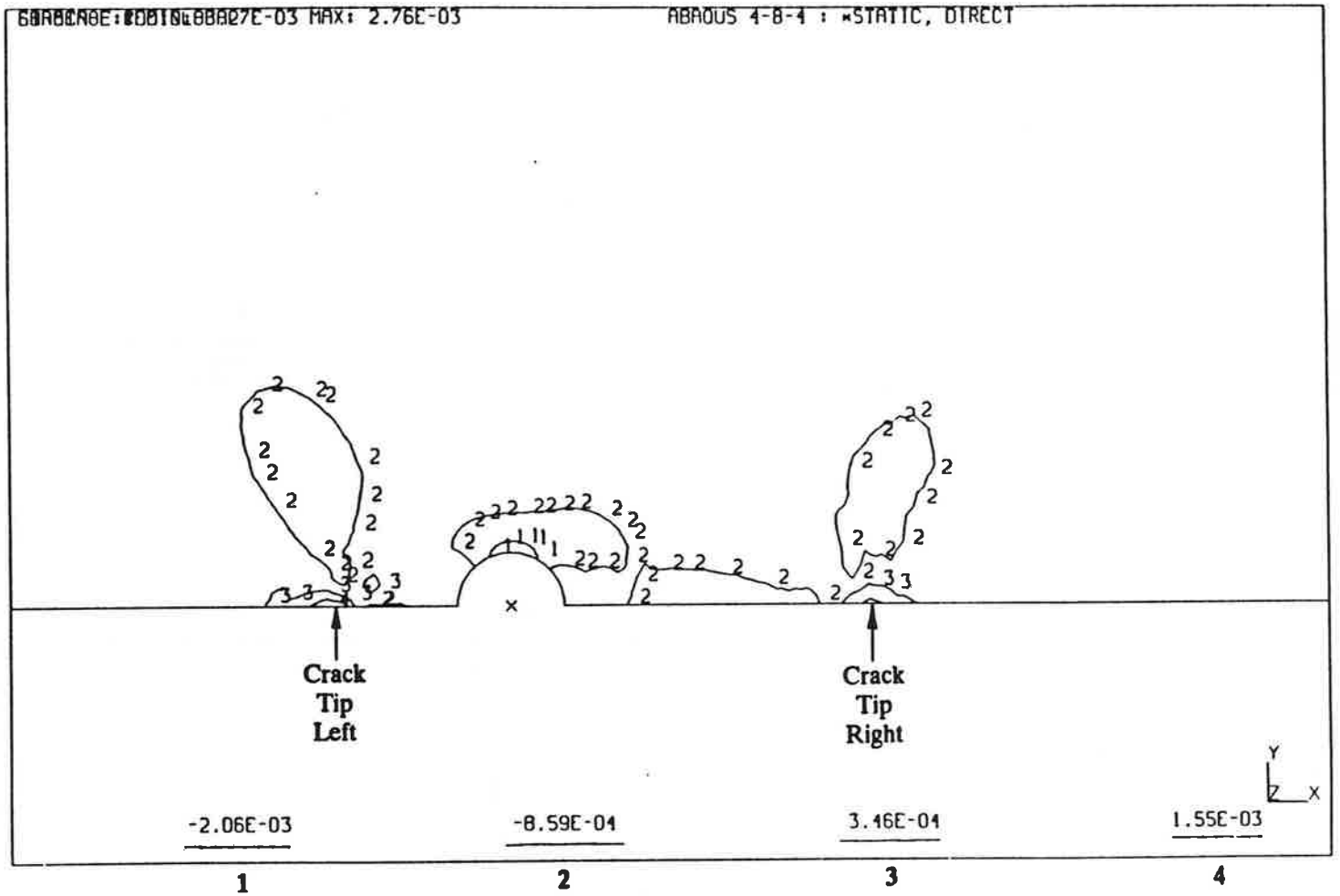

Exx Contours - 4 Levels
Hole Area Enlarged
Uniform Loading

FIGURE 4-18. STRAIN CONTOURS FOR SHORTER CRACK

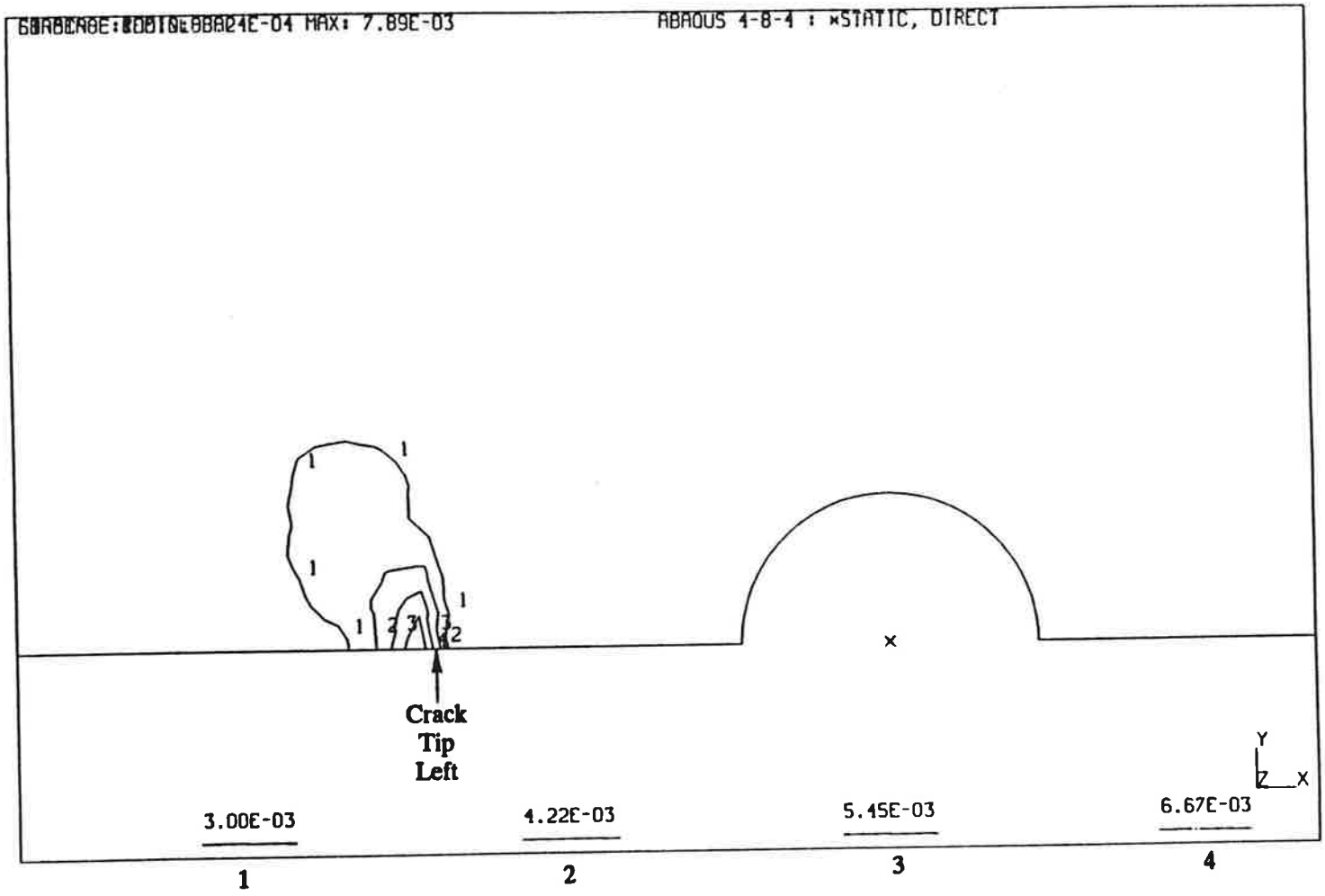

Eyy Contours - 4 Levels
Left Area Enlarged
Uniform Loading

FIGURE 4-19. OVERALL CRACKED RIVET HOLE STRAIN CONTOURS

5.0 STANDARDIZED LOAD SPECTRA

5.1 Fuselage Loading

5.1.1 Loading Segments. An aircraft fuselage is subjected to flight segments with different loading content during a typical flight. The loading consists of the 1.0 g stationary load and dynamically induced loadings. The flight segments within which the dynamic loading occurs are taxiing and take-off, ascent/climb with pressurization, cruise, descent with depressurization, landing impact and taxiing. Over the years NASA and the FAA have conducted several flight loading surveys on the response of commercial aircraft to gust and maneuver loadings. The experimental data taken in the form of velocity, g-levels and altitude (VGH) are reduced to basic exceedance curves for the various types of aircraft such as large or medium size and commuter aircraft. The cyclic content and magnitude of stresses at a particular fuselage location are determined from exceedance diagrams for gust and maneuver loadings[11]. Detailed data on the most recent NASA/DOT/FAA program on VGH flight loadings data for the B727, L-1011, DC10, and B747 aircraft are provided elsewhere[12].

The stress history development for a given location in the fuselage must consider the pressurization, gust and maneuver loadings. The primary loadings in the fuselage are the pressure loads with superimposed maneuver and gust loadings. The stresses at the location selected for an analysis are determined by structural load transfer functions which account for the response of the aircraft fuselage to gusts and maneuvers. The determination of pressurization stresses is straightforward.

5.1.2 Gust Loadings. The normal coordinate system for the aircraft structure is shown in Figure 5-1. Besides pressurization, the next primary source of cyclic loading on a commercial aircraft fuselage is gust. Gust loads on the wing will cause cyclic fuselage bending; lateral gusts on the tail fin will cause fuselage torsion. As such, the gust spectrum is relevant to the definition of fuselage cyclic loads. Figure 5-2 explains the elements of gust loading. During normal stationary flight the lift is equal to the aircraft's weight ($L = W$), regardless of altitude, airspeed or angle of incidence. Note that the tail load, T, is generally small (positive or negative) and ideally equal to zero. The tail is needed only to equilibrate the total moment and to account for maneuvers.

A gust causes a ΔL up or down, as shown in Figure 5-2c. For a ramp-type or *(1-cosine)* gust, a gust alleviation factor, G_{al}, must be included, which depends upon aerodynamic inertia. A large, sluggish aircraft (B747 or DC10) has a lower G_{al} than a smaller one (B737 or DC9). Equation (5-1)

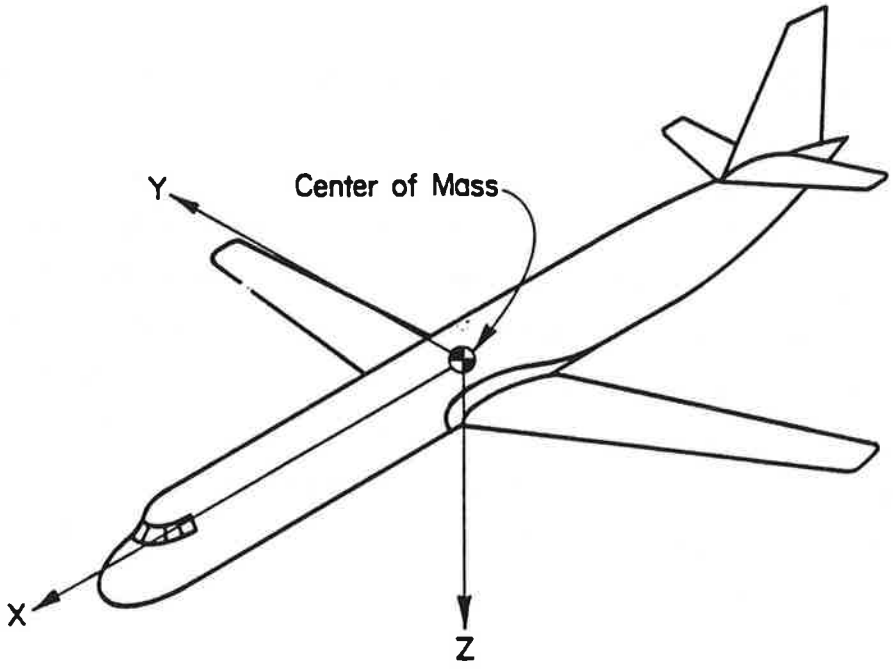

FIGURE 5-1. COORDINATE SYSTEM

shows that for a particular aircraft type the ΔL is always proportional to the gust velocity, U, and the airspeed, V, regardless of altitude.

$$\Delta L = \frac{1}{2} \rho V^2 S \, G_{al} \frac{dC_L}{d\alpha} \Delta\alpha$$

$$= \frac{1}{2} \rho V^2 S \, G_{al} \frac{dC_L}{d\alpha} \frac{U}{V} \qquad (5\text{-}1)$$

$$= \frac{1}{2} \rho S \, G_{al} \frac{dC_L}{d\alpha} UV = C \, UV$$

where

ρ	=	Density of the air
S	=	Wing area
G_{al}	=	Gust alleviation factor depending on aircraft and altitude

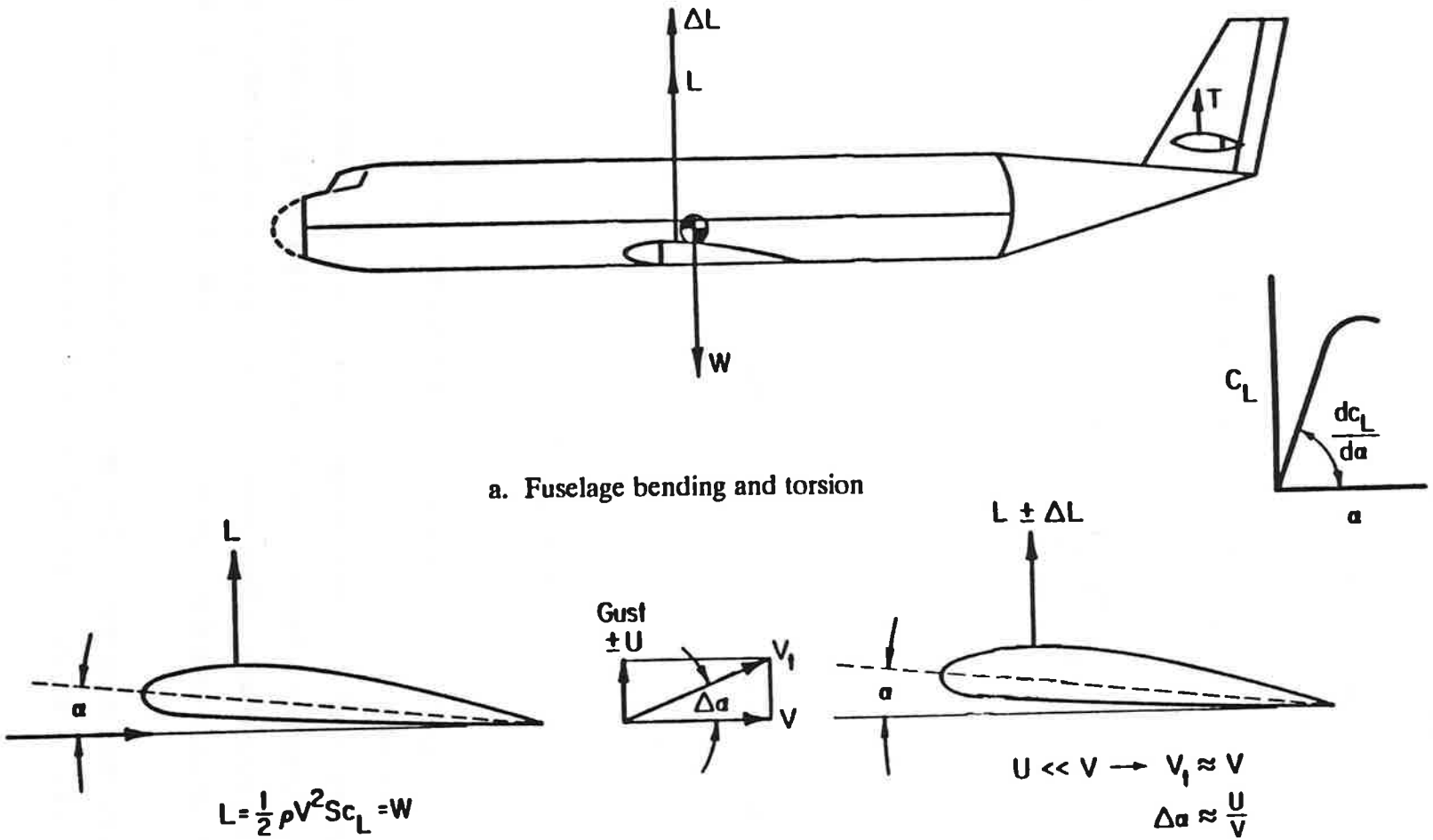

a. Fuselage bending and torsion

b. Stationary flight

c. Gust

FIGURE 5-2. GUST LOADING DELTA ΔL

C_L	=	Three dimensional lift coefficient
α	=	Angle of attack, angle between free-stream and wing velocity and wing chord line
$\frac{dC_L}{d\alpha}$	=	Slope of C_L vs. α curve
C	=	½ product of above factors.

Substituting L (with $L = W$), one can also derive Equations (5-2a) and (5-2b), where $\overline{A}$ and $\overline{\overline{A}}$ depend upon the aircraft type.

$$\Delta L = L\, G_{al} \frac{dC_L}{d\alpha} \frac{1}{C_L} \frac{U}{V} = \overline{\overline{A}}\, W \frac{U}{V} = \overline{A}\, WU \tag{5-2a}$$

$$n_z = \frac{L + \Delta L}{L} = \frac{W + \Delta L}{W} = \frac{W + \overline{A}WU}{W} = 1 + \overline{A}\, U \tag{5-2b}$$

Note that most airliners fly at nearly the same average airspeed. This leads to the equation for vertical acceleration, n_z, as in Equation (5-2b). Hence, the bending moment, and, therefore the cyclic stress (per Equation (5-3)), is proportional to U, where C depends upon the aircraft type weight distribution and fuel load.

$$\sigma = \sigma_{1g} \pm C\sigma_{1g} \tag{5-3}$$

It follows that fuselage cyclic loading can be derived directly from gust spectra, especially wing spectra, as shown in Sections 5.2-5.4.

5.1.3 Maneuvers. Cyclic loads due to maneuvers are a consequence of inertia forces. As shown for two typical maneuvers in Figures 5-3 and 5-4, the center of gravity (c.g.) acceleration, n_z, can be determined for any maneuver. Although maneuvers are the primary source of cyclic loads for fighters and trainers, for commercial aircraft, maneuver loads are small and infrequent compared to gust loads.

5.1.4 Basic Fuselage Stress History. Gust and maneuver loads are not the only source of cyclic stress on a fuselage. The pressurization cycle, occurring once per flight, is a major

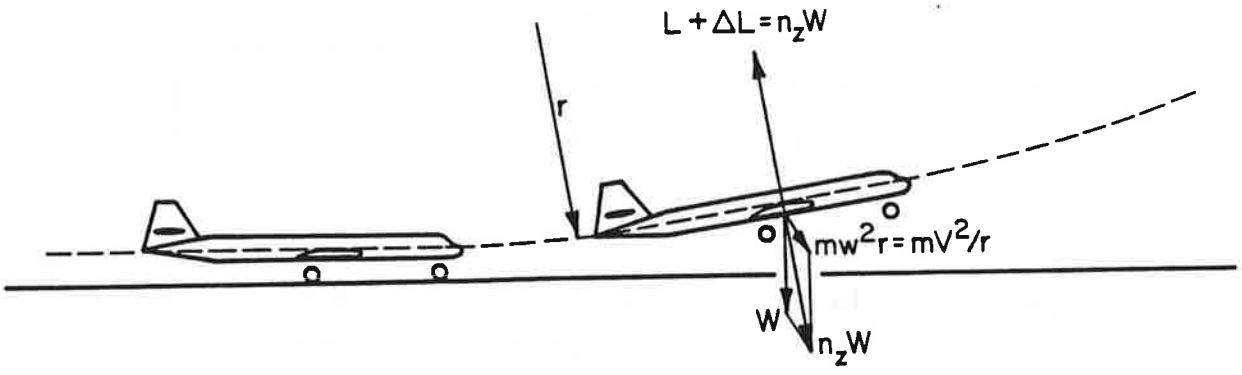

FIGURE 5-3. MANEUVER LOADING TAKE-OFF ROLL

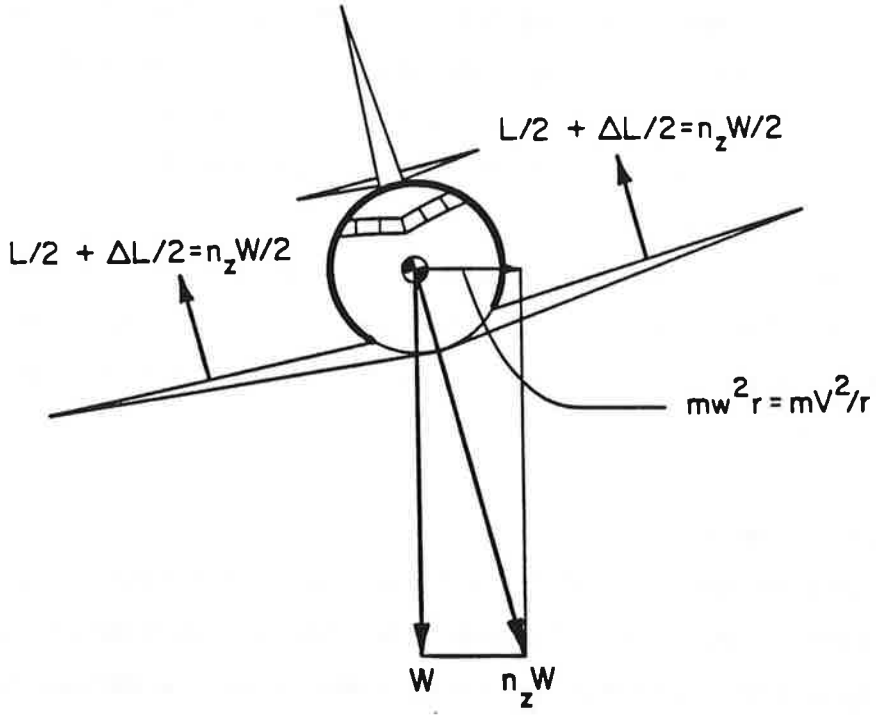

FIGURE 5-4. MANEUVER LOADING BANKING IN CURVE

contributor, especially for circumferential stresses. Table 5-1 provides a summary of typical pressurization stresses for common commercial aircraft. Combination of the appropriate pressurization stresses with the gust and maneuver induced stresses leads to the stress histories shown in Figure 5-5.

TABLE 5-1. VARIATION IN AIRCRAFT HOOP STRESSES

Hoop Stress, ksi	Aircraft	Alloy	Minimum Skin Thickness, inches
9.8	DC9	2014/24-T6	0.050
12.8	DC-8	2014-T6	0.050
14.8	L-1011	7075-T76	0.068
15.0	DC-10	2024-T3	0.068
15.7	B737	2024-T3/T4	0.036
15.9	B707/B727	2024-T3/T4	0.040
18.3	B747	2024-T3	0.063

For circumferential stresses, the hoop stress, σ_p, is the basic flight-by-flight cycle, essentially the ground-air-ground (GAG) cycle. Longitudinal stresses for the stationary flight have two contributors, one due to pressurization (roughly half the hoop stress) and one due to fuselage bending, following from the "normal" weight distribution in the fuselage. Thus the GAG cycle consists of two superimposed components, as shown in Figure 5-5b.

Cyclic stresses due to bending by inertia forces from vertical gusts and maneuvers are superimposed on the GAG cycle. Torsional loadings are generally small and have a zero mean because tail fin loads are normally zero. However, cyclic torsional stresses do occur due to lateral gusts and maneuvers.

5.2 The Exceedance Diagram

5.2.1 Measured Spectra and the TWIST Standard. As demonstrated in Section 5.1, and especially in Figure 5-5, the major fuselage cycle is the GAG cycle due to internal pressurization; the superimposed cyclic stresses are due primarily to the fuselage response to the wing, which is subjected to gust and maneuver loadings. The fuselage stresses are due to inertia loads, which in turn are due to wing loads. Thus, the fuselage spectrum for the bending loads can be obtained from the wing spectrum using the proper load-to-stress conversions (stress transfer functions) obtained from structural analyses.

The best way to obtain the cyclic stress spectrum due to gusts and maneuvers is from measurements. Extensive measurements on wings were made[12,13]; they are shown in Figure 5-6 (many more are presently available). Obviously, different aircraft types have somewhat

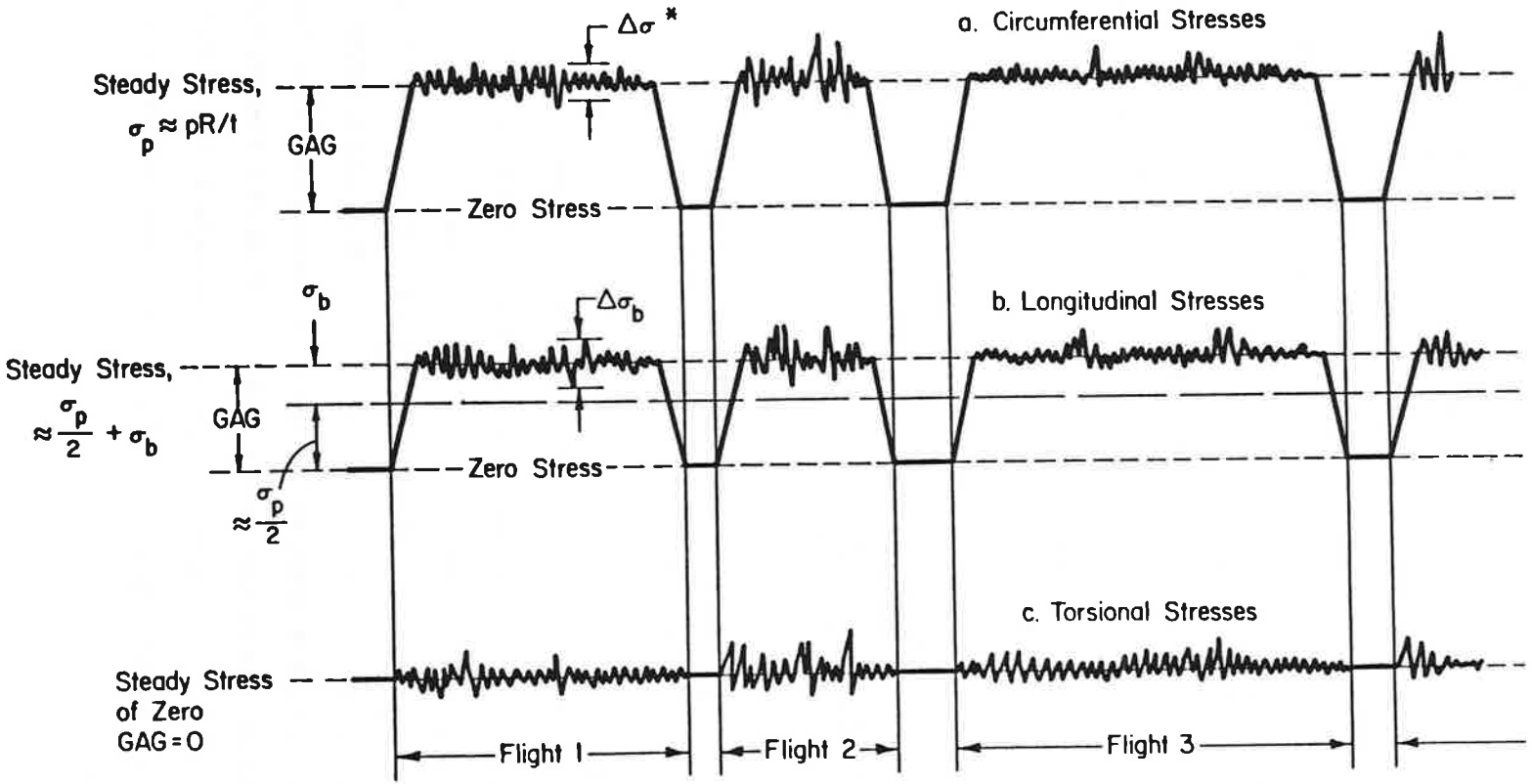

* $\Delta\sigma$ due to bending + torsion

FIGURE 5-5. TYPICAL STRESS HISTORIES FOR AIRCRAFT FUSELAGE

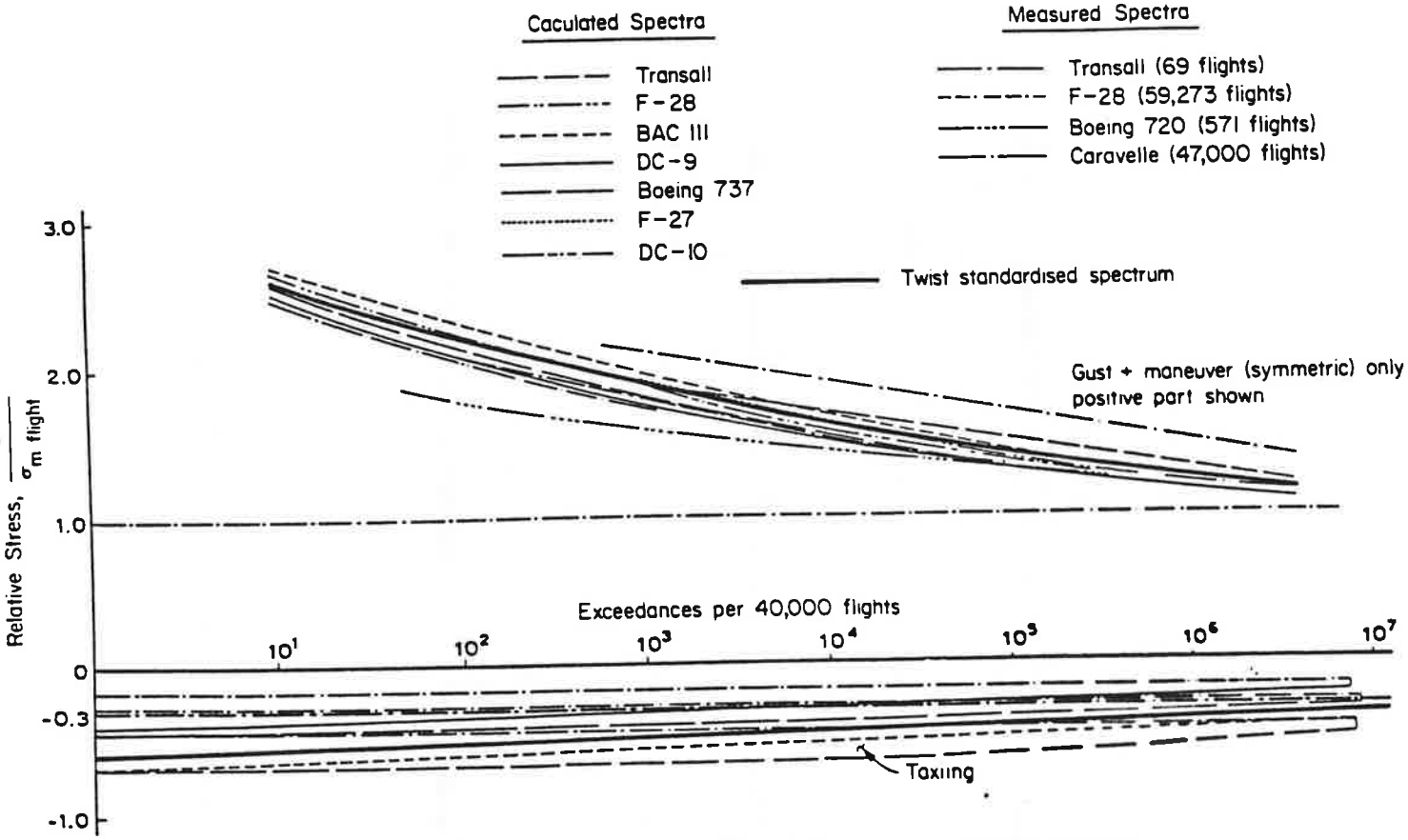

FIGURE 5-6. LOAD SPECTRA PERTAINING TO 40,000 FLIGHTS FOR DIFFERENT AIRCRAFT

different spectra, which is mainly due to the difference in the gust alleviation factor G_{α}, or α and C, the parameters shown in Equations (5-1) and (5-2). Also note that these measured spectra inherently include maneuver loads. The latter are small compared with the gust loads. The spectra are essentially symmetric and nearly linear on a semi logarithmic scale.

These measured spectra were used[13] to establish a standard spectrum, called TWIST, which is also shown in Figure 5-6 and in more detail in Figure 5-7. Note that the stresses are expressed as a ratio to the 1g stationary flight stress, so that adjustments can be made for the stress level: the stress axis can be obtained when the 1g stress level is known. It should be pointed out that TWIST was developed for comparative testing. It is *not* a standard spectrum *for design*. Nevertheless, it can serve as a basis for the present purpose *provided* the stress levels are adjusted for fuselages of different aircraft systems.

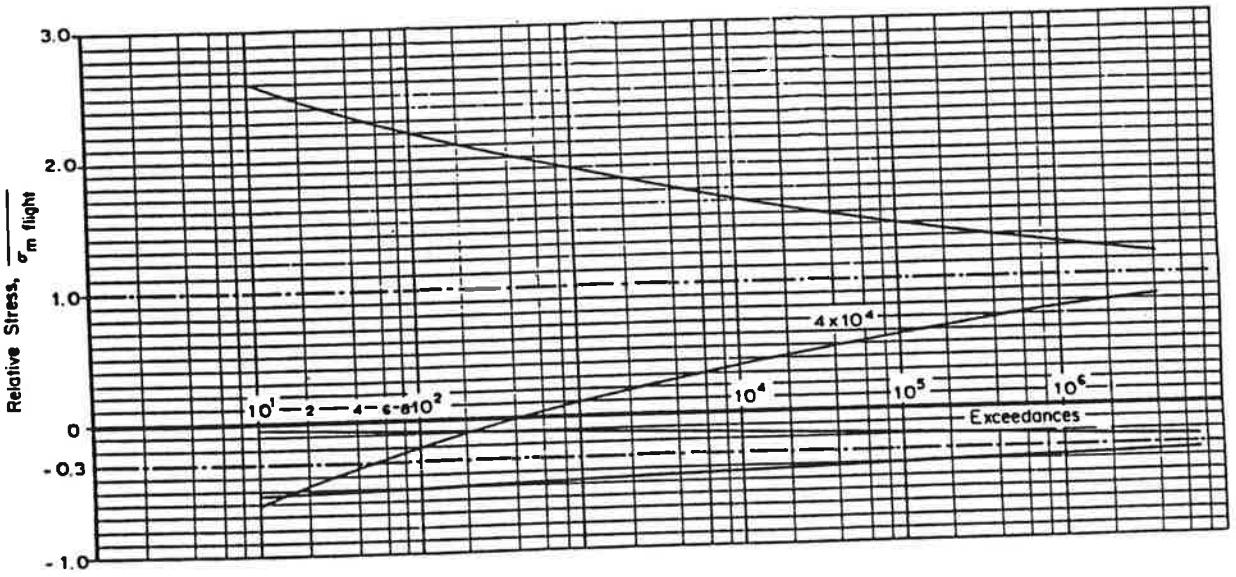

FIGURE 5-7. STANDARDIZED SPECTRUM FOR 40,000 FLIGHTS TWIST

Since TWIST is used for testing, detailed procedures have been developed to generate stress histories from the exceedance diagram of Figure 5-6. Although such histories are useful for testing, they are cumbersome, to say the least, for analysis; easier, but similar ways to derive stress histories can be devised, as will be shown in Section 5.3.

5.2.2 Proposed Spectrum. The TWIST exceedance diagram is repeated in Figure 5-8, together with a proposed simplification. The simplification is not essential; the TWIST exceedance diagram could be used as is. However, since it is an average, some streamlining is justified, especially since the stress axis must be adjusted for different fuselages types (Section 5.4).

TWIST is a spectrum for 40,000 flights of an estimated average duration of 1.5 hours; hence it is a spectrum for about 60,000 hours, the normal aircraft design life. In the case of fuselages for aircraft with largely different flight durations, the GAG cycle occurs more or less frequently. As the GAG cycle is of major importance (Figure 5-5), the spectrum must be considered to be for 60,000 hours instead of for 40,000 flights. This is perfectly legitimate, because the number of gusts per hour is of more importance than the number of gusts per flight.

The TWIST spectrum ends at a minimum of 10 exceedances. This essentially means that it is clipped at 10 exceedances per 60,000 hours. Clipping and truncation of the spectrum is of no consequence if crack growth retardation due to overloads is not accounted for in the fatigue crack growth analysis of the repair [11]. However, it is of great importance if retardation is to be

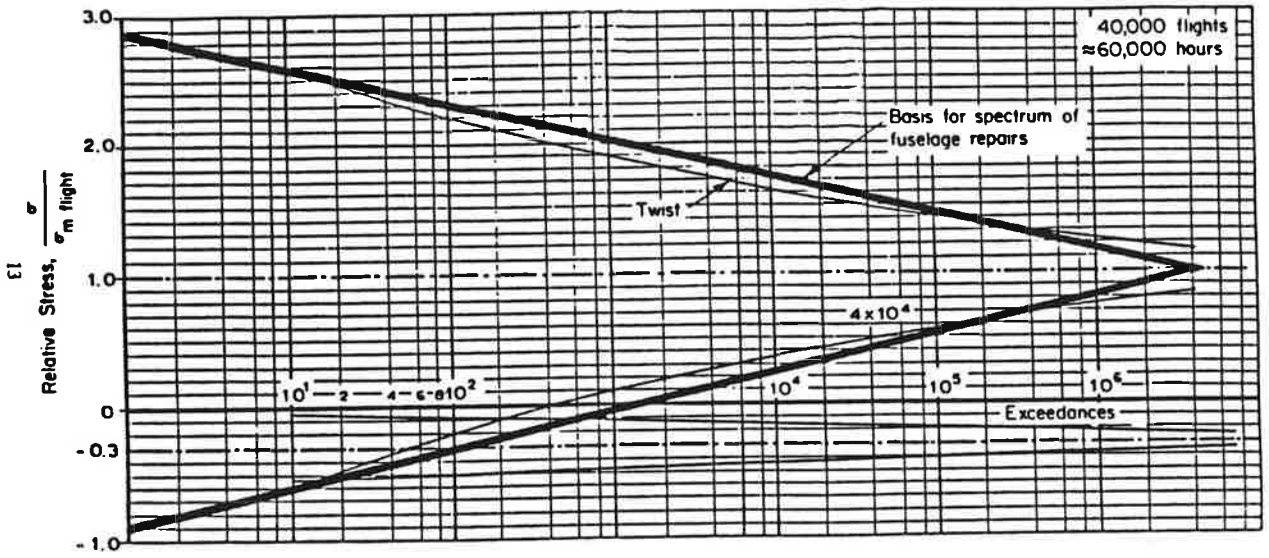

FIGURE 5-8. PROPOSED SIMPLIFICATION TO STANDARDIZED TWIST SPECTRUM FOR 40,000 FLIGHTS

considered [11,14-15]. Performing linear crack growth analysis without consideration for retardation effects is generally conservative.

As discussed in Section 5.3, a 60,000 hour spectrum is unwieldy and unnecessary for stress history generation, especially when it is clipped anyway. Therefore, the proposed spectrum is reduced to one for 600 hours. The logic for the reduction can be understood by comparing Figures 5-9 and 5-10. The 600 hour spectrum of Figure 5-10 is the same as the one in Figures 5-8 and 5.9, but it is more suitable for the stress history generation explained in Section 5.3. Note that this spectrum is "automatically" clipped at the once per 600 hours exceedance (100 times per 60,000 hours), which is more conservative if retardation is accounted for [11,14]. The spectrum shown in Figure 5-10 can be converted to stress quite easily, since the fuselage pressurization stress and the limit load stress are known for all certified aircraft. This will be explained in Section 5.4.

5.3 Stress History Generation

5.3.1. Stress Levels. Depending upon the counting procedure, the exceedance diagram shows the number of times a positive or negative stress excursion is exceeded; i.e., it shows the size of the stress range and their frequency. In the schematic example in Figure 5-11, stress Level 4 is exceeded

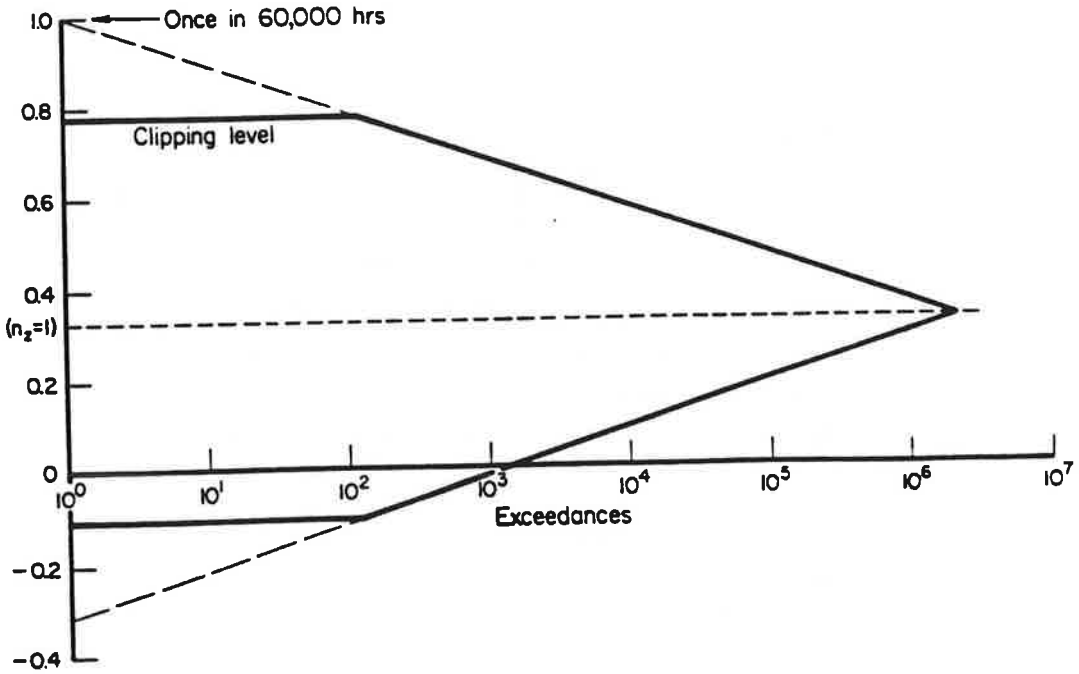

FIGURE 5-9. REPAIR SPECTRUM (SEE FIGURE 5.8) IN TERMS OF N_Z

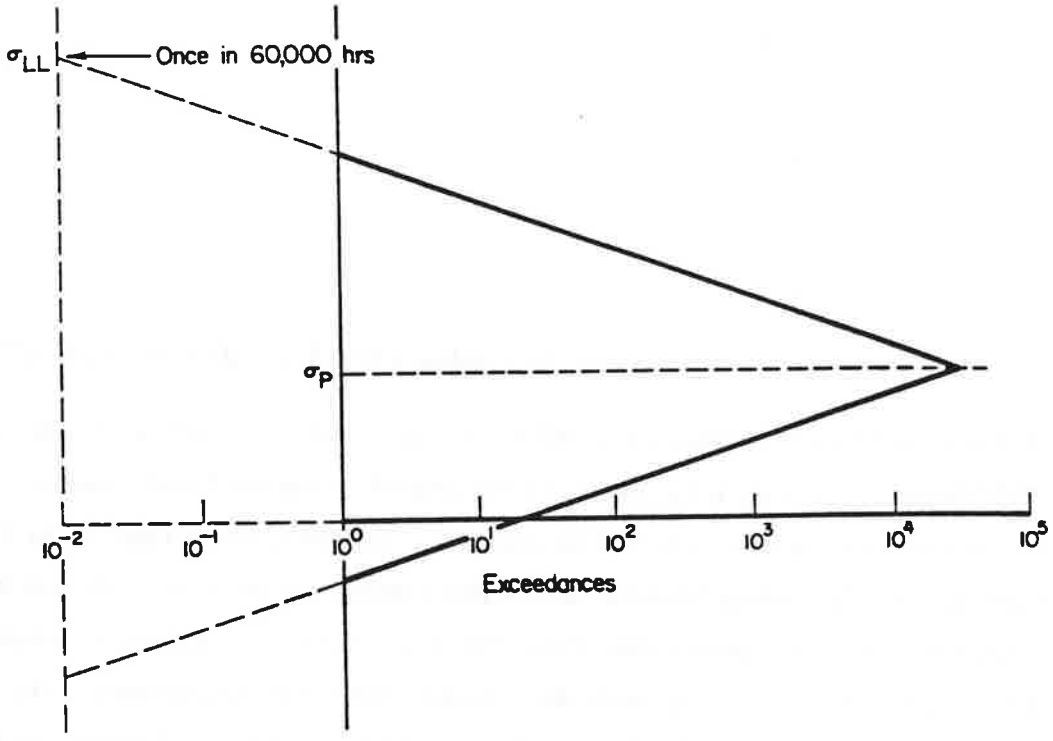

FIGURE 5-10. REPAIR SPECTRUM FOR 6700 HRS (COMPARE TO FIGURE 5.9)

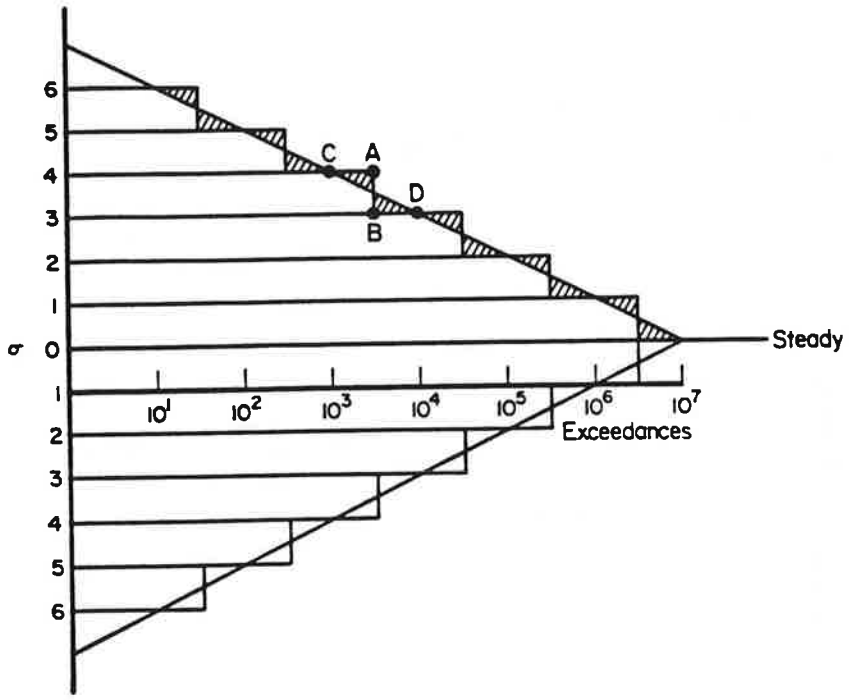

Example of level approximation (only 6 levels shown for clarity)

Level	Exceedances
6-6	30
5-5	300
4-4	3000
3-3	30000
2-2	300000
1-1	3000000

FIGURE 5-11. OBTAINING STRESS LEVELS AND EXCEEDANCES

3,000 times and Level 3 is exceeded 20,000 times. As a result, there will be 20,000 - 3,000 = 17,000 events in which the stress reaches a level somewhere between Levels 3 and 4.

In reconstituting a stress history the exceedance diagram is always idealized by a number of discrete levels. Considering too many stress levels is impractical and ignores the fact that the spectrum is a statistical representation of *past* experience and that the analysis is a prediction of the *future*. Accounting for too many stress levels would be presuming that stresses can be predicted to occur in the future exactly as they have in the past, which they will not. The discrete levels do not have to be evenly spaced, but they usually are. Experience shows that 10 to 12 levels (each positive

and negative) are sufficient for the desired accuracy; use of more than 12 levels does not significantly change the results. This can be appreciated from the fatigue crack growth analysis results, shown in Figure 5-12, for one particular exceedance diagram. The calculated life remains essentially the same once the number of levels is greater than 10.

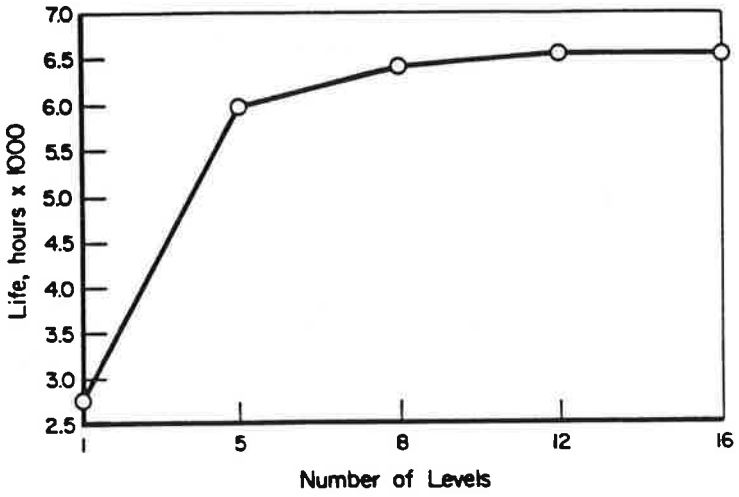

FIGURE 5-12. EFFECT OF LEVELS IN EXCEEDANCE DIAGRAM APPROXIMATION; COMPUTED NUMBER OF HOURS FOR CRACK GROWTH AS A FUNCTION OF NUMBER OF LEVELS. ONE LEVEL IS CONSTANT AMPLITUDE

For clarity only 6 levels (6 positive and 6 negative) are shown in the example in Figure 5-11. At each level a line is drawn intersecting the exceedance curve. Steps are completed by vertical lines (such as AB) so that the shaded areas shown in Figure 5-11 are essentially equal. Figure 5-11 also shows how the exceedances, and from these the number of occurrences of each level, are obtained.

Positive and negative excursions still have to be combined to create stress cycles. One might be tempted to select positive and negative excursions in random combinations, as is done in TWIST. This is often done to define aircraft component test conditions. However, when this is done as part of an analysis, a rainflow counting of the history will again be necessary to determine the stress ranges. This is a legitimate approach, but a simpler procedure can be employed. Since the spectrum was developed from a counted history in the first place, it should not be necessary to disarrange it, and then count it again. The result is known a priori. The result of counting will generally be that the largest positive peak will be combined with the lowest valley. Foreseeing this, it is reasonable to

combine positive and negative excursions of equal frequency. Stress ranges so established can be applied (semi-) randomly, as they are *already* pre-counted and interpreted. This leads to the largest possible load cycles (conservative), and the computer code does not need a counting routine. It is also *realistic*, because air is a continuous medium, and a down-gust is often followed by an up-gust of approximately equal magnitude (Figure 5-13).

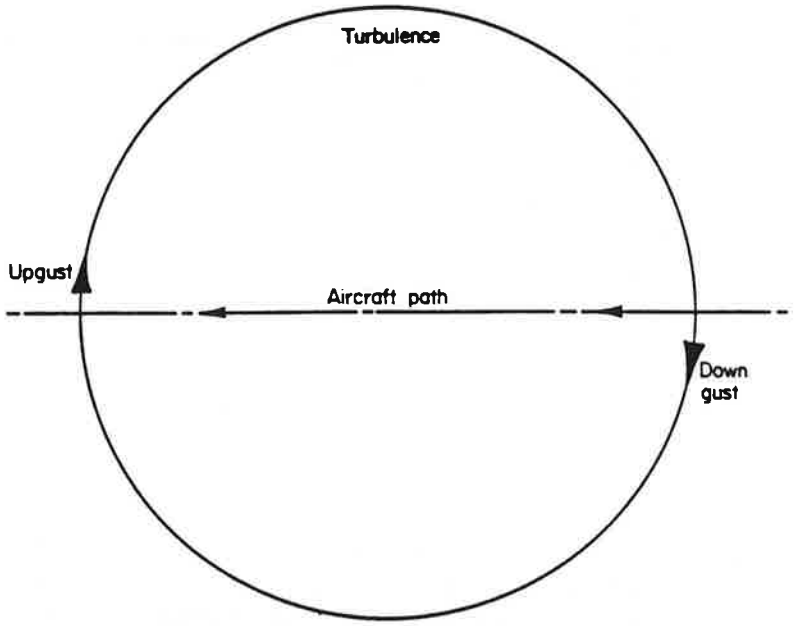

FIGURE 5-13. TURBULENCE, GUSTS, AND CONTINUITY OF AIR UP AND DOWN GUST OF ABOUT EQUAL MAGNITUDE OFTEN OCCUR IN CLOSE SUCCESSION

5.3.2 Different Flight Types. The content of the stress history is now known, but the sequence must still be determined. If retardation is not an issue, sequencing of stresses is irrelevant. If load interaction must be considered, stress sequencing is of eminent importance. In many analyses the loads are applied in random order. However, with retardation, a *random* sequence *does not provide correct answers* when actual service loading is semi-random. A commercial aircraft experiences many smooth flights and occasionally a rough flight. This means that the loading is not truly random, but clusters of high loads do occur (Figure 5-14). Were these high loads (e.g, A, B, and C in Figure 5-14a) distributed randomly as in Figure 5-14b, as is sometimes done in analyses, they would each cause retardation. Because of the clustering, the retardation will be much less (in Figure 5-14a, only A will cause retardation, B & C are overshadowed by A). Realistically then,

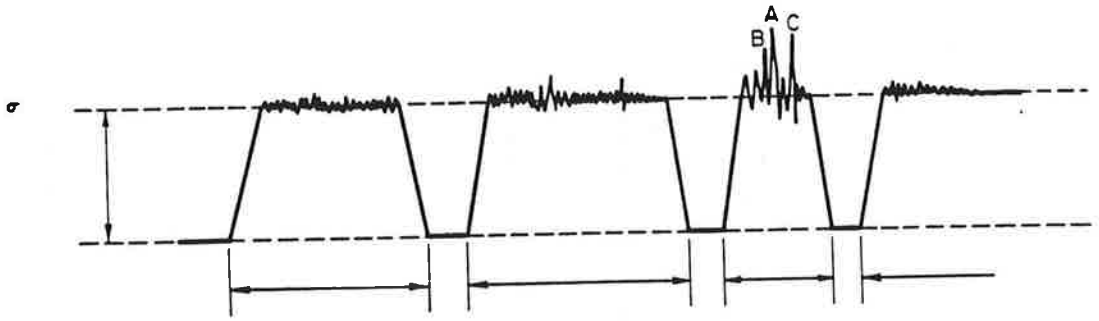

a. Truly Semi-random (Real Situation)

b. Random (Commonly done, but very wrong if there is retardation).

FIGURE 5.14. REAL (SEMI-RANDOM) AND WRONG (RANDOM) HISTORIES

fatigue crack initiation and growth analyses must principally account for a mixture of flights of different severity. This is defined as semi-random loading. There will be fewer severe flights than mild flights, as shown in the example in Figure 5-14. In the computer analysis flights of different severity must be applied in random sequence, and the cycles within each flight must be random. Such a semi-random sequence can be developed in many ways. A simple algorithm is shown in Table 5-2 on the basis of Figure 5-15. Mild and severe flights are constructed by recognizing that the exceedance diagrams for the individual flights are of the same shape, as demonstrated by Bullen[16], but with different slopes as shown in Figure 5-15c. Their total makes up the diagram of total exceedances (Figure 5-15a). The following example is based upon a schematic exceedance diagram for 100 flights; again only 6 levels are used.

The different flights are constructed as illustrated. The total number of exceedances is 100,000, so that the average number of exceedances per flight is 100,000/100 = 1,000 [6]. This provides the end-point in Figures 5-15b and 5-15c. The highest level occurs 3 times (Figure 5-15 and Table 5-2, Column 3). Naturally, it will occur only in the most severe flight denoted as A. Letting this level occur once in A, the exceedance diagram for A is established as shown in Figure 5-15b, because the highest level (6) provides the point of 1 exceedance. Flight A can occur only three times,

TABLE 5-2. GENERATION OF STRESS HISTORY WITH DIFFERENT PERIODS BASED ON FIGURE 5.15

1	2	3	4	5	6 3 x 5	7 3 - 6	8	9	10 12 x 9	11 6 - 10
Level	Exceedances Fig. 15a	Occurrences	Type A exceed. Fig. 15b	Occur in A	Occur in 3 types A	Remainder	Type B exceed. Fig. 15c	Occur in B	Occur in 12 types B	Remainder
6	3	3	1	1	3	—	—	—	—	—
5	21	18	3	2	6	12	1	1	12	—
4	132	111	12	9	27	84	5	4	48	36
3	830	698	48	36	108	590	20	15	180	4110
2	5750	4920	158	110	330	4590	100	80	960	3630
1	43650	37900	575	417	1251	36649	480	380	4560	32089
			Total number of periods						12 + 3 = 15	

12	13	14 36 x 13	15 11 - 14	16 15/49	17 16 x 49	18 15 - 17	19 18/12	20 9 + 19	21	22
Type C exceed. Fig. 15c	Occur in C	Occur in 36 types C	Remainder for 49 type D	Occur in type D	Occur in 49 types D	Remains	Distributed in 12 type B	New type B	Exceed. of D	According to diagram Fig. 15c
—	—	—	—	—	—	—	—	—	—	—
—	—	—	—	—	—	—	—	1	—	—
1	1	36	—	—	—	—	—	4	—	—
8	7	252	158	3	147	11	1	16	3	1
52	44	1584	2046	42	2058	-12	-1	79	45	20
400	348	12528	19561	399	19551	10	1	381	444	300
		15 + 36 = 51			51 + 49 = 100					

Same for negative levels if applicable. Periods: 3A + 12B + 36C + 49D = 100 total.

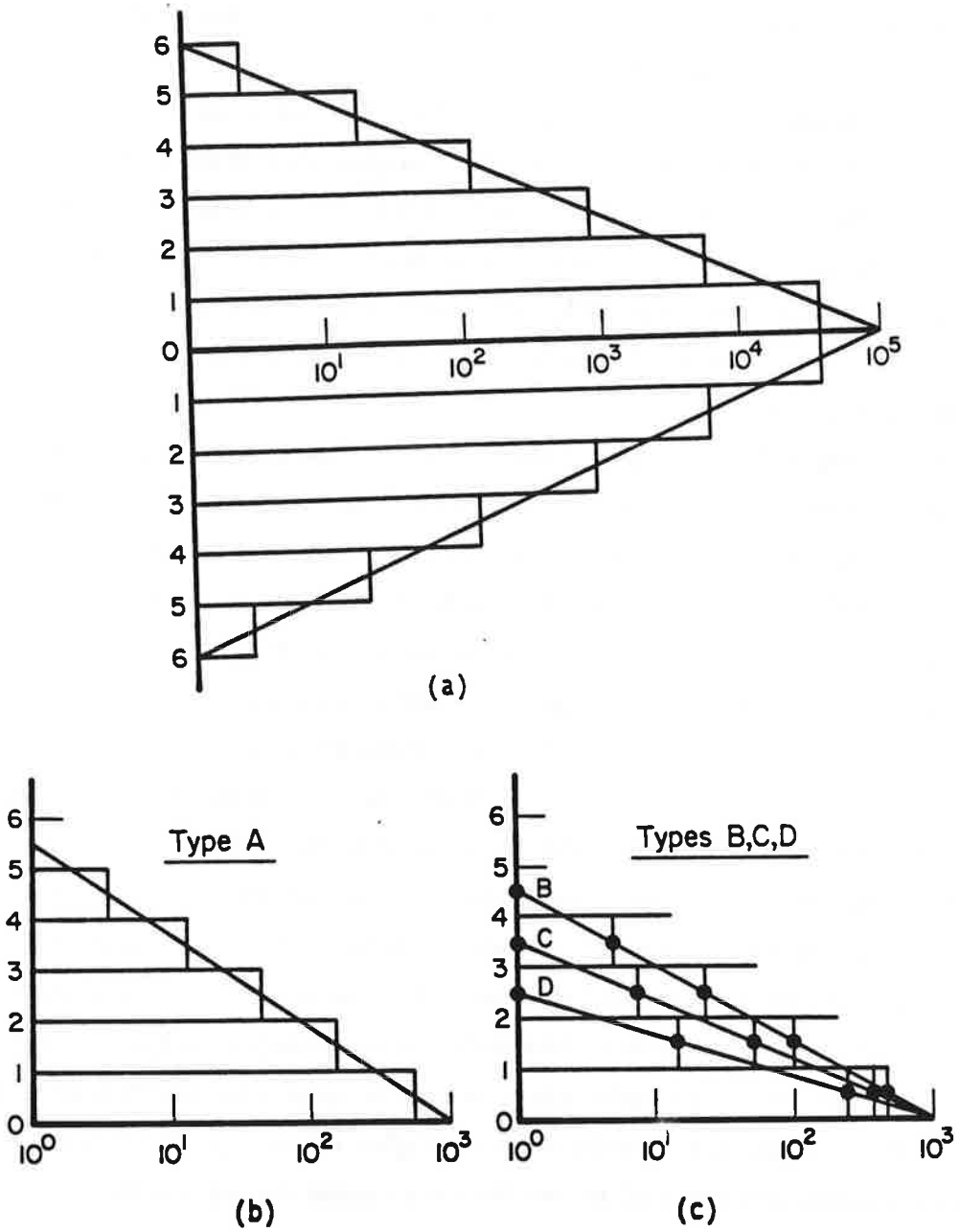

FIGURE 5-15. STRESS HISTORY WITH DIFFERENT FLIGHTS (SEMI RANDOM)

because then the cycles of Level 6 are exhausted. The exceedances for A are read from the exceedance diagram of A (Figure 5-15b), and from these the occurrences (number of cycles) are determined as in Columns 4 and 5 of Table 5-2. There being three Type A flights, the total cycles

for all A flights are shown in Column 6. These cycles are subtracted from the total so that the remainder for the other 97 flights is as shown in Column 7.

The next most severe flight is Type B. Its highest level will be Level 5, which will occur once. This information permits construction of the exceedance diagram for B as shown in Figure 5-15c, Level 5 being at 1 exceedance. The exceedances and occurrences are determined as in Columns 8 and 9 in Figure 5-15. Since there were only 12 cycles of Level 5 left after subtraction of three Type A flights (Column 7), there can be 12 Type B flights. These 12 flights will use the number of cycles shown in Column 10, which must be subtracted from those in Column 7 to leave the remaining cycles in Column 11.

Flight C is constructed in the same manner. There can be 36 Type C flights and then the cycles of Level 4 are exhausted. One could go on in this manner, but since there now are only 49 flights left, it is better to divide the remaining cycles in Column 15 by 49 in order to distribute them evenly over 49 Type D flights. This is done in Columns 15-17. There are some cycles unaccounted for, and a few too many cycles were used as shown in Column 18. These are of lower magnitude, contributing little to crack initiation or growth — and since the diagram is only a statistical average — this little discrepancy could be left as is. However, if one wants to be precise, they could be accounted for by a little change in the content of Flight C, as shown in Columns 18-20.

If more than 6 levels are used, more (and different) types of flights can be generated. However, this was an example only, and there is no need to go to extremes as long as a semi-random history is obtained, recognizing that flights of different severity do occur and that the higher loads are clustered in those flights. No matter how refined the procedure, the actual load sequence in practice will be different. In accordance with the nature of the loading, there are only three Type A flights of a high severity in the total of 100. The majority consists of mild flights of Types D (49) and C (36). Regardless of the number of levels chosen and the number of flights, the above procedure will reflect this reality. Other procedures can be devised, but the above is a rational one and easy to implement[14].

In crack initiation and growth analyses the various flights must be applied in random order and the cycles within each flight applied randomly. Thus, the second occurrence of any flight type will have a different sequence than its first occurrence, but the total cycle content will be the same. If the "basket" with 100 flights is empty, it is "refilled", and the process started anew; yet because of the randomization the flights and the cycles within each flight will appear in different order.

5.3.3 Issues of Importance. The stress history generated in the manner discussed provides the most realistic results when the total exceedances are on the order of 2,000 to 100,000 and the number of flights on the order of 50 to 1000. Therefore, it may be advantageous to adjust exceedance diagrams for smaller or larger numbers to the above ranges, as was done in Figure 5-10.

To summarize, the following issues are important in the generation of a stress history, namely:

a. Flights of different severity must be applied. Random application of stresses derived by complicated means will negate all the efforts.

b. Deterministic loads must be applied at the point where they occur: GAG cycles must occur *between* flights; *random* application may defy all other sophisticated procedures.

c. A reasonable number of stress levels (10-16 positive and negative) must be selected. More levels will complicate the procedure without improving the results and make the generation of different flight types much more cumbersome.

d. Positive and negative excursions of equal frequency must be combined. Random combinations will require subsequent counting, the result of which can be foreseen, while the stress history was based on an already counted history in the first place.

e. The total number of flights and cycles must be in accordance with the total exceedance diagram.

The above criteria account for what may be called the *signature* of the loading. Small changes in these, including clipping[11,14,15], will usually have more effect on crack initiation and growth than any complicated means of establishing stress levels.

It is important to emphasize that the TWIST spectrum is based on measurements and used for demonstration in this report; it should be compared with spectra furnished by the OEM. Another important data source is the NASA/DOT/FAA aircraft loadings data[12]. In developing a stress history for a given repair in an aircraft fuselage, the repair engineer may be well advised to compare the stress history he or she develops with the proposed history and to use the most severe of the two.

5.4 Fuselage Stresses

The basic spectrum and stress history have now been established. What still needs to be done is adjustment of the stress axis (actual stress) for the fuselage. There are two relatively simple ways to accomplish this:

a. Approximate fuselage stress analysis

b. Limit load analysis.

These two possibilities are discussed in the following sub-sections.

5.4.1 Approximate Fuselage Stress Analysis. Figure 5-16 shows an aircraft's weight distribution. Only the *fuselage* weight is of importance for fuselage bending; it is assumed to be

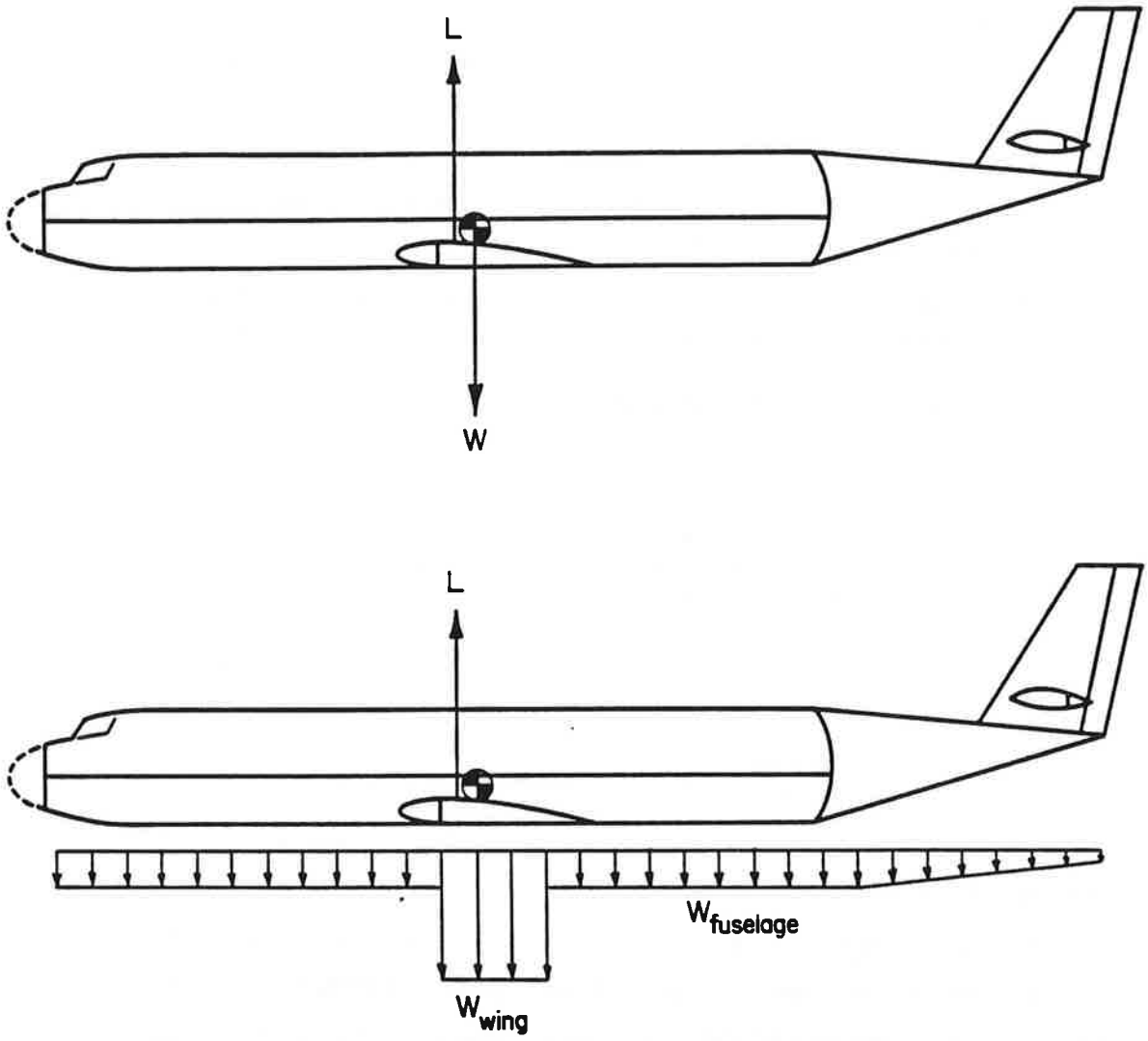

FIGURE 5-16. FUSELAGE LOADING

evenly distributed. As shown in Figure 5-17, local bending moments due to vertical gusts are determined from static equilibrium requirements. Given the Station No., x, of the repair, which is always known, the moments (M_b and M_t) are determined, and from these the approximate stresses can be readily calculated as shown in Figure 5-18.

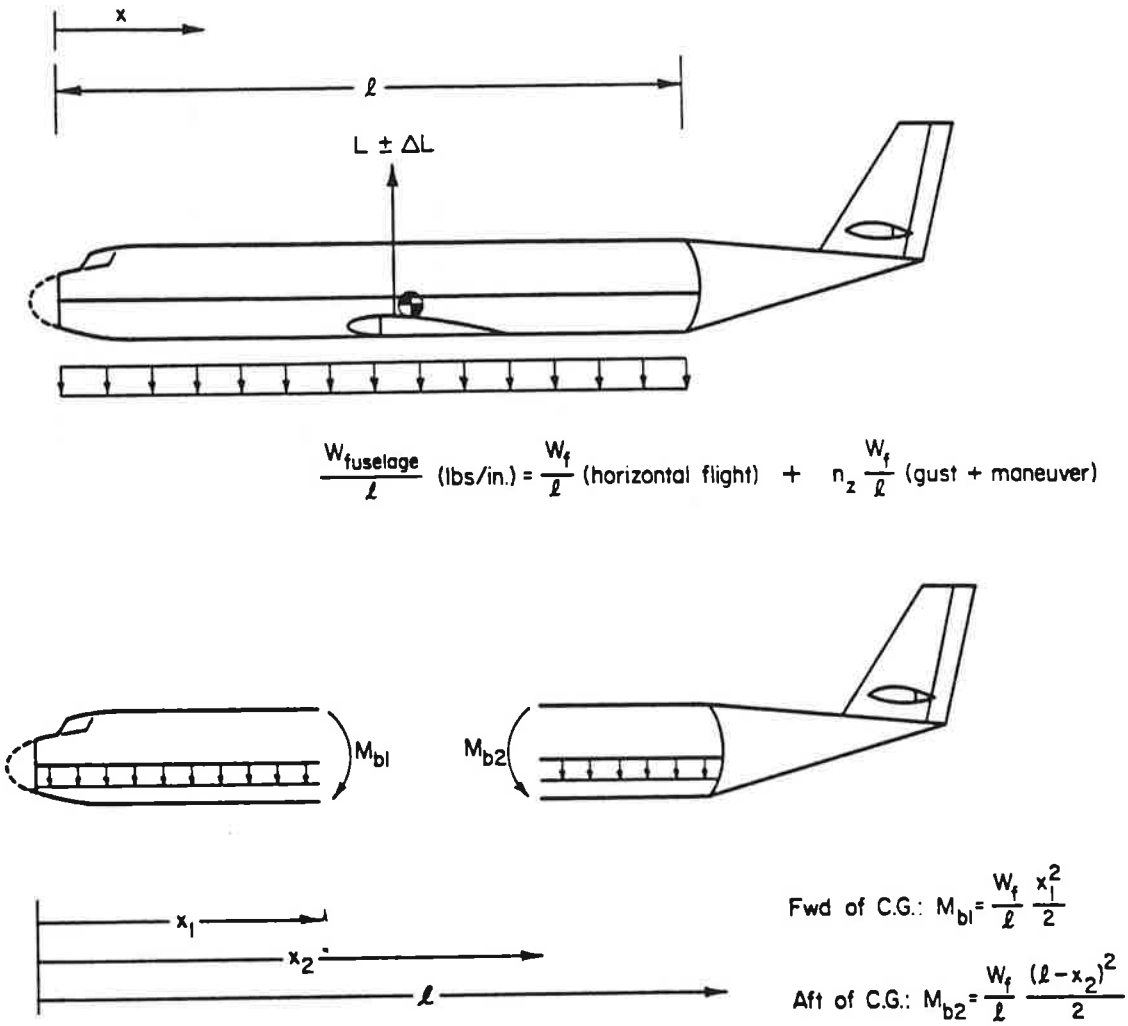

FIGURE 5-17. FUSELAGE BENDING

Circumferential stresses can be calculated as follows:

$$\sigma_p = \frac{pR}{t} \tag{5-4}$$

This pressurization stress cycle occurs once per flight. The circumferential stresses are generally reduced by approximately 20 percent near frames and 10 percent near tear straps.

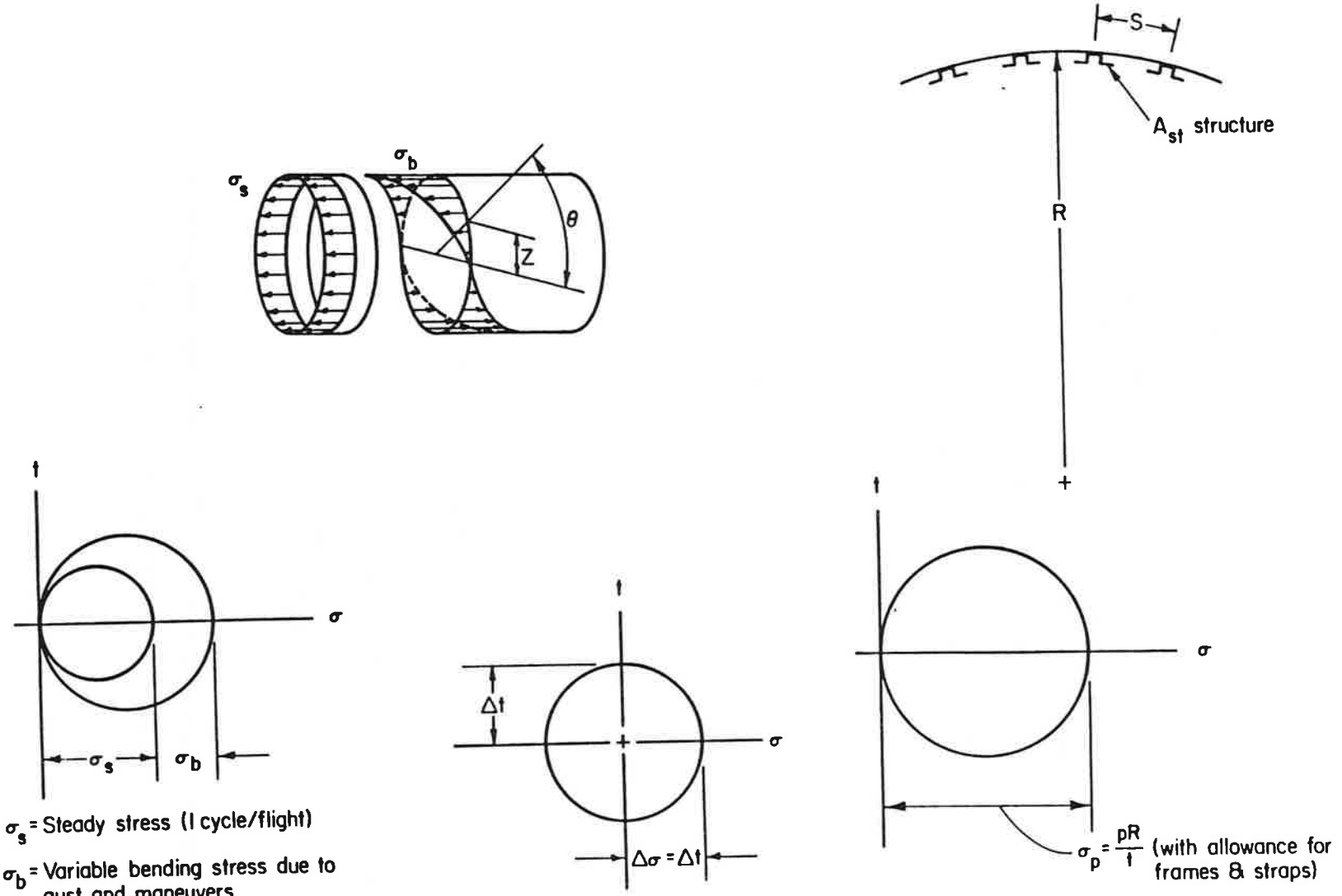

a. Longitudinal

b. Torsion — variable amplitude stress due to lateral gust and maneuvers

c. Pressurization and longitudinal cracks: steady stress part (1 cycle per flight)

FIGURE 5-18. FUSELAGE STRESSES

Longitudinal stresses are due to pressurization, σ_{pl}, and bending at the 1 g load (L - W), $\sigma_{bl\text{-}g}$. The pressurization stress is:

$$\sigma_{pl} = \frac{p\pi R^2}{2\pi Rt + k\,A_{st}} \tag{4-5}$$

where

k = number of stringers
kA_{st} = $\alpha_1\, 2\,\pi\, Rt$ and $\alpha_1 \approx 0.8$ (based upon a typical stiffening ratio of 0.4, but can be determined for each aircraft type).

This leads to:

$$\sigma_{pl} = \frac{p\pi R^2}{2\pi Rt(1 + \alpha)} \approx \frac{p\pi R^2}{2\pi Rt(1 + 0.8)} = \frac{p}{3.6Rt} \tag{4-6}$$

The bending stress is:

$$\sigma_{bl} = \frac{M_b\, Z}{\pi R^3 t + \frac{k}{2} A_{st}\, R^2} = \frac{M_b\, R \sin\theta}{\pi R^3 t + \alpha\, \pi\, RtR^2} \approx \frac{M_b \sin\theta}{1.8\pi\, R^2 t} \tag{4-7}$$

The total stress at 1-g loading, σ_1, is then

$$\sigma_1 = \sigma_{pl} + \sigma_{bl} \tag{4-8}$$

where σ_{bl} is the bending stress from Equation (5-7) for the 1-g bending moment. Superposed on this 1-g stress is the cyclic bending stress due to inertia during gust and maneuvers.

The spectrum (Figure 5-8) shows that the once per 600 hours stress excursion (at 100 exceedances in 60,000 hours) is 1.3 times the "steady" stress, which in this case is the 1-g bending stress. Calculation of the 1-g bending stress therefore defines the entire exceedance diagram of Figure 5-10 in terms of real stresses.

The stress history can then be generated in accordance with the following procedure. Every cycle will be an excursion due to bending from the 1-g steady stress $\sigma_{bl\text{-}g}$; so that the stress history is described as:

$$\sigma_1(\text{time}) = \left(\sigma_{pl} + \sigma_{bl}\right)_{\text{constant}} + \Delta\sigma_{bl}(\text{time}) \tag{4-9}$$

where

$\Delta\sigma_{bl}$ reaches $\pm$ 1.3 ($\sigma_{b1\text{-}g}$) once in 600 flights, as shown below:

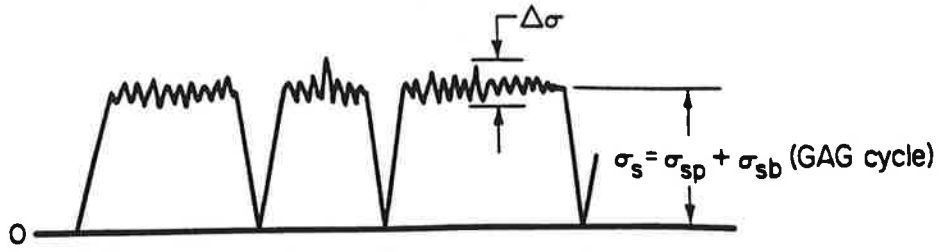

If necessary the shear stresses due to torsion and bending can be included.

$$\Delta\tau_t = \frac{\Delta M_t}{2\ \pi\ R^4 t}\ R = \frac{\Delta M_t}{2\pi\ R^3 t};\ \Delta\sigma_t = \Delta\tau_t \qquad (4\text{-}10)$$

With the other stresses already obtained, this permits calculation of the largest principal stress — the one to be used in the fatigue and crack growth analyses.

A complication that must be considered is that fuselage bending stresses due to wing gusts and torsional stresses (due to lateral gusts) vary independently. It is likely, however, that the torsion contribution will be small for circumferential cracks, and the bending contribution will be small for most longitudinal cracks.

Of course the value of α_1 in σ_{pl} in Equation (5-6) can be adjusted in a stress analysis program for different aircraft types. The effect of longitudinal stringers on bending stresses and longitudinal pressurization stress is properly accounted for. Some adjustments to the circumferential stresses to account for the effects of straps and frames must be made, and appropriate adjustments must be made for door and window cut-outs and framing.

When the stresses in the basic structure are known in this manner, the stresses in the repair can be calculated by compatible displacements (or other local stress analysis techniques) for any repair.

5.4.2 Limit Load Analysis. An alternative, but simplified, way to obtain the stress conversion is as follows:

> Limit load is basically the load that is expected to occur once in the aircraft life (i.e, once in 60,000 hours as shown in Figures 5-9 and 5-10). The structure is sized such that the stress at ultimate load is equal to the material's design allowable strength. The safety factor between ultimate and limit load is 1.5 (the airworthiness requirement).

Hence, the limit load stress follows immediately as the design allowable stress divided by 1.5. One small limitation to this approach is that different manufacturers do use different allowables, and these allowables are often lower than the "true" statistical allowable of the material.

In any case, given the material and hence the design allowable stress, the limit load stress follows as above. Since this is the stress which is assumed to occur once in about 60,000 hours, the beginning points in Figures 5-9 and 5-10 are known, and hence the whole exceedance diagram can be estimated. Another rule of thumb to consider in this analysis is that limit load stresses (in 2024-T3) are usually set no higher than about 35 ksi.

As aircraft structures are seldom designed exactly to the design allowable limits (there is always a margin of safety, which varies from location to location), the disadvantage of this method is a loss in accuracy, but the accuracy may suffice for comparative analyses. Its advantage is that no special allowances have to be made for location and structural details. (The assumption being that the original structure was designed to conform to limit load margins).

5.5 Comparison of Proposed Stress History Generation Scheme With Manufacturer's

To provide an appreciation of how representative crack growth curves, as calculated with the proposed stress history and spectrum, compare with those calculated by manufacturers, a comparison was made of crack growth computations based upon the proposed procedure and those based on stress histories for the KC-135 and EC-135[17]. The latter were kindly provided by the US Air Force. Only longitudinal stress estimates are considered in these examples.

The following discussion is based on the word "spectrum" meaning the total load experience (in terms of an exceedance diagram or otherwise), while the specific sequence of loads or stresses used in an analysis or test is called a "stress history". These definitions were adhered to earlier in Section 5, but in the general literature they are often confused, or used alternatively without explanation. The two are essentially different — a stress history may be a loose interpretation of the spectrum, as will be shown below. In practice the word "spectrum" is often used for both, which may lead to confusion.

Before presentation of the results of the comparison, the stress histories for the military versions of the B707/B720[17] require some discussion, because otherwise a fair comparison is not

possible. The details of the analysis leading to the stress histories are not elaborated upon in Reference [17]. Therefore, only the results are reviewed briefly.

The fuselage of the aircraft is divided into Areas A through O, as shown in Figure 5-19. Stress histories for these areas were derived, and these were assumed to be valid throughout the area without regard to stress gradients or detail design. (It should be noted that the bottom of Figure 5-19 roughly represents the neutral axis for fuselage bending.) The stress histories in each of these areas were derived on the basis of the load spectrum, taking into account flight conditions (point-in-the-sky approach accounting for different flight segments as discussed earlier). Although details are not given, other evidence[18] shows that the manufacturer used a loose interpretation of TWIST (the spectrum used here) for the stress history in a recent full-scale fatigue test; it is therefore reasonable to assume that similar considerations were used in the derivation of the stress histories discussed here.

Apparently, stress histories for a variety of missions of the different military versions of the aircraft were derived[17]. By means of crack growth calculations, details of which are not specified, one particular mission (identified as Mission 3) was determined to be the most severe. This led to a typical mission profile (stress history) as shown in Figure 5-20. Similar stress histories were developed for all areas specified, using only Mission 3 for all areas. The number of cycles in these missions, and the maximum stress in each area, are shown in Figure 5-19.

The first thing to be noted is that the most severe mission (which was taken as representative for all versions) pertains to the AWACS version. The radar disk above the fuselage may explain the fact that in Areas A through I the number of cycles is much larger than elsewhere and that the stresses do not follow the anticipated pattern. For this reason, Areas A through I could not be used for comparison with a commercial aircraft. This leaves Areas J through O, from which Areas J, K, and L were selected as the basis for comparison.

The cycle numbers per mission for these areas (Figure 5-19) do not seem to be consistent, as (one must assume that) the cyclic stresses are due to bending cycles, the number of which is the same for all areas in the fuselage. Be that as it may, Mission 3 includes 5 touch-and-go landings as illustrated in Figure 5-21. Because normal airline practice does not include touch-and-goes, the cycles concerned were eliminated. The stress histories for Areas J, K, and L are shown in Figure 5-22. It seems reasonable to assume that the cycles for the five touch-and-goes are as indicated. Eliminating these leads to the stress histories shown in Figure 5-22.

The total number of cycles per mission (flight) is still inconsistent and remains unexplained. The stress histories in Figure 5-22 were considered representative for three areas over which the

Note: Maximum stress in history, σ_{max}, and number of cycles in Mission 3, N, are shown.

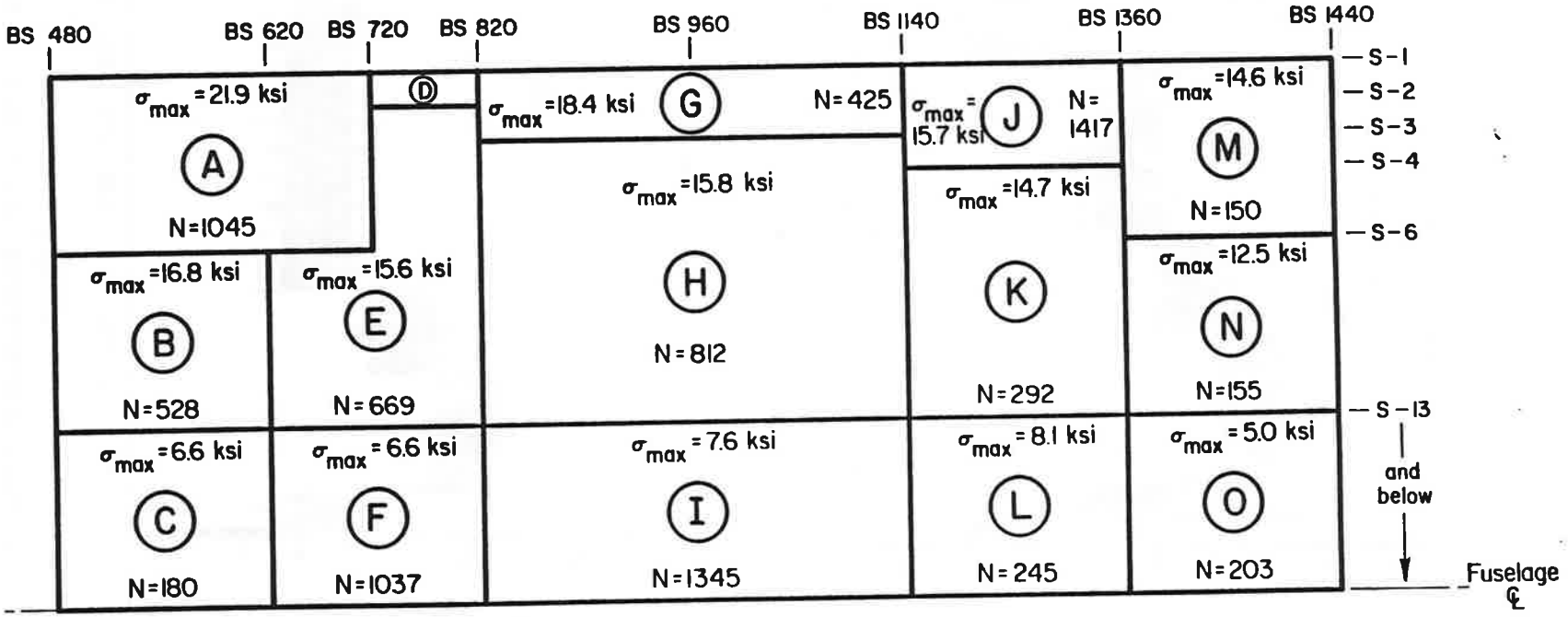

BS = Fuselage station
S = Stringer

FIGURE 5-19. AREAS OVER WHICH STRESSES ARE ASSUMED THE SAME

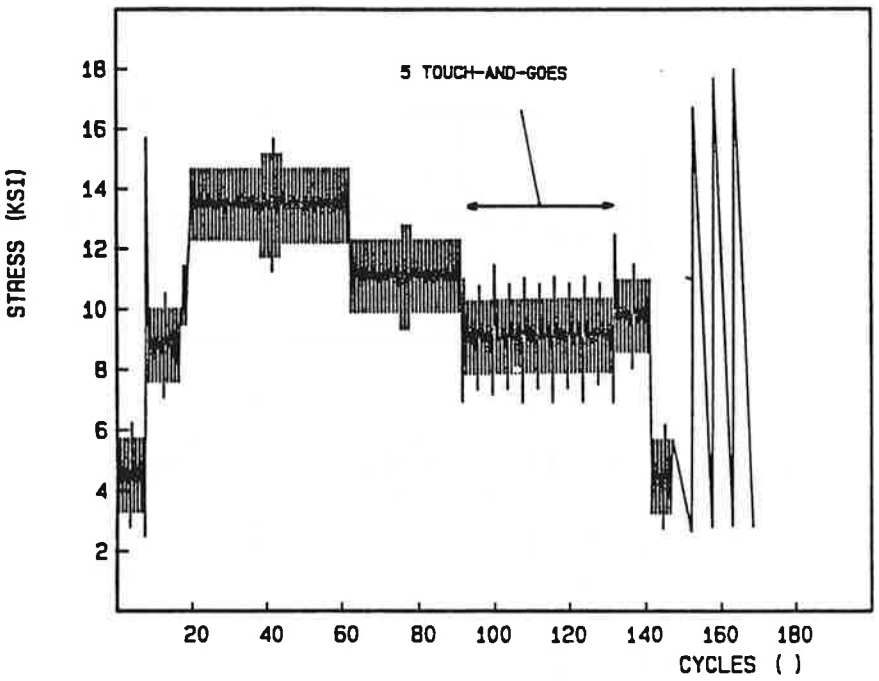

a. Area J

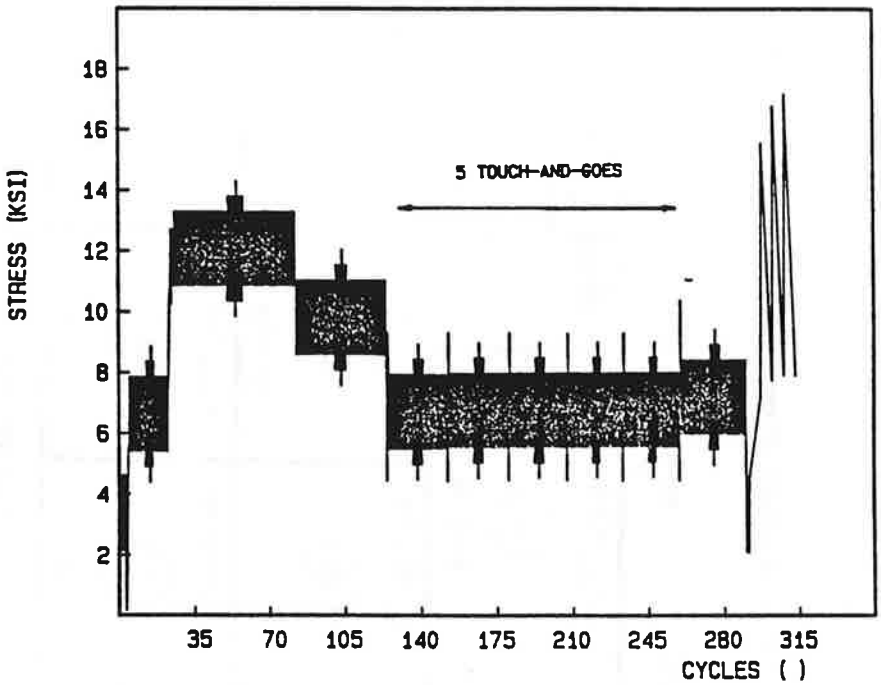

b. Area K

FIGURE 5-20. BOEING SPECTRUM; ALL FLIGHTS ARE THE SAME, LAST 3 CYCLES ARE MAKE UP CYCLES

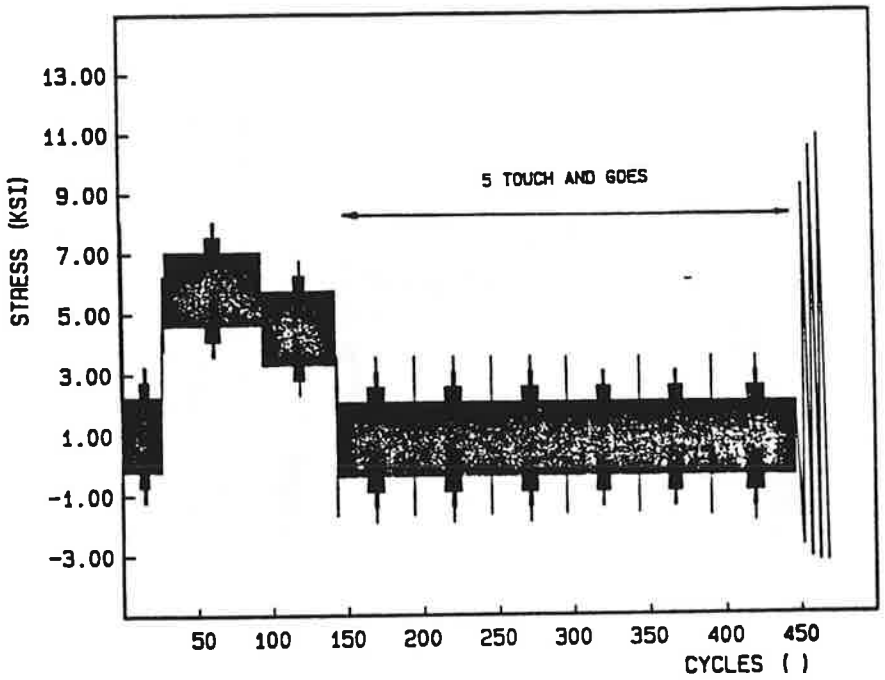

c. Boeing Spectrum for Area L

FIGURE 5.20 BOEING SPECTRUM; ALL FLIGHTS ARE THE SAME, LAST 3 CYCLES ARE MAKE UP CYCLES(CONCLUDED)

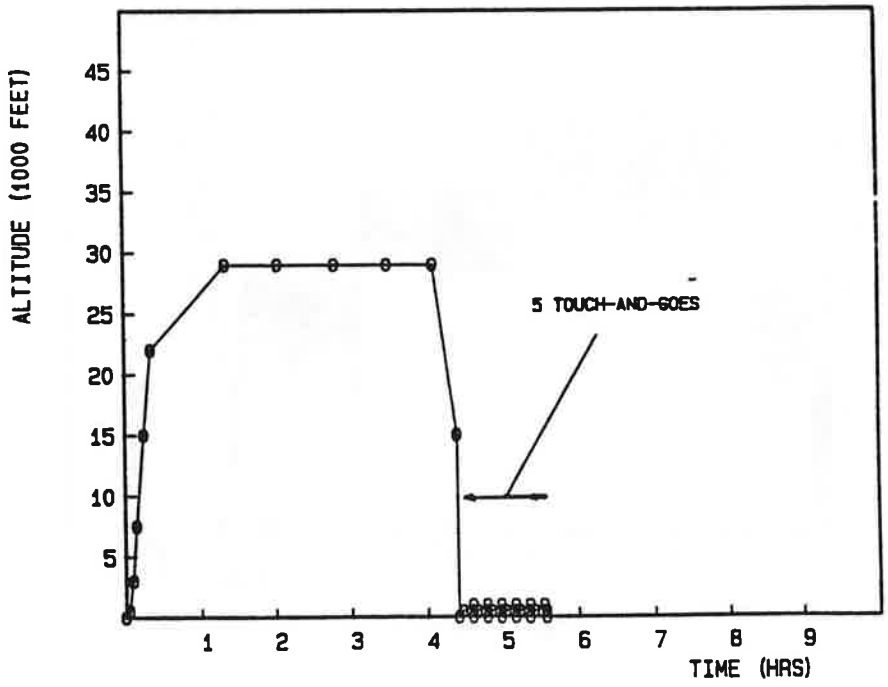

FIGURE 5-21. MISSION 3 ALTITUDE PROFILE

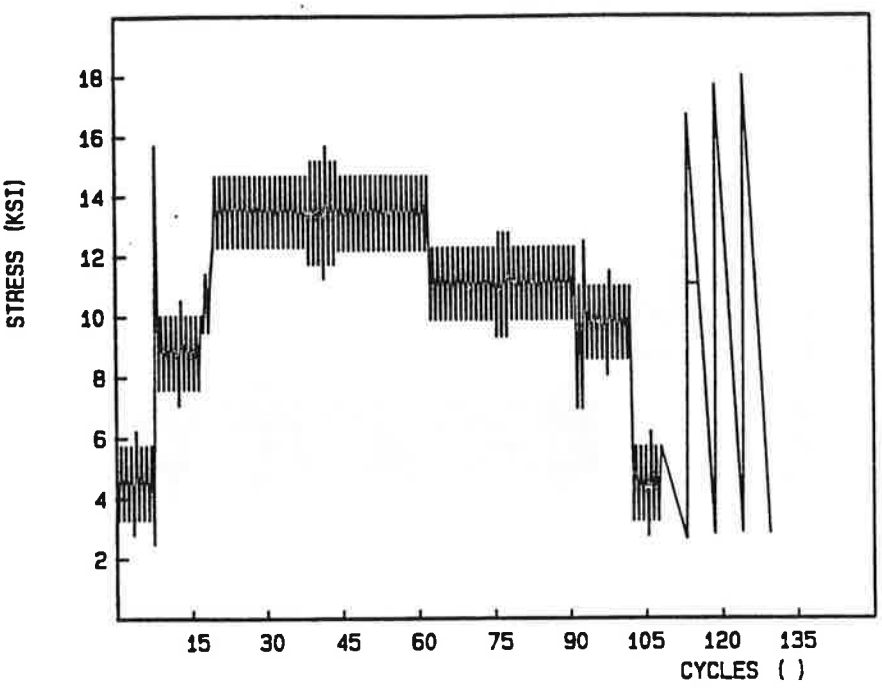

a. Area J

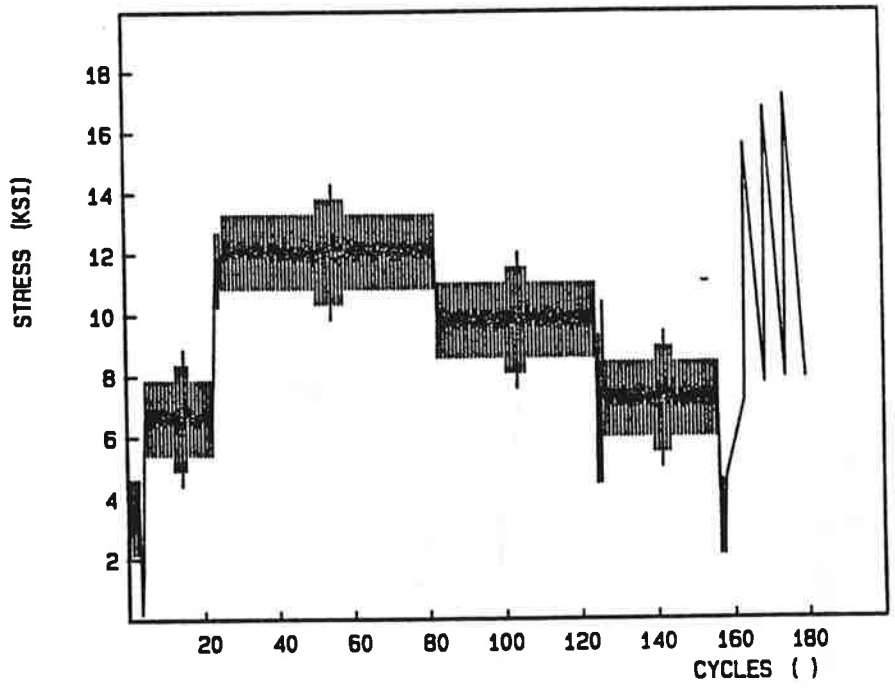

b. Area K

FIGURE 5-22. SHORTENED SPECTRUM, TOUCH AND GOES DELETED

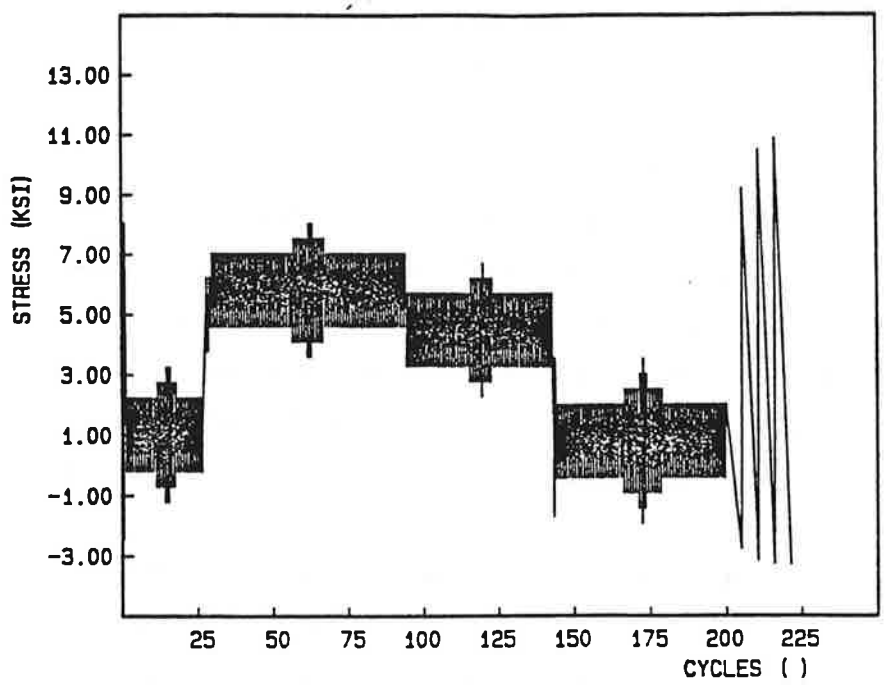

c. Area L

FIGURE 5-22. SHORTENED SPECTRUM, TOUCH AND GOES DELETED (CONCLUDED)

stresses vary appreciably. Also, the particular mission in the stress history is the only one: all flights are assumed to be equal. However, it should be noted that a small compensation is made for the fact that higher loads do occur from time to time. For this reason the last three cycles in all histories in Figures 5-20 and 5-22 are "make-up cycles". The first of the three occurs once in every 10 flights, the second occurs once in every 100 flights, and the third occurs once in every 200 flights.

For a comparison with the stress histories proposed here the following conditions were considered:

- Maximum differential pressure of 9 psi
- Fuselage weight of 65,000 pounds (for the military version for which the comparison was made)
- The critical points covered by Areas J, K, and L are at the forward and top of these areas which are the worst, as the stresses will be decreasing from there.

The stresses were calculated for these conditions using the procedure described in Section 5.4. From these the spectrum was obtained, and subsequently stress histories were determined, all in

accordance with the procedures described earlier in this section. The stress histories for Area J are shown in Figure 5-23. Note that there are five different types of flights. The stress histories for Areas K and L are similar, except that the stress values are different.

The objective of the computations was to show the effect of different methods of computing stress histories on predicted crack growth behavior. Therefore, the configuration and basic crack growth rate data used are immaterial, as long as the same situation and data are considered for both stress histories. Nevertheless, a configuration was chosen that is reasonably representative for aircraft structures, namely a through crack at a fastener hole (no load transfer), while the crack growth rate data were represented by a Walker equation with a coefficient of 3×10^{-9}, and exponents of 2 and 1, respectively.

The results of the computations for the three areas are shown in Figure 5-24. For Area J (the most critical for longitudinal stresses) the present history is conservative by a factor of two with regard to the manufacturer's history. For Area K they come out about the same, but for Area L the manufacturer's spectrum is far more conservative. Anticipated crack growth in the three areas according to the manufacturer's method of developing a stress history and according to the proposed method are shown in Figure 5-25. The proposed stress history would produce a much longer crack growth life in the area close to the neutral axis. This is reasonable, but rather insignificant, because inspection intervals would be based on the most critical area (Area J), where the proposed history is more conservative by a factor of two.

These relatively similar results must be considered with caution for the following reasons:

a. The manufacturer's stress history is the same in every flight; the proposed history recognizes that all flights are different.

b. The manufacturer's stress history recognizes that some load cycles occur at altitudes less that the cruising altitude, as shown in Figure 5-22, while the proposed histories implicitly assume that all cycles have the same mean stress. (It should be pointed out, however, that the cycles at lower mean stresses do not occur at a fixed mean either as assumed by the manufacturer.)

c. The manufacturer keeps the stresses the same over large areas, while the proposed history recognizes gradual stress gradients.

The stress history for Area J as shown in Figure 5-23 seems more representative of aircraft loading than the one shown in Figure 5-22a, despite the fact that Figure 5-22a reflects altitude differences. In reality the cycles at lower altitude (mean stress) are spread over different altitudes.

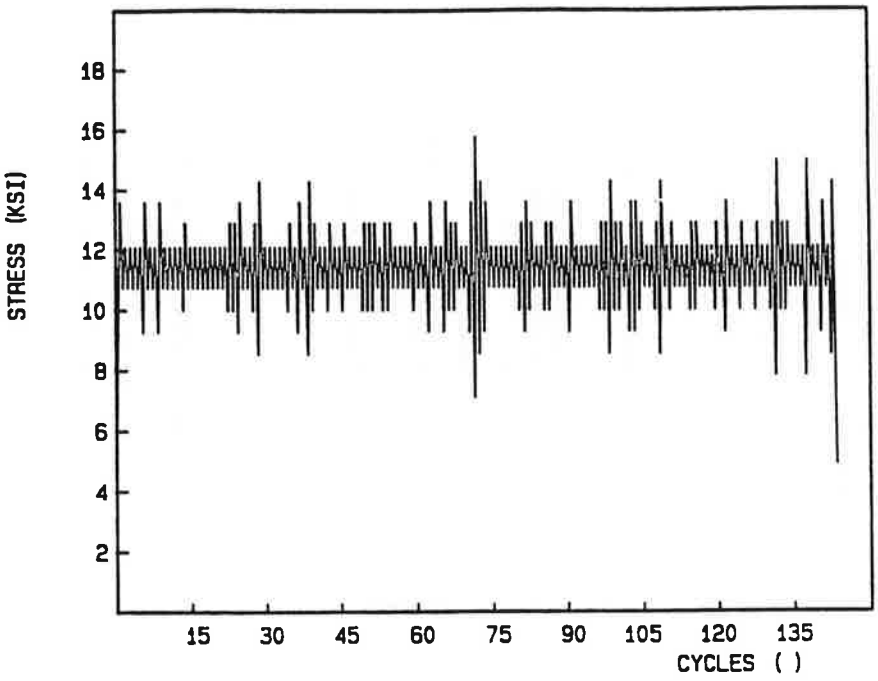

a. Flight Type 1 — Occurs 106 times in 133 flights

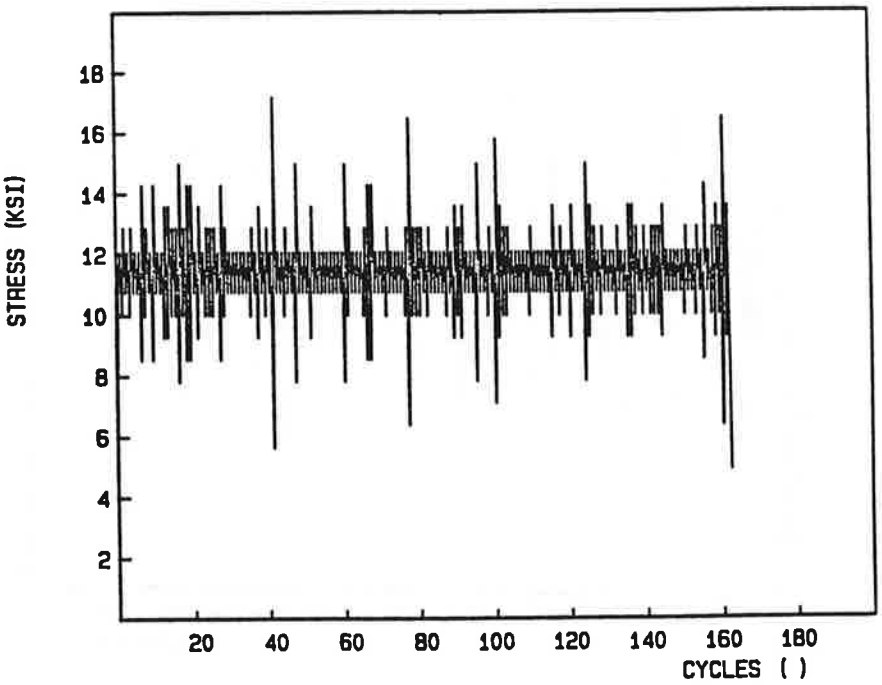

b. Flight Type 2 — Occurs 21 times in 133 flights

FIGURE 5-23. FLIGHT TYPES, EVERY OCCURRENCE WITH DIFFERENT SEQUENCE

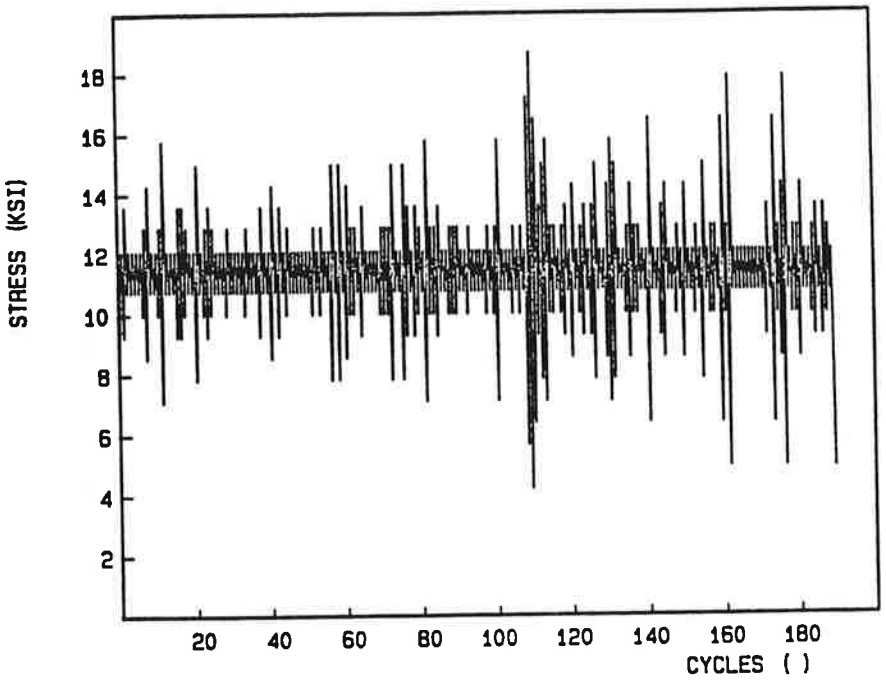

c. Flight type 3 - Occurs 4 times per 133 flights

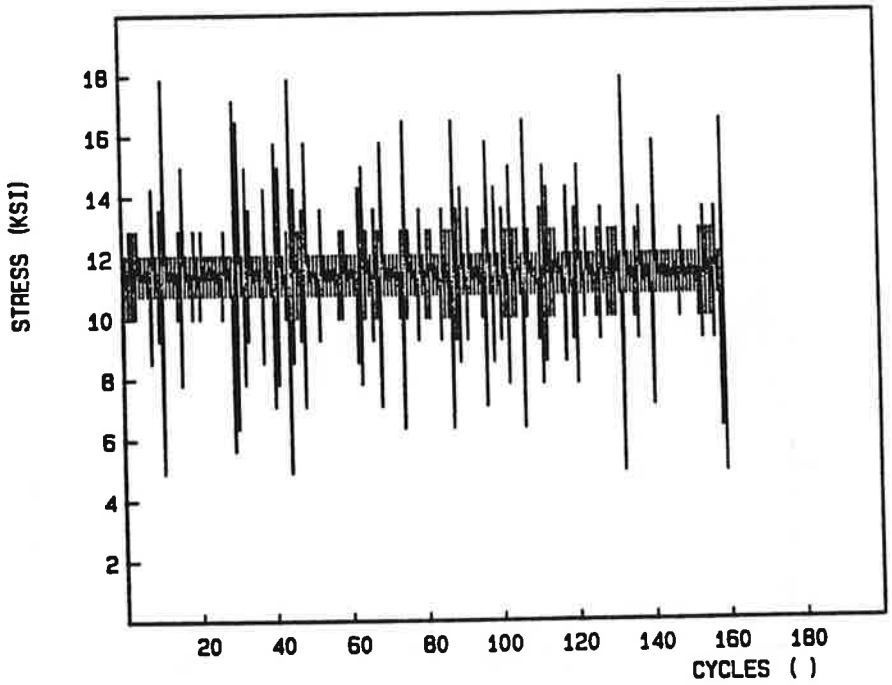

d. Flight Type 4 — Occurs once per 133 flights

FIGURE 5-23. FLIGHT TYPES, EVERY OCCURRENCE WITH DIFFERENT SEQUENCE(CONTINUED)

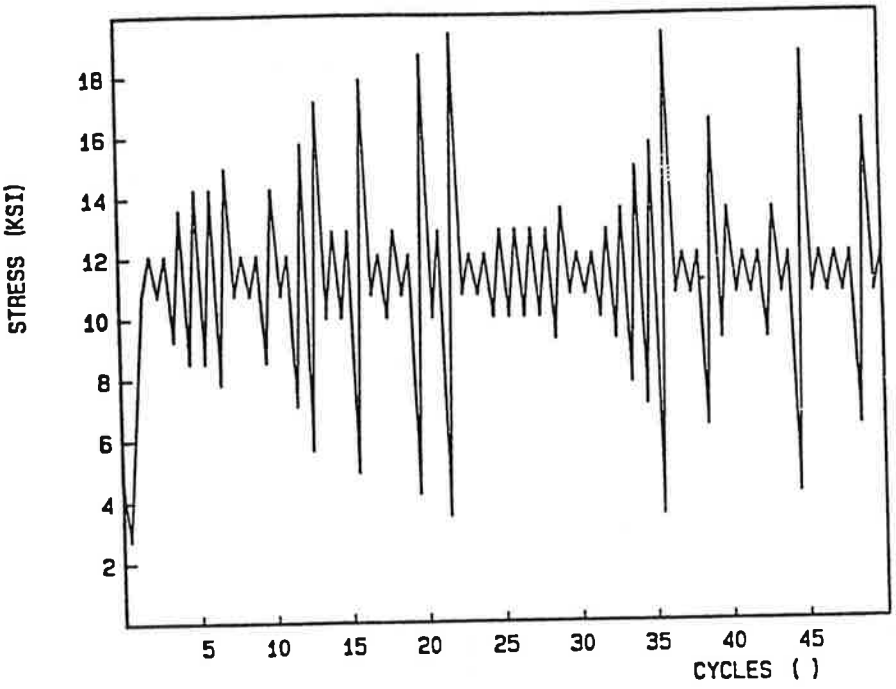

e. Flight Type 5 - Occurs once per 133 flights

FIGURE 5-23. FLIGHT TYPES, EVERY OCCURRENCE WITH DIFFERENT SEQUENCE (CONCLUDED)

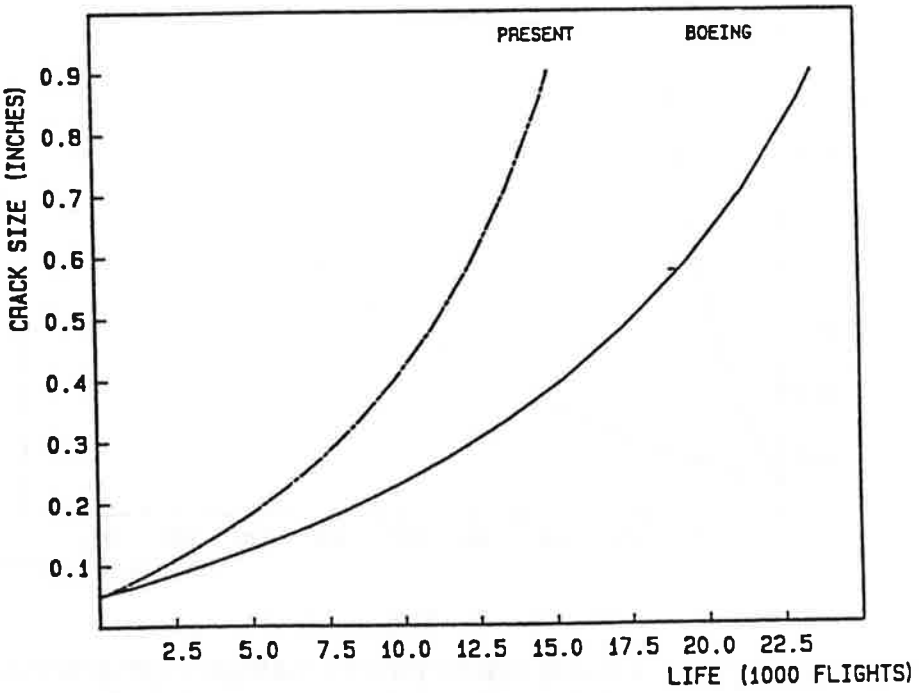

a. Run ID: 5742 — Area J

FIGURE 5-24. CRACK GROWTH COMPARISON OF BOEING AND PRESENT SPECTRUM

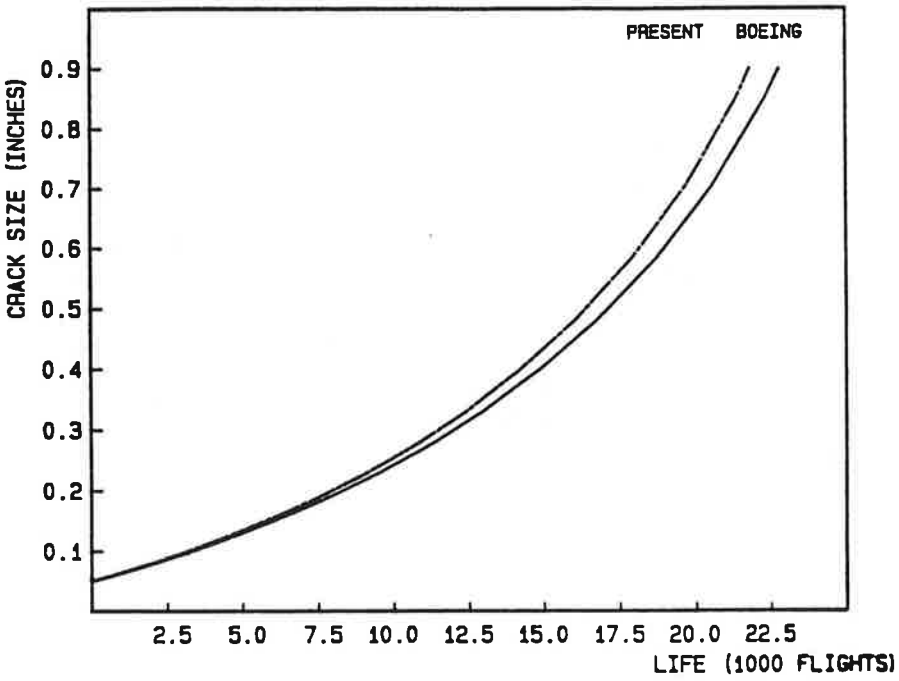

b. Run ID: 24657 — Area K

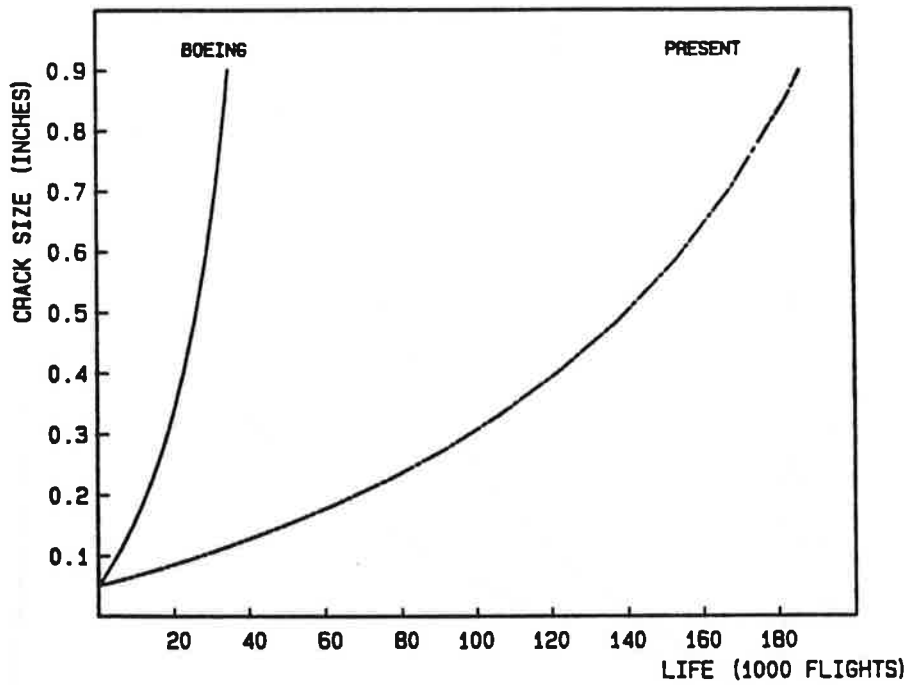

c. Run ID: 7387 — Area L

FIGURE 5-24. CRACK GROWTH COMPARISON OF BOEING AND PRESENT SPECTRUM (CONCLUDED)

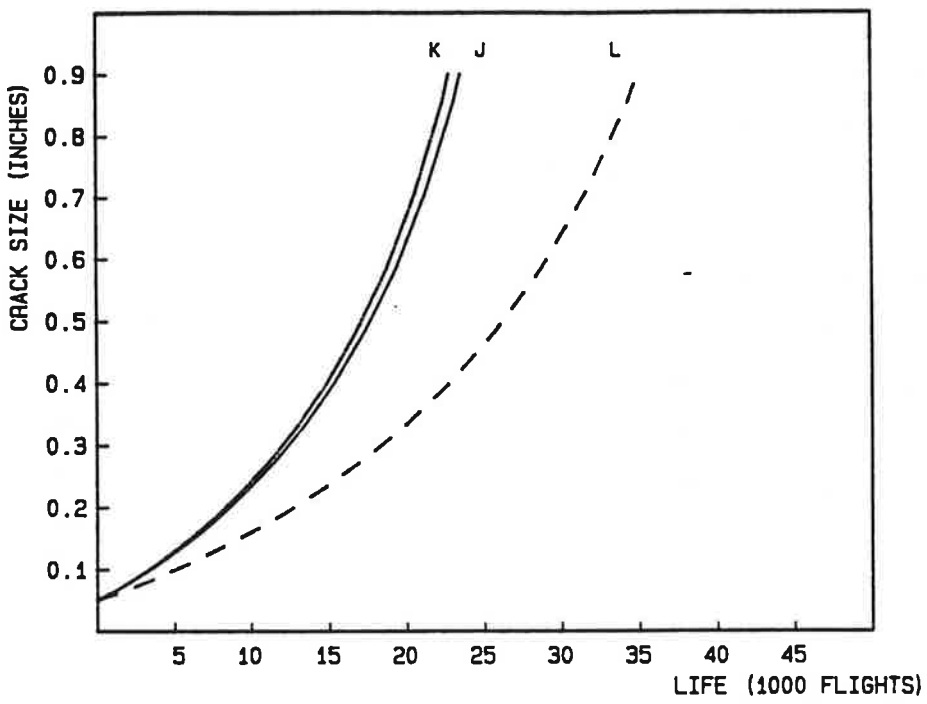

a. Run ID: 14835

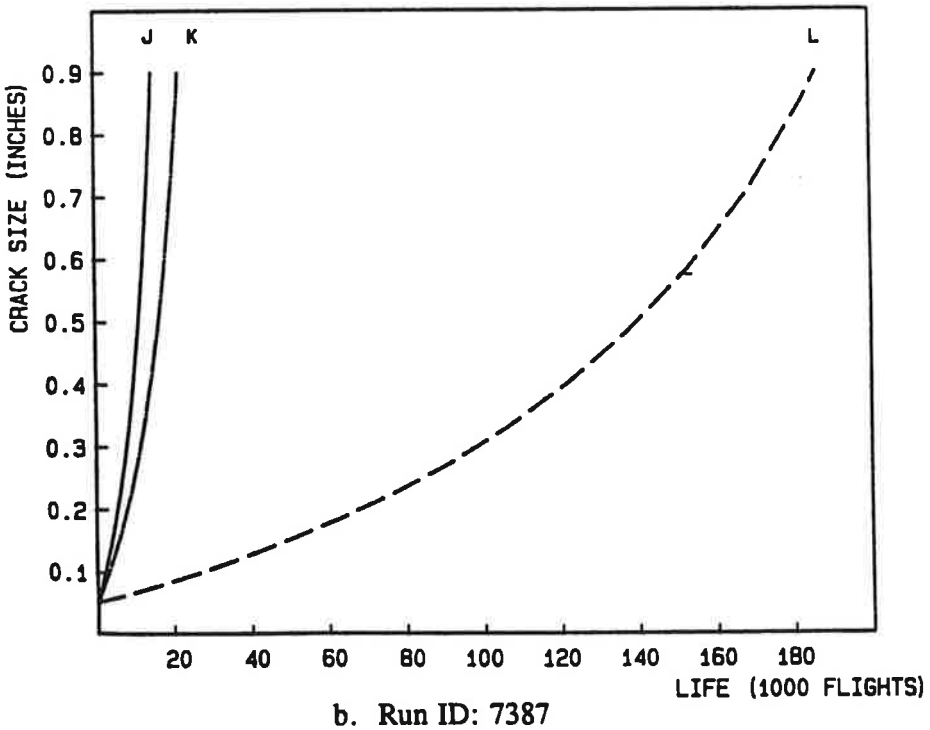

b. Run ID: 7387

FIGURE 5-25. CRACK GROWTH, PRESENT SPECTRUM FOR AREAS J, K, AND L

The manufacturer assumes that they will occur at a fixed (lower) altitude, while the present procedure assumes them at a fixed higher altitude (conservative). In any case, the issue is of secondary importance, because it affects only the R-ratio. The effect can be assessed by estimating the relative number of cycles occurring at lower R; the result is that the effect is at most a factor of 1.3. Considering the simplifications in taking all flights to be the same in the history and by assuming this history is valid for large areas, the effect of R is probably inconsequential.

Both stress histories are based on numerous assumptions; the proposed history is based upon measurements, is conservative with regard to R-ratio effects, and is more realistic in accounting for different flight profiles. While the proposed method derives the stresses from generalization and simplification of the structure, the manufacturer's method does also, and results in essentially the same stress history.

6.0 REPAIRED PANEL TESTING

The goal of this effort was to select some common repairs, analytically predict their behavior, and conduct fatigue experiments on them to substantiate the predictions. The plan was to test simple flat panel doubler designs, 20 inches in width, evaluate the relative fatigue quality of a range of commonly used simple fuselage panel repairs to verify anticipated trends and provide basic data for designated engineering representatives (DER's) and airline repair engineers. The loading was to be uniaxial constant amplitude cycling to simulate pressurization cycles only.

6.1 Specimen and Fixture Designs

The three commonly used fuselage doubler repairs are shown schematically in Figure 6-1. A Type I (or Type A)[19] fuselage repair is a permanent repair that restores the aircraft's normal inspection requirements. Such a repair often incorporates internal doublers, layered external doublers and solid fasteners. By comparison, a Type II (or Type B) fuselage repair has a design life less than the original design goal for the aircraft, and it generally requires repetitive inspections. A Type II repair often incorporates layered external doublers and solid fasteners (but not internal doublers).

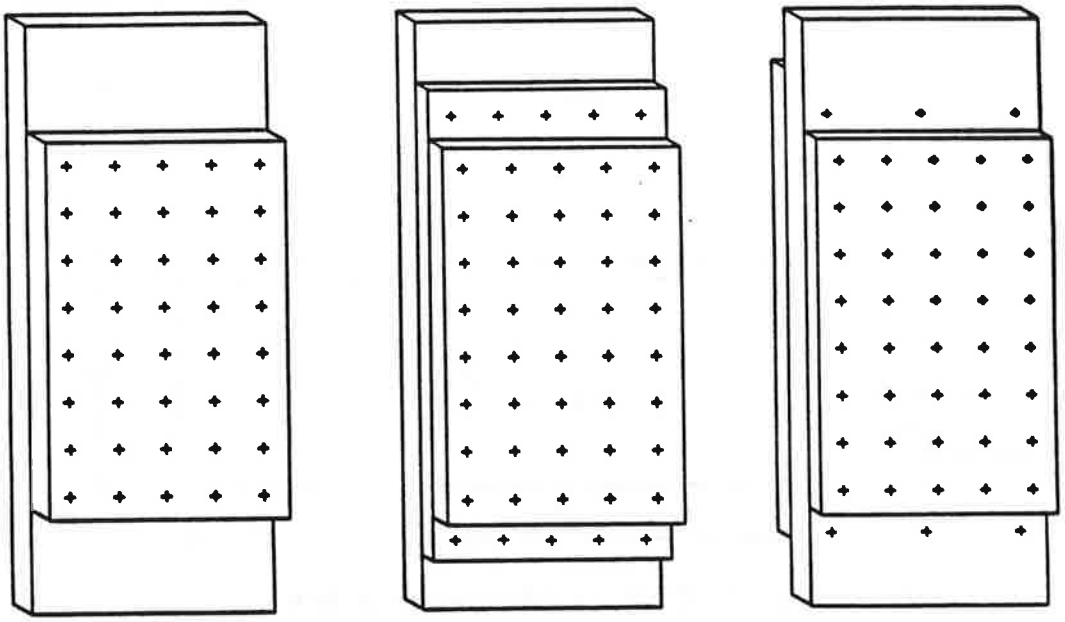

FIGURE 6-1. COMMON FUSELAGE DOUBLER DESIGNS

Type III (or Type C) fuselage repairs are temporary repairs. The expected life of a Type III repair will generally be less than the life of a Type II repair. The design of a Type III repair is often similar to a Type II repair, except that blind, protruding head fasteners are often used, instead of solid fasteners, because internal access during installation of the repair is not required. Drag increases with Type III repairs may result in some performance penalties, but these repairs are normally replaced by a Type I or II repair at some prescribed number of flights.

In actual practice different types of repairs are often used depending on the specific situation. The choice between a Type I repair and a less permanent repair depends on the tradeoff between the time and cost of periodically removing major components when performing inspections, and the added time and cost of performing a Type I repair.

The test specimen was 20 inches in width with a single row of countersunk rivets along the specimen centerline (to simulate a pre-existing row of rivets at a stringer) as shown in Figure 6-2.

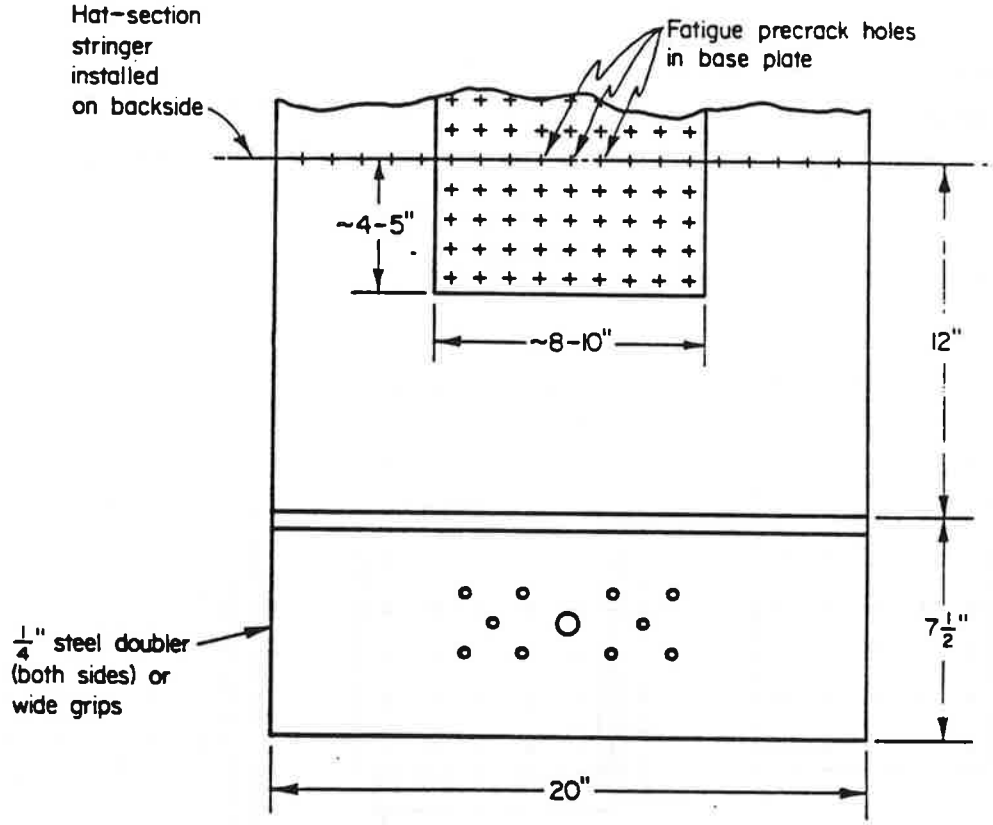

FIGURE 6-2. TYPE III, DOUBLER SPECIMEN DESIGN

The material chosen was 2024-T3 clad sheet, in 0.040 and 0.050 inch thicknesses. The specimen shown here represented a Type III, or temporary repair. It consisted of a single doubler applied on the outside of the "fuselage" over a cutout (to remove prior damage). To simulate the lack of

internal access, blind rivets were specified. Beyond Type III repairs, both Type I and Type II doubler repairs were also to be examined, but the experimental effort was discontinued before that work could be undertaken.

Before proceeding with testing it was necessary to demonstrate that the loading arrangement for the samples was adequate to produce nearly uniform stresses across the test section of the test samples. A finite element analysis of the first candidate loading arrangement showed an uneven stress distribution over the central section of the repair panel. One simple solution that was considered was a substantial elongation of the test sample, but this was deemed impractical because of the available panel widths and practical constraints imposed by the available test systems. As a relatively simple alternative, in order to obtain a more uniform stress distribution across the center of the repair panel, a spreader bar (or "whiffletree") assembly was designed. Figure 6-3 shows a plan view of the assembly.

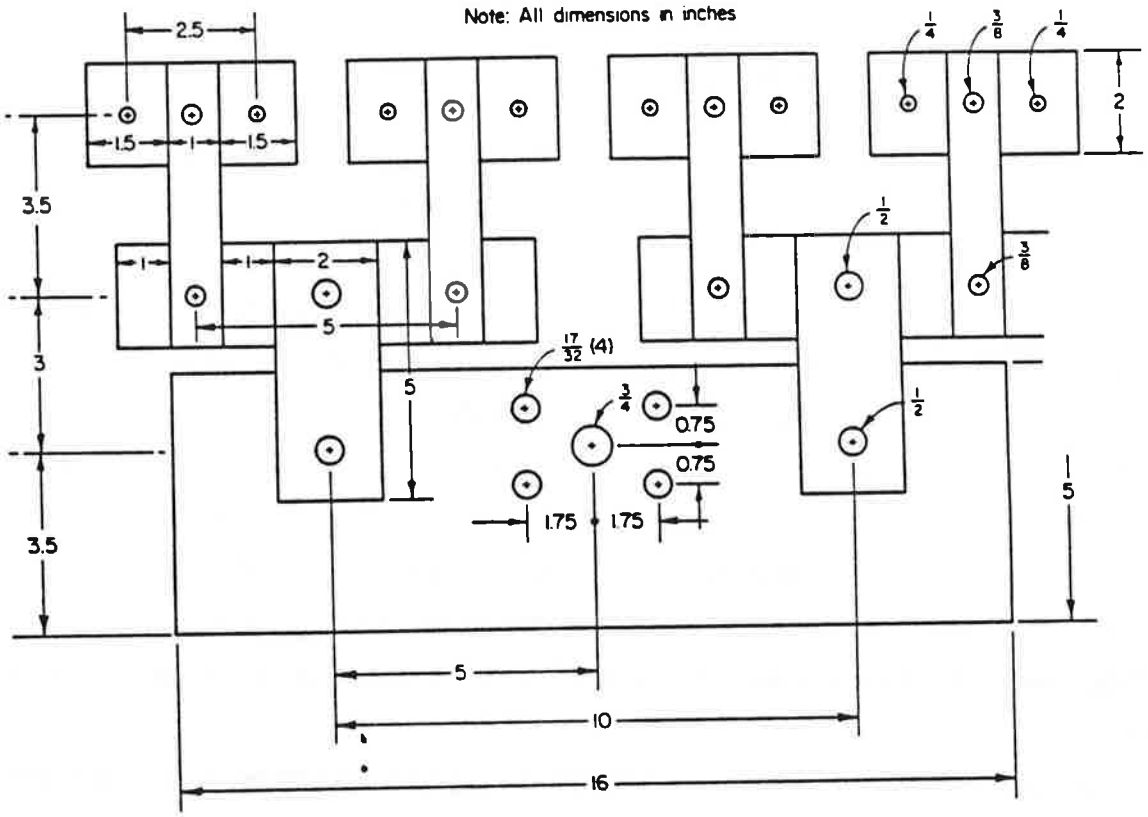

FIGURE 6-3. SPREADER BAR OR WHIFFLETREE FIXTURE DESIGN

Figure 6-4 shows the results of a finite element analysis on a symmetrical 1/4 section of the specimen loaded with these grips. The computed stresses in the repair section were constant across the center of the sample within 98 percent accuracy.

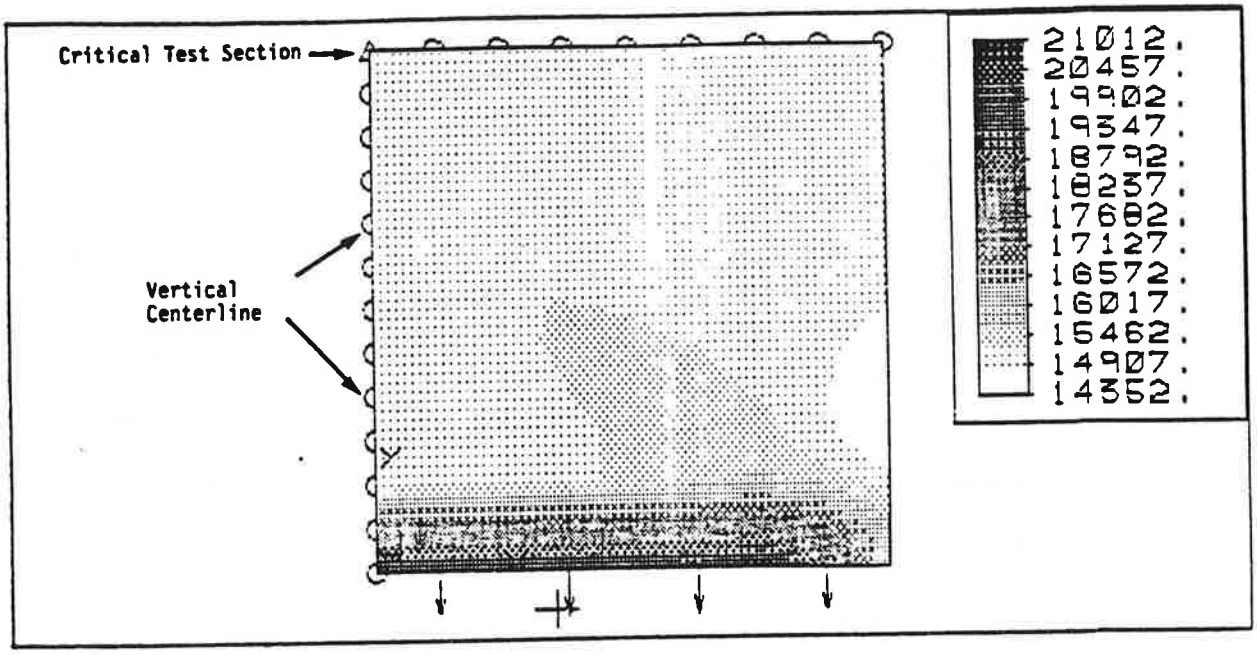

FIGURE 6-4. FINITE ELEMENT ANALYSIS OF 1/4 REPAIR PANEL

When the grip assembly was completed, a blank specimen was prepared and strain gaged and the uniformity of the stress field in the repair section was confirmed experimentally. This was done by fabricating a test panel without fastener holes and then strain gaging it. Figure 6-5 shows the test panel with the gage locations identified. The panel was loaded in increments to 16,000 pounds and strain readings were taken at 0, 5000, 10,000, and 16,000 pounds (which corresponded to stress levels of approximately the same magnitude in ksi, since the cross-sectional area of the sample was about 1 in^2). The range of variation in strains within the row of gages 7 inches off of the centerline was within $\pm$ 6 percent, with the higher readings near the center of the sample as expected. The variation in strains from nominal along the centerline of the sample was smaller (within $\pm$ 3.5 percent), again with the lower readings near the edges. These results were considered sufficient evidence that the nominal stress variations within the region of the doubler repairs would be small.

It is required by the FAA that known fatigue cracks be removed before a repair is completed. As a result, the removal of fatigue damage prior to repair is common practice in the field, as indicated by detail procedures recommended in SRM's for both B737 and DC-10 aircraft. Therefore, it was decided that the damaged condition should be represented by the insertion of a cut-out in the base sheet, just as is recommended in most SRM's for a fuselage skin repair over a stringer.

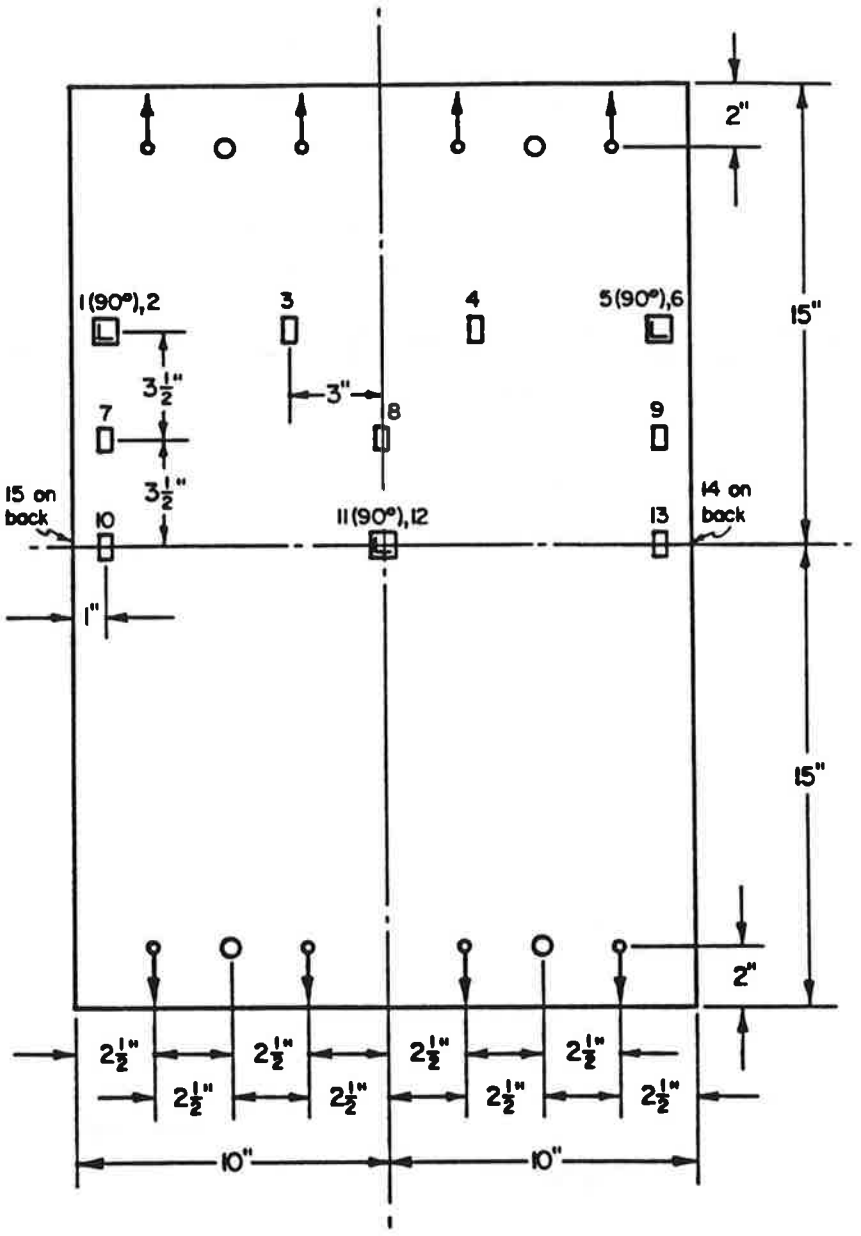

FIGURE 6-5. STRAIN UNIFORMITY VERIFICATION SAMPLE

An OKUMA MC-5VA numerically controlled machine was used to automatically and accurately position all of the fastener holes in the repair sections. Typical aircraft fastener installation procedures were used by experienced technicians. Installation tooling was loaned to Battelle by the fastener supplier (Allfast Fastening Systems). First, BAC R15CE4D 3C countersunk solid rivets were installed in the repair panels. Then NAS 1398D 5AZ blind rivets were used to install the doublers on these panels.

6.2 Experimental Plan

This test plan investigated the effects of skin thickness for baseline samples and Type III repairs. The test matrix is shown in Table 6-1. The focus of these experiments was to provide baseline fatigue properties for undamaged fuselage skin material and demonstrate the effect of doubler

TABLE 6-1. MATRIX OF EXPERIMENTS

Test Series	Inner Layers	Skin	Outer Layers	Fastener System	Damage Cutout?
1a	–	Small coupons			
(5 ea)	–	0.04"			No
(5 ea)	–	0.05"			No
1b	–	Single row unfilled holes			
(5 ea)	–	0.04"			No
(5 ea)	–	0.05"			No[1]
1c	–	Single row filled holes			
(5 ea)	–	0.04"			No[1]
(5 ea)	–	0.05"			No[1]
2a	–	Standard hole pattern			
(3 ea)	–	0.04"	0.5 X Skin	Blind, Protruding	No[1]
(3 ea)	–	0.04"	"	"	Yes[1]
(3 ea)	–	0.05"	"	"	No[1]
(3 ea)	–	0.05"	"	"	Yes[1]
2b					
(3 ea)	–	0.04"	1 X Skin	Blind, Protruding	No[1]
(3 ea)	–	0.05"	"	"	Yes[1]
(3 ea)	–	0.05"	"	"	No[1]
(3 ea)	–	0.05"	"	"	Yes[1]

thickness on the fatigue resistance of Type III repairs. They also provided important information on the actual stress distributions within these simple repairs as compared to analytical predictions.

Five specimen designs were used in the first series of experiments. Simple, unnotched dogbone specimens, as shown in Figure 6-6 were used for the Test Series 1a experiments. The

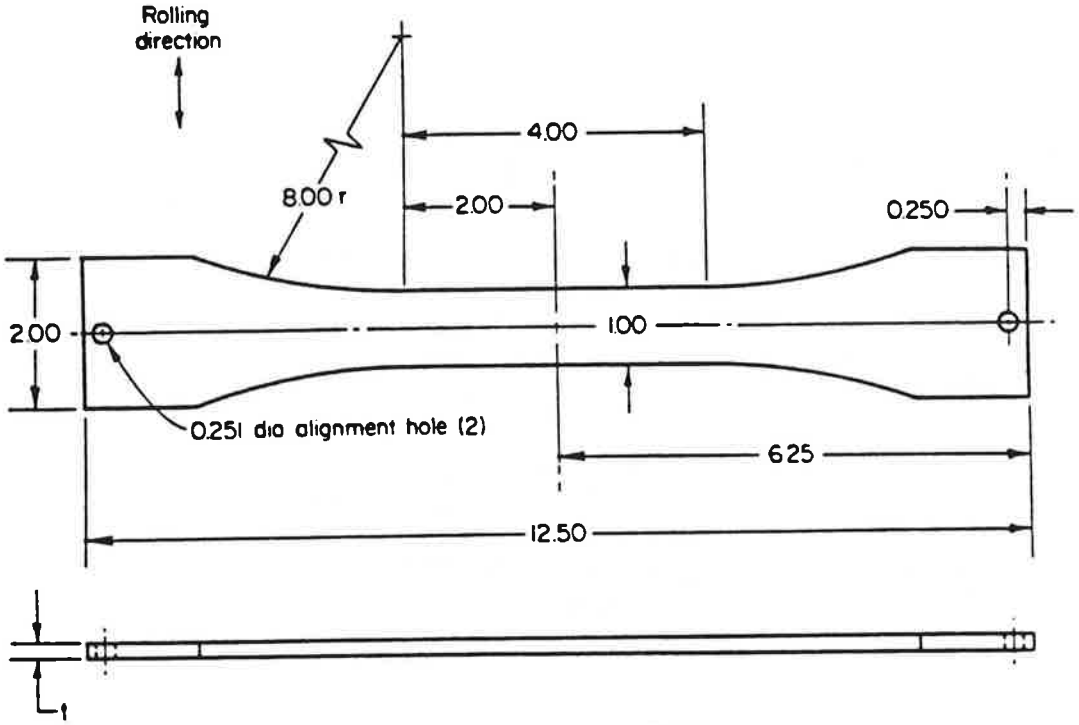

Notes: 1. Reference: ASTM designation E466.
2. All dimensions in inches.
3. Scale: 0.5" = 1"

FIGURE 6-6. UNNOTCHED DOGBONE SPECIMEN DESIGN

Series 1b and 1c specimen design is shown in Figure 6-7. These tests provided baseline fatigue properties for the skin material with countersunk holes drilled but no fasteners installed. These tests also provided information on the amount of time spent in propagating a fatigue crack from the inside of the countersunk hole to the surface of the skin, where it would normally be visually inspectable. The filled-hole experiments also provided baseline fatigue properties for a simulated fuselage skin at a longitudinal stringer.

Test Series 2a and 2b focussed on simple variations in Type III doubler repairs to isolate effects of base skin thickness, doubler thickness and skin repair (cutout) on fatigue crack initiation and growth properties. Blind protruding head rivets were used for all of these doubler repairs as shown in Figures 6-8 and 6-9.

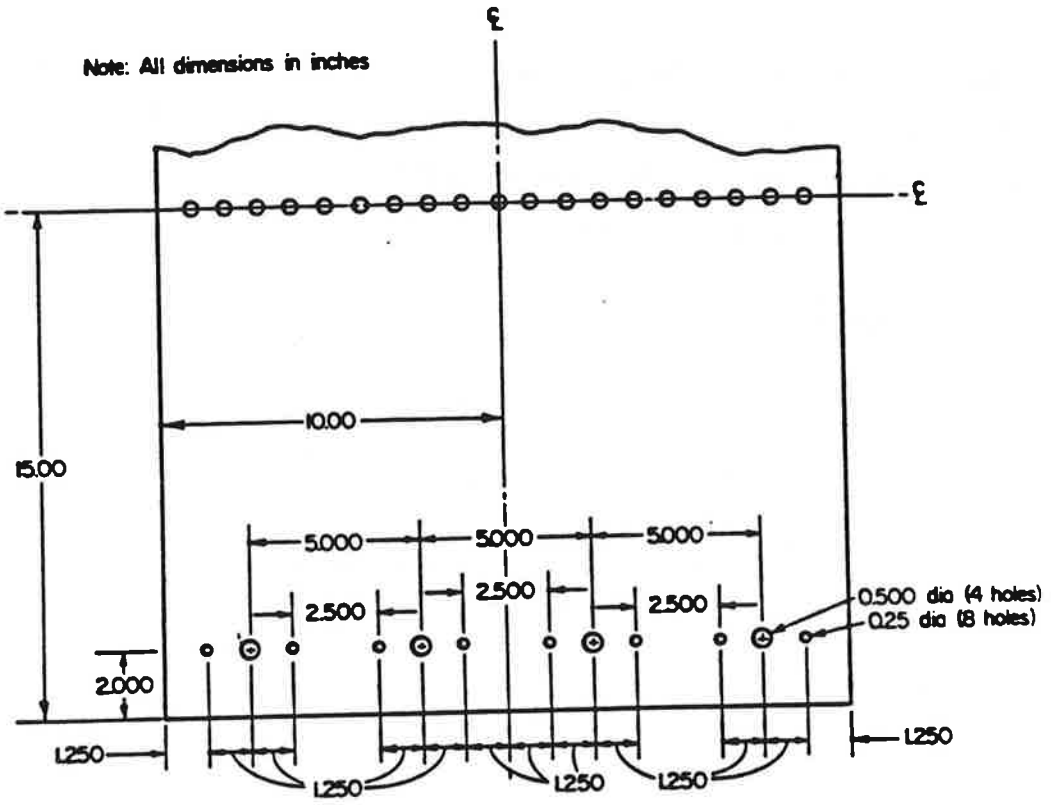

FIGURE 6-7. BASELINE REPAIR SAMPLE WITH UNFILLED AND FILLED COUNTERSUNK HOLES

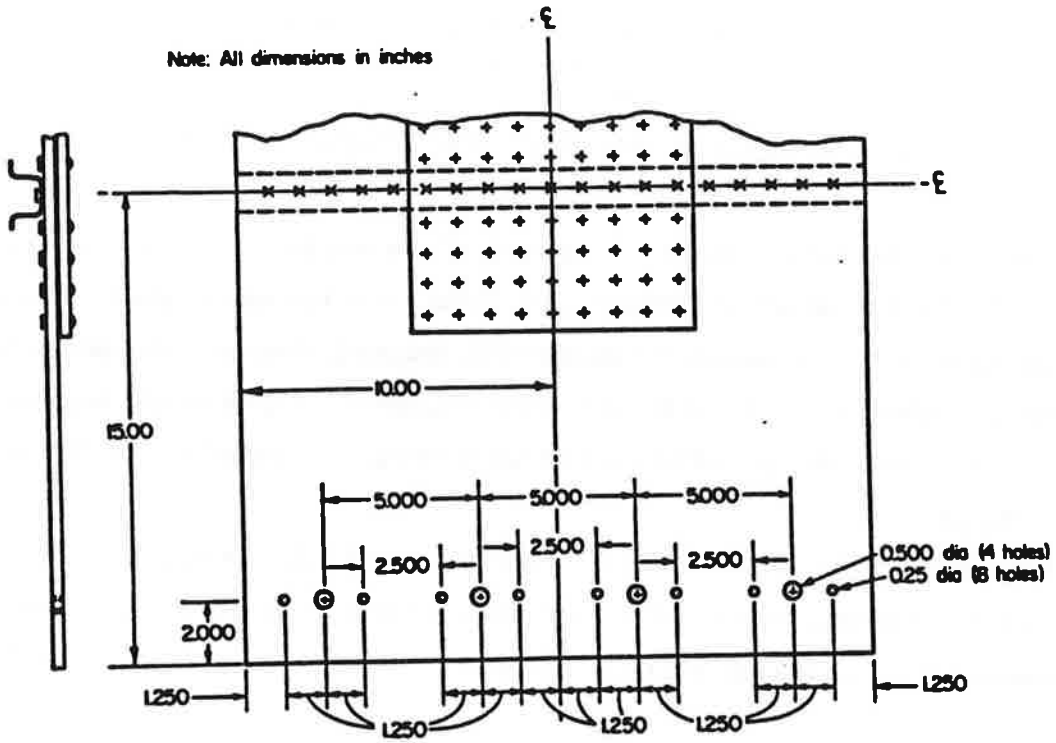

FIGURE 6-8. REPAIR SAMPLE WITHOUT CUTOUT

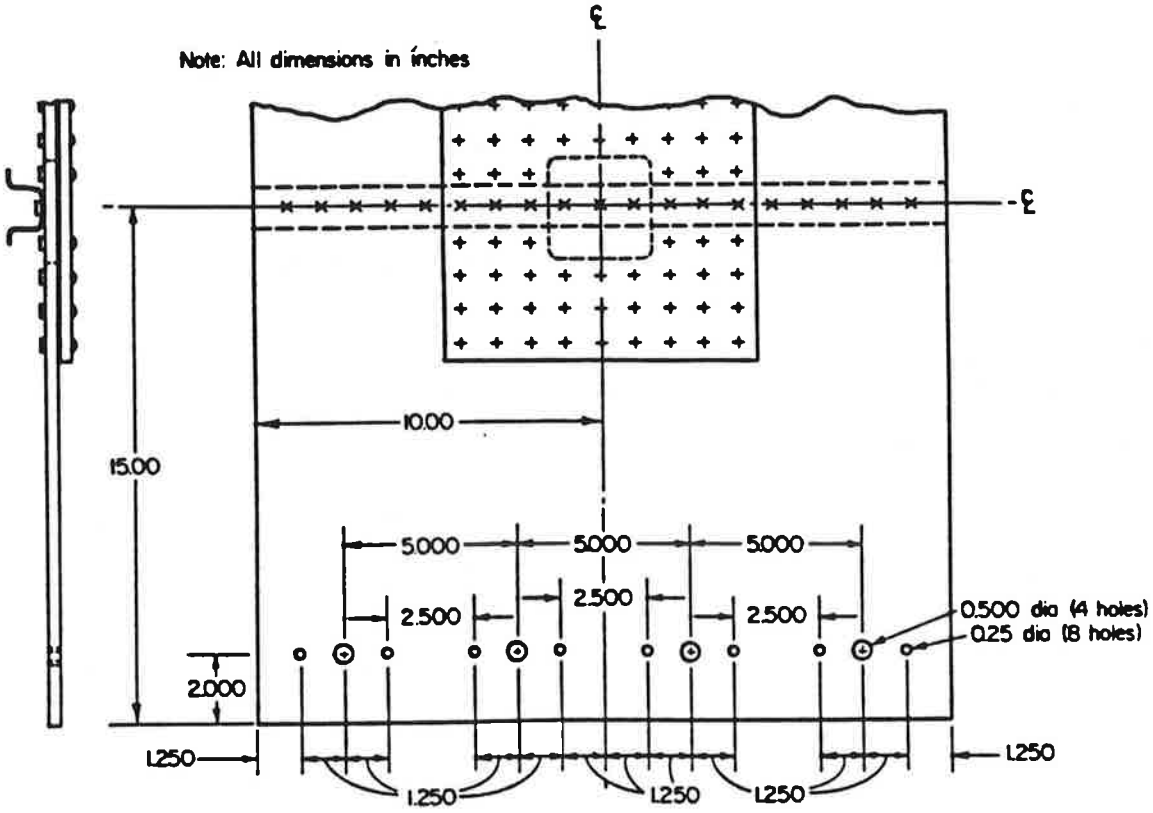

FIGURE 6-9. REPAIR SAMPLE WITH CUTOUT

6.3 Repair Program Fatigue Experiments

6.3.1 Baseline Fatigue Experiments. Table 6-2 documents Phase I baseline fatigue experiments that were completed. A total of 12 samples were tested, six of the 0.040-inch-thick material and six of the 0.050-inch thick material. All samples were tested at a stress ratio of 0.10. The scatter between test results for comparable test conditions was relatively small. The cycles to failure diverged slightly at the lower stress levels for the different material thicknesses. This difference was not considered significant for this study, though, since fatigue lives ranging from 100,000 to 250,000 cycles were the primary focus for repair panel testing. In this range, the fatigue behavior for the two aluminum thicknesses did not vary appreciably. Limited data are available in the literature on 2024-T3 clad sheet. A 1955 NACA report[20] provided some data on 0.032 inch sheet material. However, these data were generated at constant mean stress levels different than those of interest in the current study. To produce approximately comparable fatigue life estimates for the same conditions tested with the new base material, fatigue lives were estimated from the following equivalent stress expression[21], which was optimized to fit the NACA data:

$$\text{Log } N_f = 6.91 - 1.48 \log (S_{eq} - 15) \qquad (6\text{-}1)$$

where, with the exponent, m, equal to approximately 0.55

$$S_{eq} = S_{max}[1.0-R]^{m} \quad (6\text{-}2)$$

TABLE 6-2. SUMMARY OF BASE MATERIAL FATIGUE TEST DATA

Sample Thickness, in.	0.039	0.048	0.032[1]
Maximum Stress[2], ksi	(Specimen Number) Cycles to failure		
45	(2) 67,200	(9) 59,600	59,500
45	(3) 80,700	(8) 62,000	
30	(1) 239,100	(7) 338,000	174,000
30	(4) 228,700	(10) 320,300	
20	(5) 1,145,500	(11) 10,361,500[3]	1,090,000
20	(6) 1,162,000	(12) 10,358,000[3]	

(1) 1955 NACA Report, Reference [18].
(2) Stress ratio of 0.10 for all samples.
(3) Did not fail.

In the mid-life range of interest both thicknesses of the current material corresponded reasonably well in terms of fatigue resistance with the previously reported clad sheet data. As might be expected the 0.040 clad sheet material more closely matched the fatigue trends of the previously studied 0.032 clad sheet material.

6.3.2 Repair Panel Fatigue Experiments. Table 6-3 summarizes the results of repair panel fatigue experiments that were completed. A coordinate system based on rivet location, as shown in Figure 6-10, is used in the comments section of this table to describe the sites of crack initiation. Specific observations made on selected samples are summarized in the following paragraphs.

Repair Sample 15. This sample contained a single row of countersunk, unfilled holes along the center line. This sample was not instrumented for crack detection. The first cracks were observed in the third, fourth and fifth holes to the right of the center of the sample at 163,000 cycles. The cracks grew from this area, and subsequently, in adjacent holes. At 164,000 cycles cracks were detected in the third and fourth holes to the left of center of the sample. The cracks on both sides of

TABLE 6-3. RESULTS OF TEST ON BASELINE AND TYPE III REPAIRS

Type of Specimen	No.	t(Skin) (in.)	t(Patch) (in.)	σ_{max} (ksi)	Cycles (to initiation)	Cycles (to failure)	Comments
Baseline (unfilled holes)	14	0.039	--	15		42,530	Failed in Grips
	15	0.039	--	15	163,000	167,430	Init @ (3,0), MSD
	16	0.048	--	15	106,780	148,050	Init @ (-1,0), No MSD
	21	0.039	--	18	68,360	93,580	Init @ (5,0)
	26	0.039	--	18	76,170	104,030	Init @ (-9,0), (12,0), MSD
Baseline (solid rivets)	17	0.048	--	15		657,800	Did not fail
	17	0.048	--	18	86,580	106,950	Init @ (-11,0), No MSD
	22	0.039	--	18		320,800	Did not fail
	27	0.049	--	18		567,860	
Type III (no cutout)	18	0.048	0.048	15		315,100	Did not fail
	18	0.048	0.048	18	unknown	21,730	
	19	0.039	0.038	18	94,110	96,620	Init @ (0,4) (Top rivet row)
	23	0.038	0.039	18	135,680	136,580	Init site unknown
	24	0.048	0.024	18	192,760	196,510	Init @ (4,-4),(0,-4), MSD
	30	0.039	0.019	18	126,000	152,210	Init between (-4,-4) and (-4,-3)
	31	0.048	0.048	18	156,870	160,920	Init (3,4) and (4,4)
Type III (Cutout)	25	0.039	0.039	18	148,480	149,220	Init @ (2,-4), (-1,4)(-2,4) (-3,4)(-4,4) MSD
	20	0.049	0.024	18		105,670	Failed @ edge of cutout
	28	0.048	0.048	18	181,670	187,910	Init @ (-4,4), MSD
	29	0.038	0.019	18	159,920	166,410	Init @ (-3,-4)

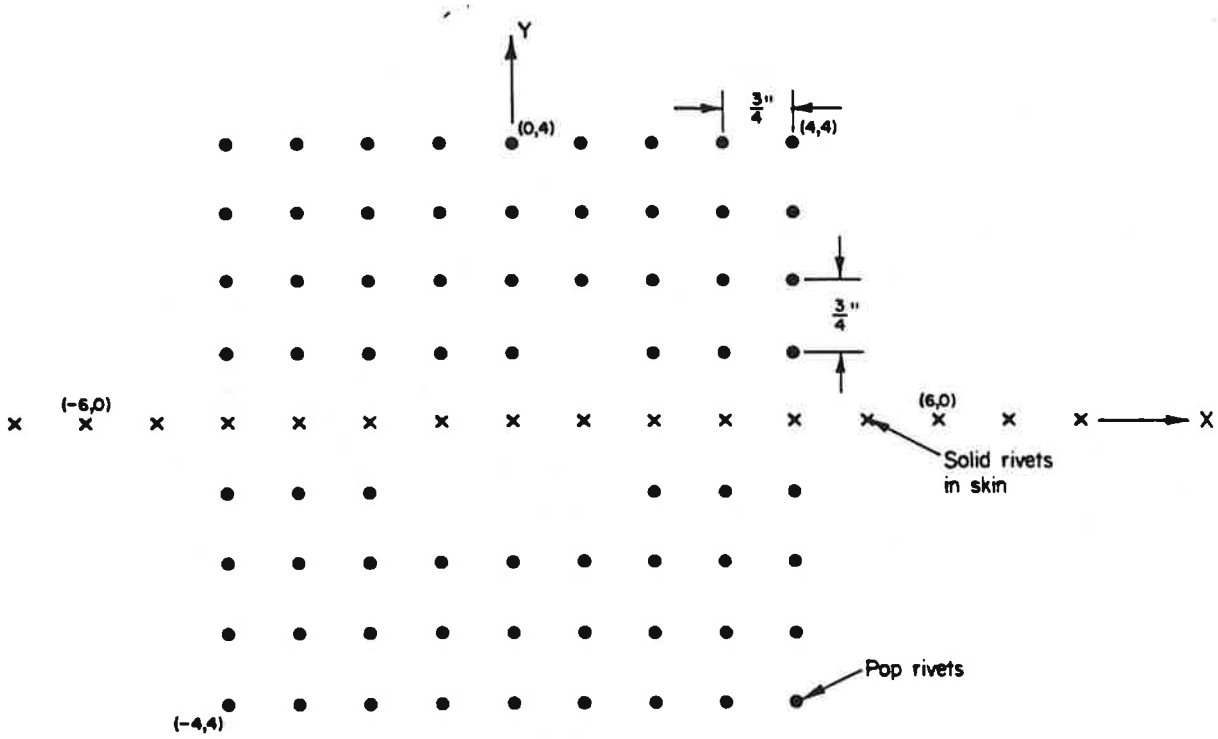

FIGURE 6-10. RIVET LOCATION COORDINATE SYSTEM

the sample continued to grow and join up until approximately the center third of the sample was cracked. At this point the entire sample failed. The total cycles to failure was 167,430.

Repair Sample 16. This sample also contained a single row of countersunk, unfilled holes along the center line. This sample was instrumented with crack detection gages on both sides of each hole. The first crack was detected on the right side of the first hole to the right of center at 106,780 cycles. A crack was detected on the other side of the first hole at 115,880 cycles. Cracks were detected at the third and fourth holes to the right of center at 136,060 cycles. The sample failed at 148,050 cycles.

Repair Sample 17. Sample 17 contained a single row of countersunk, solid rivets along the center line. The sample was instrumented with crack detection gages on each side of the rivet heads. No detectable cracks formed after 657,800 cycles at a maximum stress of 15 ksi, so the maximum stress was raised to 18 ksi and the test continued. The first crack was detected on the right side of the fifth hole to the right of center at 86,580 cycles. A crack was detected on the left side of Hole 5 at 92,050 cycles. The crack in Hole 5 grew to Hole 4 and another crack was detected at the right of Hole 3 at 93,020 cycles. A crack was detected to the right of Hole 4 at 103,780 cycles and another was detected in the left of Hole 6 at 105,280. The sample failed at 106,950 cycles beyond the initial 657,800 cycles.

TABLE 6-4. FATIGUE LIFE STATISTICS FOR REPAIR PANELS TESTED AT A MAXIMUM STRESS OF 18 KSI, R = 0.10

Sample Type	Skin Thickness, inch	Skin to Doubler Thickness Ratio	Average Fatigue Life	Specimen Numbers
Repair Panels				
With cutout	0.039	1.0	149,220	25
	0.048		187,910	28
With cutout	0.039	2.0	166,410	29
	0.048		105,670	20
Without cutout	0.039	1.0	116,604	19, 23
	0.048		160,920	31
Without cutout	0.039	2.0	152,210	30
	0.048		196,510	24
Baseline Panels				
Unfilled holes	0.039	N/A	98,805	21, 26
Filled holes	0.039	N/A	320,800	27
	0.048		567,860	27

[1] Failed at edge of cutout.
[2] Did not fail, test discontinued.

Each of these variables was found to be significantly correlated with fatigue life. The positive correlation between fatigue life and skin thickness most likely resulted from the somewhat superior fatigue resistance of the thicker material, as reflected in the simple coupon fatigue experiments (Table 6-2). The negative correlation of fatigue life with doubler thickness is attributable to the fact that thinner doublers pick up less load from the base panel, thereby producing lower local cyclic stresses at the outer rivet rows.

For the range of conditions tested, variations in skin thickness produced the greatest impact on fatigue life, with variations in doubler thickness producing a secondary, and opposite effect on fatigue life. However, without a broader range of experimental data to support these trends, Equation (6-3) should not be used to attempt an optimized doubler fatigue design.

A modest positive correlation between cutout width and fatigue life is also evident. However, this relationship only holds when correlating cutout width with outer rivet row fatigue failure modes. If the possibility of cutout fatigue failure is considered, it is evident that cutouts above a certain size,

Repair Sample 18. This sample contained a repair patch that was of the same thickness as the base material. There was no cutout in the base sheet. This sample was used for the rivet displacement measurements described in Section 6.4. The sample ran for 315,100 cycles at a maximum stress of 15 ksi without developing any visible cracks. The maximum stress was raised to 18 ksi and the counter reset. The sample failed along the bottom row of rivets in the repair panel at an additional 21,730 cycles. Fatigue cracks were evident in three of the interior holes from this row of rivets. A single fatigue crack was detected in the opposite outer row of rivets, again near the center of the patch. For this configuration the early indications were that fatigue cracking would generally not begin at the corners of the patch, but would start at one or more of the inner rivets in the outside rows. This result was not anticipated because analytical predictions suggested that the corner rivets would be most critical, although only slightly more so than the inner rivets in the outside row. Slightly higher than nominal stresses at the center of the test panels probably contributed to this trend.

After these initial experiments a decision was made to use a stress level of 18 ksi as a standard for the remainder of the Phase I repair experiments. The requirement to use this relatively high stress level (compared to in-service fuselage pressurization stresses) to produce "reasonable" fatigue lives was not too surprising considering the fact that the countersunk rivets in the skin were selected to avoid feather edges, typical of most current aircraft designs. It was also decided that it would be prudent to use crack detection (continuity) gages along both outer rows of rivets to provide additional, detailed information concerning exactly when and where the fatigue cracks typically initiated.

Table 6-4 summarizes the fatigue crack initiation life statistics for the tested repair samples. The data are subdivided by base skin thickness because it was evident for almost all conditions that the 0.039 inch 2024-T3 clad sheet repair panels provided lower fatigue resistance than the 0.048 inch repair panels. Table 6-4 also suggests an interesting relationship between the size of the cutout and doubler thickness. For the repairs without a cutout, fatigue lives tended to go down as the thickness of the doubler was increased. The fatigue lives dropped from over 500,000 cycles with no doubler, to 131,000 cycles when a doubler was added of the same thickness as the skin.

The critical parameters related to the observed fatigue lives for these repair panels can be described in the following expression:

$$N_f\ (X\ 10^{-5}) = 2.304\ (D_1) - 0.687\ (D_2) + 0.116\ (D_3) \qquad (6\text{-}3)$$

where

D_1 = Skin thickness (X 20), inch
D_2 = Doubler thickness (X 20), inch
D_3 = Cutout width, inch.

combined with relatively thin doublers, will almost certainly move the fatigue failure site to the cutout (as occurred with Specimen No. 20), away from the outer row of rivets. Of course, this is a condition that the repair is normally supposed to remedy, but it also shows the tradeoffs that must be made in effective fatigue design of a doubler repair.

These results reinforce the concept that there should be an optimum size (as well as thickness) for the doubler for a particular skin thickness and cutout size.

6.4 Doubler Strain and Displacement Measurements

Two COD-type clip gages were developed for rivet displacement measurements. These gages were designed to span two adjacent rivets in order to precisely measure their relative displacements. One of these gages was calibrated and used to measure the displacements of the first two rows of rivets above the centerline of the sample and the displacements of the last two rows of rivets (see Figure 6-11) in one of the repair panels. Table 6-5 shows the results of these measurements.

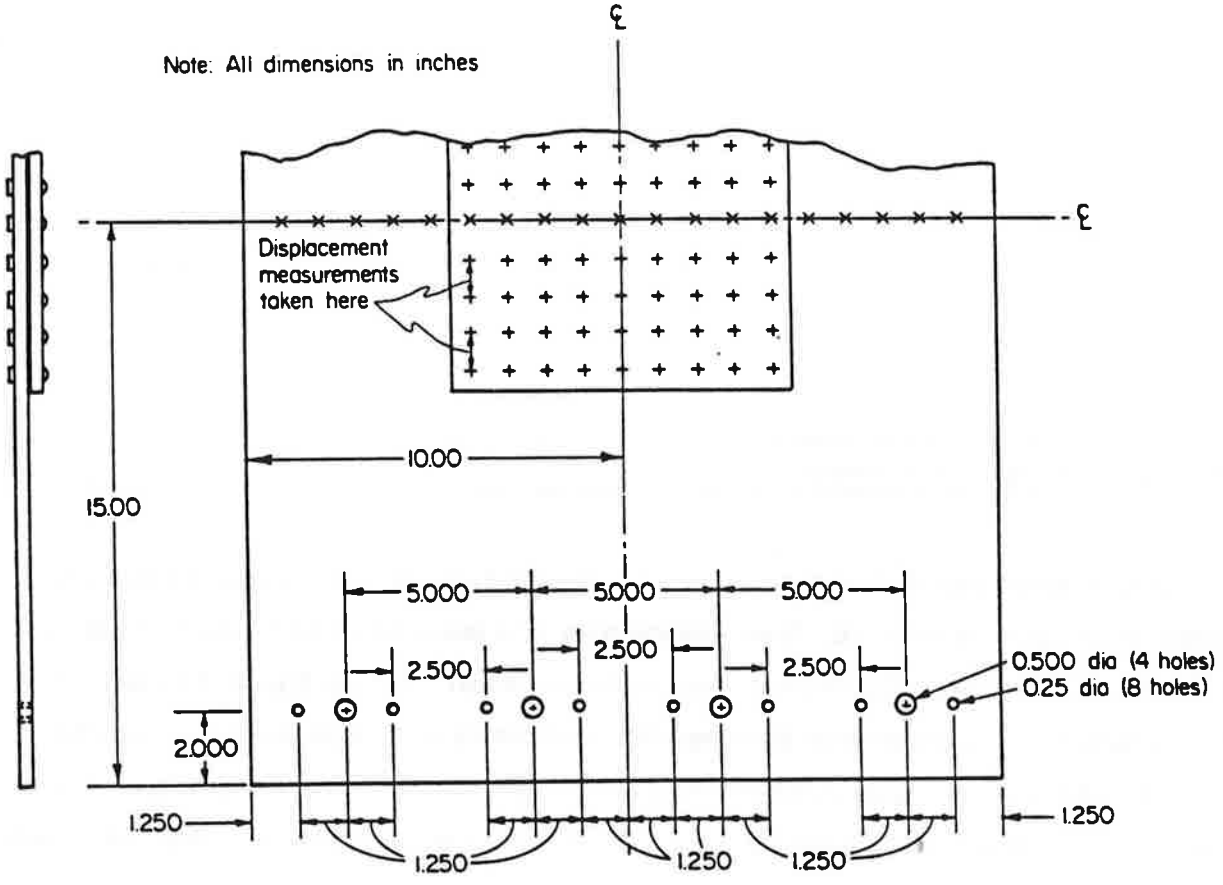

FIGURE 6-11. REPAIR PANEL WITH LOCATION OF DISPLACEMENT MEASUREMENTS NOTED

The instrumentation used to read the clip gages was not grounded to the test sample during the first two series of measurements which resulted in less precision in the measurements than in the final two sets of measurements. Once this problem was resolved, the readings were stable and repeatable. These results demonstrated the potential of these gages to measure displacements within an accuracy of ± 50 microinches, which equates to a resolution of rivet loads for 0.040-inch thick sheet/doubler combinations to within about ± 10 pounds. Calibration checks of the gages also showed them to be linear within 10 microinches over the design range of ± 0.0020 inches.

TABLE 6-5. RESULTS OF RIVET DISPLACEMENT MEASUREMENTS ON TEST SAMPLE NO. 18

Location	Stress (ksi)	Displacement (in.)
End, 1st 2 Rows of Rivets	5.2	0.00 [1]
	10.4	0.00 [1]
	15.6	0.00028[1]
End, last 2 rows of rivets	5.2	0.00 [1]
	10.4	0.00028[1]
"	15.6	0.00076[1]
"	5.2	0.00014
	10.4	0.00035
	15.6	0.00076

[1] Instrumentation not grounded to sample.

One of the test panels, Specimen No. 25, was extensively strain gaged to measure skin and doubler stresses between the rivets. Rivet displacements were measured on both sides of the sample for all adjacent rivet rows. The results of these measurements are shown in Figures 6-12 and 6-13. The comparison of these results with the compatible displacement analysis predictions is included in Section 4.4 of this report. Since additional, fully instrumented samples could not be completed, an accurate estimate of the uncertainty in these measurements could not be established. Additional work needs to be focused on this area, if valid comparisons are to be made between the repair panel experiments and any model that will be used to explain the results.

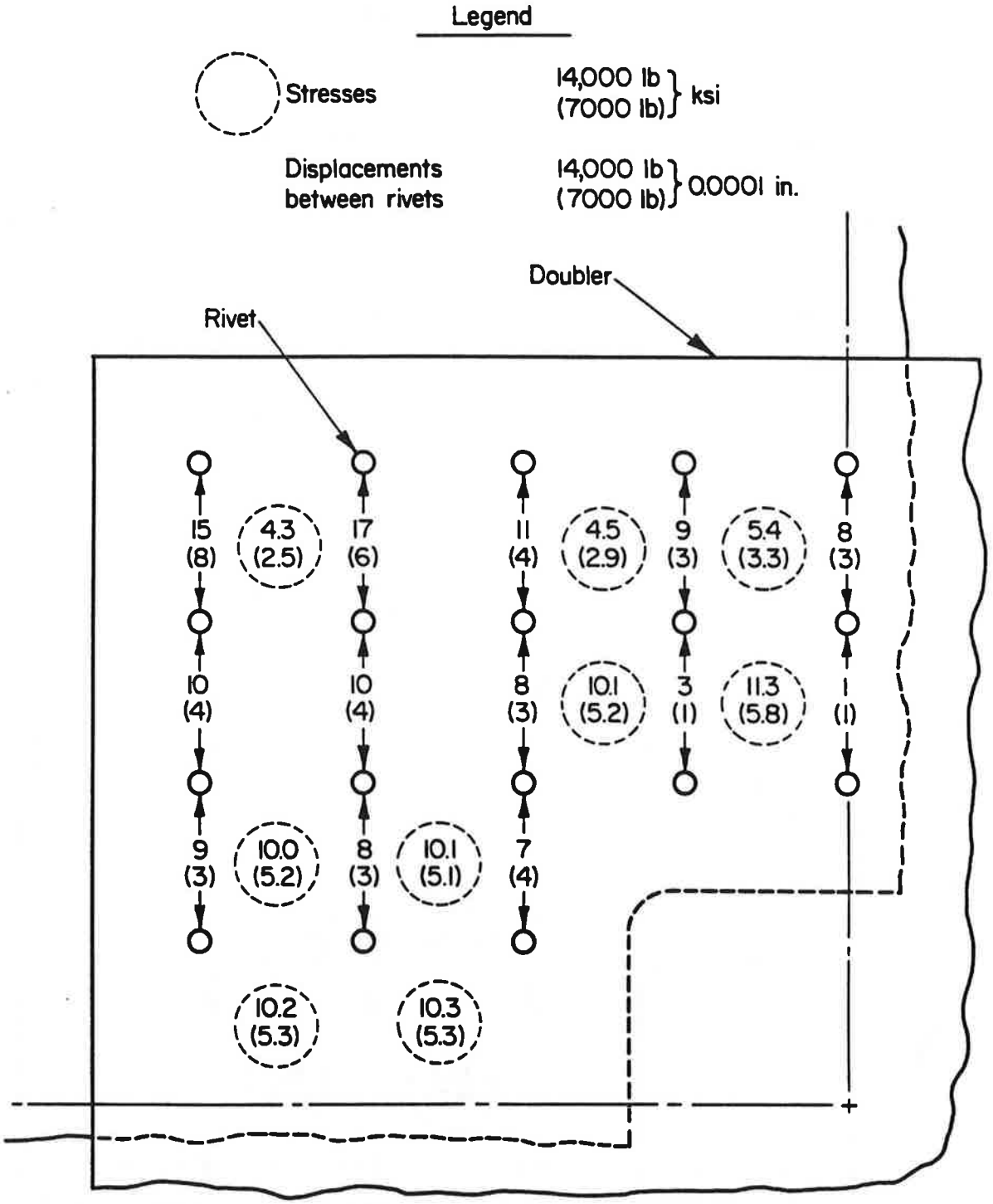

0.039 Panel with 0.039 patch
Specimen No. 25 (with cutout)

FIGURE 6-12. DOUBLER STRESSES AND RIVET DISPLACEMENTS FOR SPECIMEN NO. 25

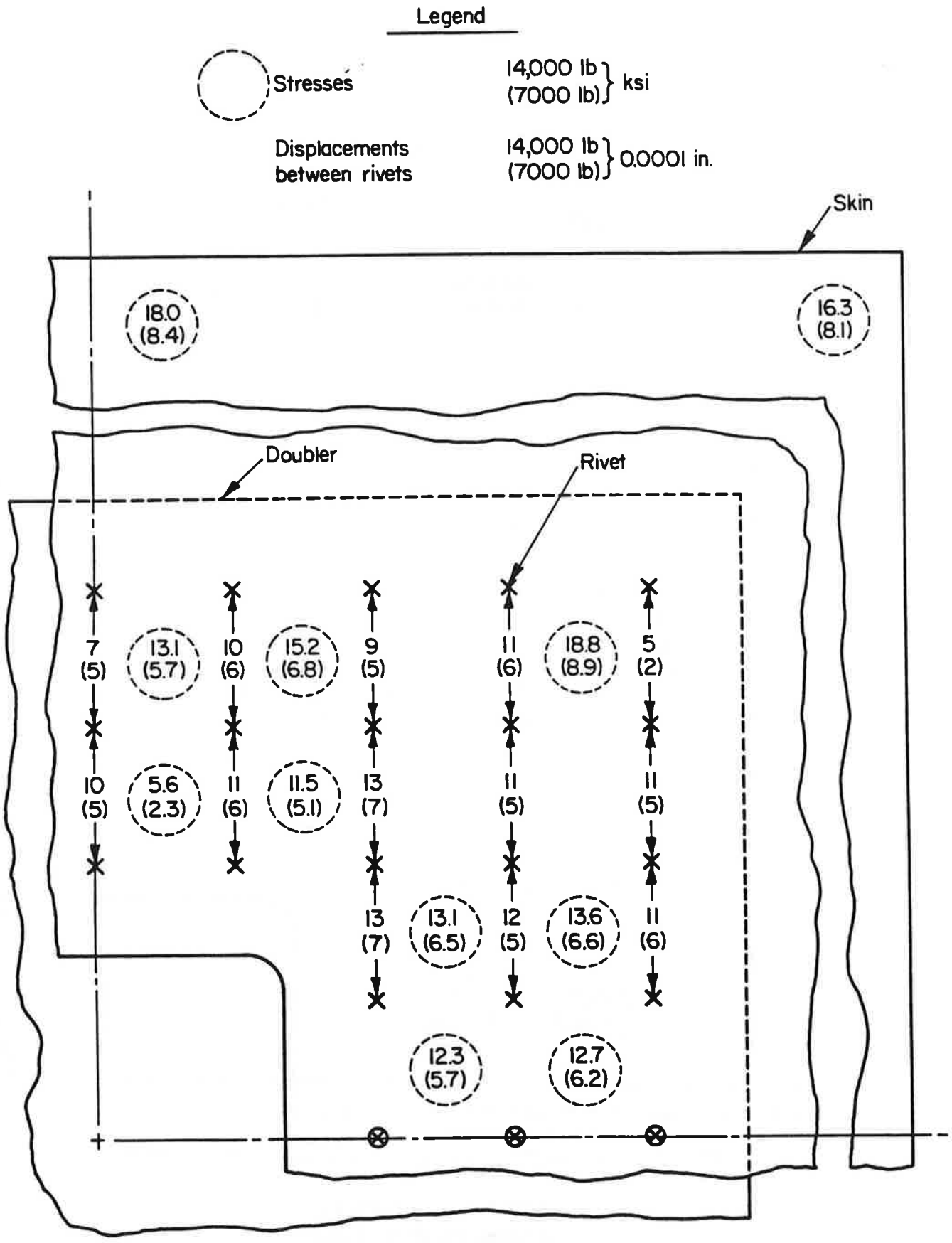

FIGURE 6-13. SKIN STRESSES AND RIVET DISPLACEMENTS (SPECIMEN NO. 25)

7.0 RELIABILITY ASSESSMENT

7.1 Introduction

In recent years, the occurrence and interaction of damage and repairs at multiple sites have been identified as important phenomena in damage tolerance assessment of older aircraft. In July 1990, a U.S. Air Force C-141 at Altus, Oklahoma was found to be close to failure when damage linked up between wing repair patches. The Aloha Air accident in Hawaii in April of 1988 showed that damage in multiple sites can lead to significant structural failures in an aircraft. Multiple site damage (MSD) is a rather general term. In the present context, MSD is defined as the existence of multiple cracks in a line of rivet holes prior to propagation of those cracks to failure (whatever the failure criteria may be).

Causative factors which correlate with MSD in aging aircraft, however, involve a number of sources of statistical uncertainty. These are due to variabilities in fatigue crack initiation, fatigue crack growth, crack detection probability, and loading environment. In particular, the predicted variability in fatigue crack growth depends greatly on the realistic distribution of initial crack sizes. Rational treatment of these uncertainties and assessment of their impact on system performance and recommended repair procedures can be achieved only by applying the theories of probability and structural reliability. Clearly, MSD is a stochastic mechanics problem.

The configuration of a repair and its associated stress field are strongly dependent on the type, size, and location of damage being repaired. The possibility of nearby MSD or otherwise damaged elements must be assessed for a complete damage tolerant analysis of the repair. The complexities involved in conducting a comprehensive reliability analysis for a commercial aircraft susceptible to MSD and requiring repairs mandate that this effort be divided into several phases. As MSD (upon detection) will require repair, and since it can significantly influence the damage tolerance of nearby repairs, it will be necessary to satisfactorily describe the initiation and growth of MSD cracks in a reliability analysis before additional issues of repair effects can be included.

This effort has focussed on the formulation of a novel probabilistic model to accurately determine the reliability of aging aircraft susceptible to MSD. Although MSD has been emphasized, the models are sufficiently flexible to accommodate other structural degradation factors that logically would be included in the future.

There are several possible enchancements to this model. For example, various existing databases could be explored to accurately characterize input variables (deterministic and random). Then, the model could be used for a significant number of specific (real world) cases. It could include the reliability assessment associated with additional sources of damage and variability such as repair location and size. Finally, the model could integrate all of these results into a framework that would provide a tool for assessing the reliability of aircraft as a function of relevant parameters such as age, probability of crack detection, inspection interval, flight load distribution, and others.

7.2 State-of-the-Art Review

Previous studies on probabilistic aspects of risk assessment for aging aircraft were critically reviewed. In recent years, there have been several research activities on multiple site damage. They have included both deterministic and probabilistic studies which were conducted by Orringer[22], Mayville[23], and Broek[24-26]. Both Orringer and Mayville investigated mainly the deterministic issues related to MSD. In Reference [24], a probabilistic model was developed in which the factors effecting initiation and growth of MSD cracks were investigated. The loading environment was assumed to be deterministic and the nominal stress distribution over a fuselage bay (as it is affected by frames, tear straps, and stringers) was obtained from linear elastic fracture mechanics analyses[27]. The statistical characterization of random parameters governing crack initiation and growth was performed by analyzing test data on lap joint specimens. An array of 100 fastener holes in a critical row of a fuselage lap joint was considered. Crack initiation and growth properties were randomly assigned in accordance with their cumulative distribution functions. They were then assessed on the basis of local stress level, in which the effects of membrane stress, fastener load, and local bending stress were included. The growth of these cracks was incremented every 100 cycles, and inspections were performed at regular intervals with the basic probability of detection (POD) curves based on U.S. Air Force (USAF) inspection data. This led to the computation of cumulative probabilities of detection (CPOD) during a series of periodic inspections from crack initiation at the first fastener hole. Figure 7-1 shows the plots of CPOD versus length of inspection interval (eddy current) for various MSD cracks obtained from Reference [23]. Results suggest that there is a precipitous drop in CPOD, if the inspection interval is longer than 3500 flights (pressurization cycles). On the basis of worst case values, it was also concluded[28] that an inspection interval of about 1800 flights would be required to provide a CPOD value of 95 percent.

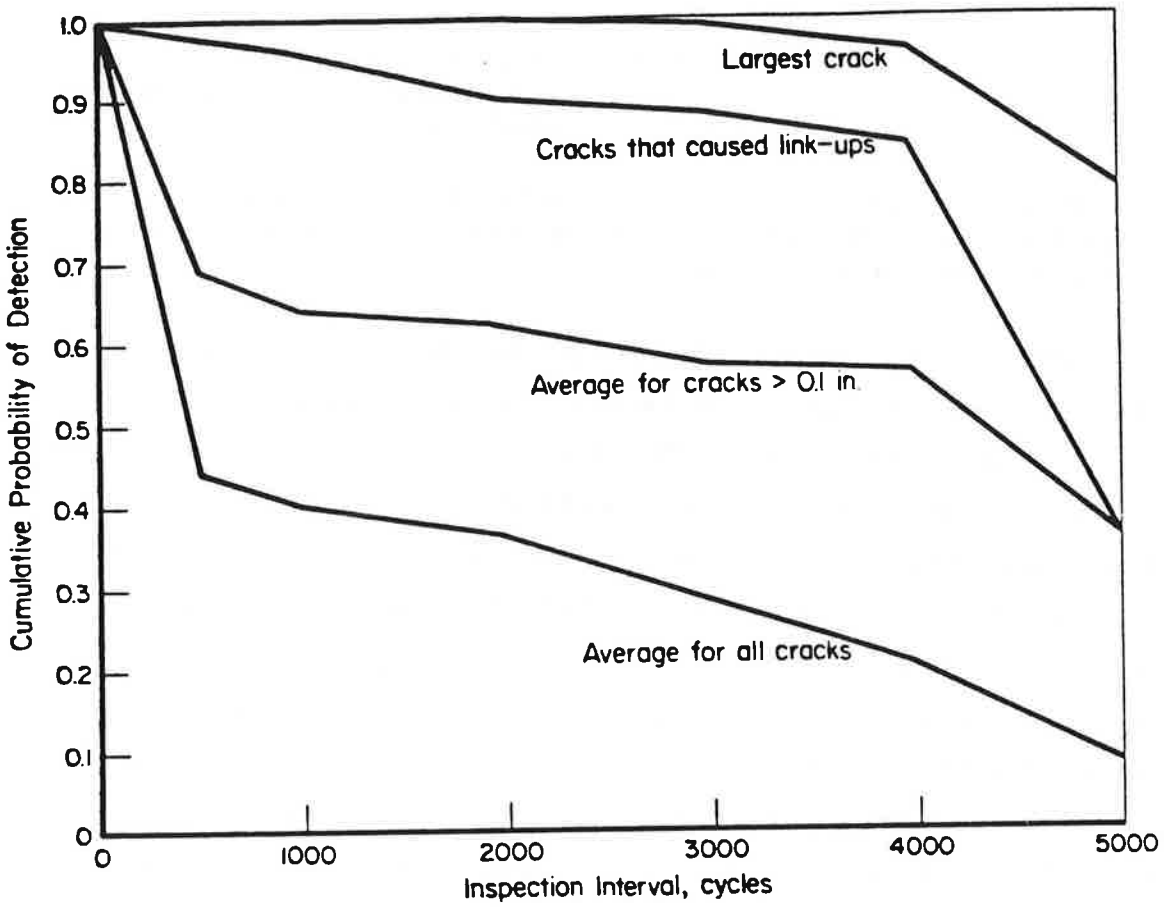

FIGURE 7-1. CUMULATIVE PROBABILITY OF DETECTION VERSUS INSPECTION INTERVAL[23]

Broek's study constitutes a significant effort in the probabilistic assessment of crack initiation and growth due to MSD. The study was systematic and was based on simple engineering methods of linear elastic fracture mechanics. However, there are several issues of probabilistic risk assessment (PRA) which were not included. They are as follows:

- Broek's probability computation was based on simple Monte Carlo Simulation (MCS). A few sample cases of results were presented by generating realizations of random variables constituting uncertainty and were surprisingly found to be insensitive due to statistical variation. Since MCS for such a small sample size may be inaccurate, these findings need to be reinvestigated carefully in the light of modern reliability and/or advanced simulation techniques.

- The probability of failure was not determined explicitly. Hence, the reliability of an aging aircraft remains virtually unknown. The quantitative measure of the reliability provides a means of structural performance and can be appropriately used in probability-based inspection planning.

- The issue regarding desirable (target) CPOD was not addressed. Obviously, this probability cannot be arbitrary. Once again, a reliability analysis needs to be performed, so that the target CPOD can be based on "acceptable" risk.

- Maintenance considerations on MSD were focussed on the evaluation of optimal interval inspection intervals. Inclusion of parameters which affect repair quality and their statistical variability (if any) were not included.

Despite these limitations, the study described in Reference [24] demonstrated the need and the feasibility of probabilistic analysis of aging aircraft subjected to multiple site damage.

The Aircraft Structural Integrity Program (ASIP) of the U.S. Air Force (USAF) traces its origin to B-47 failures in 1958. ASIP was established based on the recognition that repeated loads were a threat to the safety of an operational aircraft. This threat has been successfully controlled through the adoption of the damage tolerance approach in 1975. This approach, also referred to as "retirement for cause", was used as a basis for the inspection/modification program to maintain safety throughout the life of the aircraft. In a recent technical paper by Lincoln[29], occurrences of MSD on USAF aircraft and their influence on service lives were discussed. This was done through the experiences derived from the KC-135, C-5, and C-141 aircraft. In summary, it was shown that detection and prevention of MSD should be a major factor in the life management program for wing structures, in addition to other components of an aircraft. For an aircraft where the maintenance of fail safety is vital to the operational safety of the aircraft, it is essential that there be an assessment of the timing of the loss of fail-safety from MSD.

Initially, the USAF damage tolerance requirements were based on deterministic rather than probabilistic approaches. The initial flaw size was postulated as a specific number, and the critical crack length was based on a specific load. Also, the inspection capability was based on one point of the POD curve, i.e., all cracks longer than the one corresponding to this point value are assumed to be found when the aircraft is inspected. For example, this point was chosen to be associated with 90 percent probability of detection. The selection of the 10 percent upper fractile from the cumulative distribution function of the smallest detectable crack size is somewhat arbitrary. Questions regarding the safety, or level of reliability associated with this specific POD value were examined in Reference [29] which also presented a risk assessment methodology originally developed in Reference [30]. The study also evaluated the adequacy of a USAF damage tolerance inspection criterion for protecting the safety of an aging military trainer aircraft. This was done though the above-mentioned risk assessment methodology based on cracks found in teardown inspections of retired wings. The crack propagation was combined with stress probabilities representing service

experience to determine single flight probabilities of failure and the single aircraft probability of failure after a given time. For the case studied, the single flight probabilities of failure at a specific location with an inspection interval obtained from the deterministic damage tolerance criterion was found to be 0.4 before the next inspection was due. This failure probability is unacceptably high and hence, the inspection program obtained from the deterministic method must be treated as unconservative due to the inadequate level of reliability.

Another study on risk analysis for aging aircraft fleets was carried out by Berens[31] under the sponsorship of the Flight Dynamics Directorate of the Wright Laboratories in Dayton, Ohio. It comprises an evaluation of the probability of failure due to a flaw in a structural element as well as a determination of optimal inspection intervals based on minimization of maintenance costs. There were two basic calculations: one involved the development of a probability density function of crack size from a beginning reference time to an arbitrary time within a period of uninterrupted usage, and the other involved the quantification of the effects of inspection and repair-if-necessary actions due to periodic maintenance. In both cases, elementary principles of probability theory were applied.

The probabilistic model described above has the merit of analytical treatment as opposed to a "brute force" approach like MCS as done in Reference [24]. However, it differs from a comprehensive reliability assessment in the following ways:

- The model is primarily developed for a single flaw which considers only the probabilistic aspects of crack growth. When there are multiple flaws, it is assumed that (all) cracks have already developed and their subsequent growth is independent. In practice, however, as an aircraft ages, there will be both crack initiation and growth at the same time, mainly due to differential stress fields and crack tip stress intensities. Simultaneous crack growth at all critical locations may not be realistic.

- The model disregards uncertainty in the crack growth parameters. For example, when a Paris equation[1] is used, the model does not take into account the stochastic variability of the Paris coefficients. Crack growth data obtained from experiments on the 2024-T3 aluminum alloy have shown that the Paris coefficients are indeed random variables with possible correlation[32-33]. If the uncertainty of these coefficients and any other relevant parameters needs to be included, the evaluation of single flight probabilities of fracture proposed in Reference [31] becomes immensely difficult. This complexity arises because the dimension of the probability integral (Equation (4) in Reference [31]) increases greatly. Since analytic and/or numerical probability integration in large dimensions becomes prohibitive, alternative methods need to be developed to calculate

---

1 Assumed log-linear relationship between crack growth rate and stress intensity factor range, see Section 7.3.3.

this failure probability. This can be a very serious limitation of the risk methodology proposed in Reference [31] unless such alternative means are found.

- The probabilities were calculated for a crack in a single element (stress raiser). Global risk assessment in an airframe which comprises many identical elements is performed by invoking independent assumptions. This may not be valid unless the loading environment in these identical elements is truly independent.

7.3 Development of the Probabilistic Model

7.3.1 Structural Loading Environment. Consider a fuselage lap joint which is subjected to multiple site damage (MSD) in a large series of fastener holes. Assume that R is the fuselage radius, t is the skin thickness, D_s is the shank diameter, D_h is the fastener head diameter, s is the fastener spacing, and p is the random fuselage pressure with a known cumulative distribution function. Figure 7-2 shows an idealized model used in a linear elastic stress analysis by finite element method

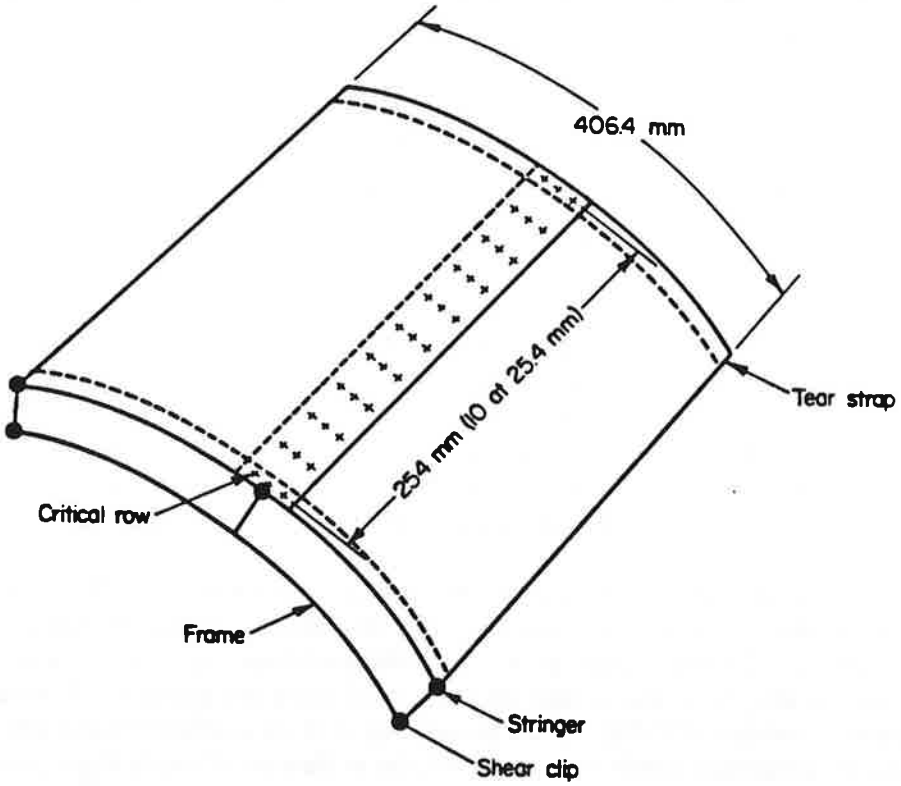

FIGURE 7-2. FINITE ELEMENT MODEL OF A LAP JOINT (REFERENCES [24] AND [27])

(FEM)[27] and obtained from Reference [24]. It consists of one half of a bay in a curved panel subjected to the distributed fuselage pressure. The three-row lap joint is considered disbonded, so that all of the load transfer occurs through the fasteners. Figure 7-3 exhibits an isolated hole which is

subjected to various stresses due to fuselage pressure p. They include membrane stress, fastener load, and local bending stress. They are discussed below.

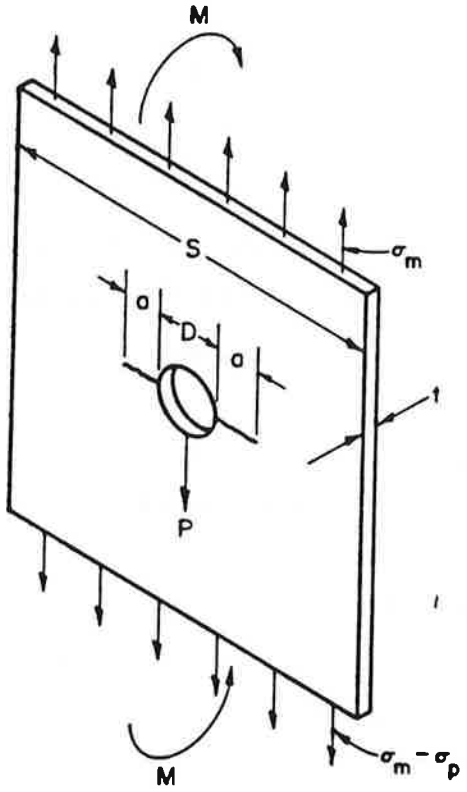

FIGURE 7-3. CRACKED HOLE AT A LAP JOINT SUBJECTED TO VARIOUS LOADS

Membrane Stress. The membrane stress, σ_m, although varying through the bay due to the frame and tear straps is proportional to pR/t and is given by[24]

$$\sigma_m(p) = \frac{A_1 pR}{t} \tag{7-1}$$

in which A_1 is a proportionality factor.

Fastener Load. The fastener load depends upon the fastener flexibility. However, it is assumed that for small changes in fastener size and skin thickness, the flexibility will not be changed significantly, and can be considered invariant for a given hole deformation. This fastener load, P, is proportional to pRs/t, giving[24]

$$P(p) = \frac{A_2 pRs}{t} \tag{7-2}$$

where A_2 is a proportionality factor.

Local Bending Stress. The local bending stress, σ_b, depends on the local bending moment due to eccentricity of the fastener forces, which in turn depends on the skin thickness. Thus, σ_b is proportional to pR/t^2 giving[24]

$$\sigma_b(p) = \frac{A_3 pR}{t^2} \tag{7-3}$$

in which A_3 is a factor of proportionality.

Using Equations (7-1), (7-22), and (7-3), the membrane stress, fastener load, and local bending stress can be calculated for each fastener hole (Figure 7-3) following determination of the proportionality factors A_1, A_2, and A_3 via a deterministic finite element analysis. The stress analysis is assumed to be linear elastic, so that results of FEM are proportional to load and geometrical parameters. On this premise, the above stresses can be easily obtained for new parameter values. Note that all these component stresses are random due to functional dependence on random fuselage pressure p, and they are all perfectly correlated.

7.3.2 Fatigue Crack Initiation. The fatigue strength for crack initiation is usually expressed through the S-N curve (Wöhler Curve), which gives the number of stress cycles N_0 under constant amplitude loading with a stress range S necessary to cause failure (initiation). Readily available fatigue test data for joints can be obtained from References [23] and [34-39]. Of these sources, some were for conditions and configurations not immediately relevant to the analysis of a fuselage lap joint. However, the large data bases generated by Hartman[34] and Mayville[23] are relevant.

Figure 7-4 shows the scattergrams of initiation life N_0 for several stress ranges obtained from the experimental data produced by Hartman and Mayville. Hartman's data were very useful, because they were generated from tests on adhesively bonded and riveted lap joints of a configuration almost identical to the one used in fuselage structures for several types of aircraft. Hartman performed well over 400 tests and investigated the effects of many parameters, such as different types of adhesives, and surface treatments, as well as variations in temperature, loading frequency, and stress intensity. The data obtained by Mayville also deserve attention. Instead of the basic lap joint as used by Hartman, Mayville, however, employed specimens with short stiffeners which were attached to their edges to simulate crack arrester straps found in some types of aircraft experiencing MSD. These test data, which are also shown in Figure 7-4, fall within (but to the low side) of the scatterband exhibited by the Hartman data.

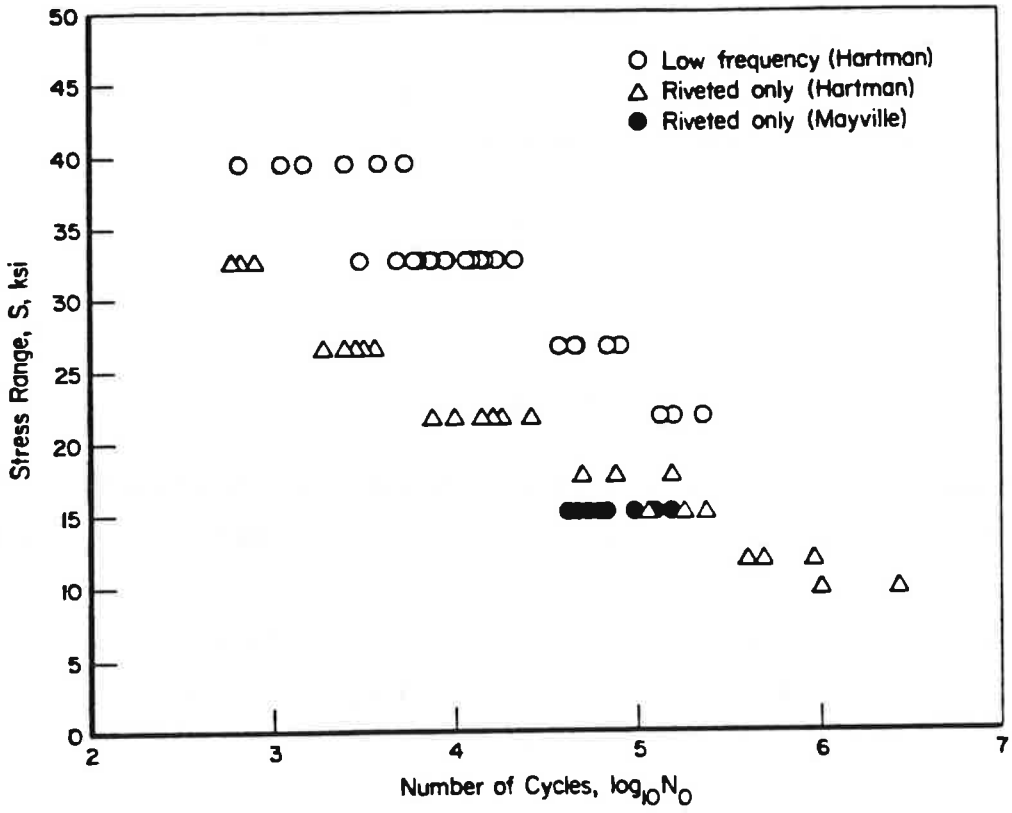

FIGURE 7-4. SCATTERGRAM OF CRACK INITIATION LIFE (REFERENCE [26])

Figure 7-4 clearly indicates that the initiation life, N_0, for a given stress range is a random variable. Broek's statistical analysis[24,25] of the consolidated Hartman data suggests that a Weibull distribution of normalized initiation life $N_0/E[N_0]$ applies fairly well, where $E[\cdot]$ is the mathematical expectation operator with $E[N_0]$ representing the expected (mean) value of random initiation life N_0.

It should be noted that the stresses are the nominal stresses away from the joint and they represent hoop (membrane) stresses in a fuselage. Furthermore, all data were obtained for a stress ratio of 0.05 or 0.10, while typical fuselage loading is essentially with stress ratio equal to zero. Consequently, an assumption has to be made on the applicability of the above test results to the slightly different fuselage loading.

7.3.3 Fatigue Crack Growth. A wide variety of mathematical models for fatigue crack growth are available in the current literature. The simplest and generally accepted model was proposed by Paris and Erdogan[40] which has the kinetic equation

$$\frac{da}{dN} = C(\Delta K)^m \tag{7-4}$$

with the initial condition

$$a(0) = a_0 \tag{7-5}$$

where $a = a(N)$ is the half crack length at N cycles, ΔK is the change in stress intensity factor due to the variation of fuselage pressure from zero to p, C and m are material constants, and a_0 is the initial value of the half crack length.

Stress Intensity Factor. The stress intensity factor K can be calculated by the theory of linear elastic fracture mechanics (LEFM). Following compounding and superposition[41-42] which are allowable in linear elastic stress analysis, K can be decomposed as

$$K = K_A + K_B + \frac{1}{2}(K_C + K_D) \tag{7-6}$$

where K_A, K_B, K_C, and K_D are stress intensity factors which correspond to the various loading cases shown in Figure 7-5. A derivation of Equation (7-6) can be obtained from Reference [24] and hence, is not repeated here. From basic principles of LEFM, the component stress intensity factors K_A, K_B, K_C, and K_D can be obtained as[41-42]:

$$K_A = 0.39\left[1 + 0.16\left[\frac{a_{eff}}{W_{eff}}\right]^2\right]\sigma_b\sqrt{\pi a_{eff}} \tag{7-7}$$

$$K_B = \sqrt{\sec\left[\frac{\pi a_{eff}}{W_{eff}}\right]}\,(\sigma_m - \sigma_p)\sqrt{\pi a_{eff}} \tag{7-8}$$

$$K_C = \sqrt{\sec\left[\frac{\pi a_{eff}}{W_{eff}}\right]}\,\sigma_p\sqrt{\pi a_{eff}} \tag{7-9}$$

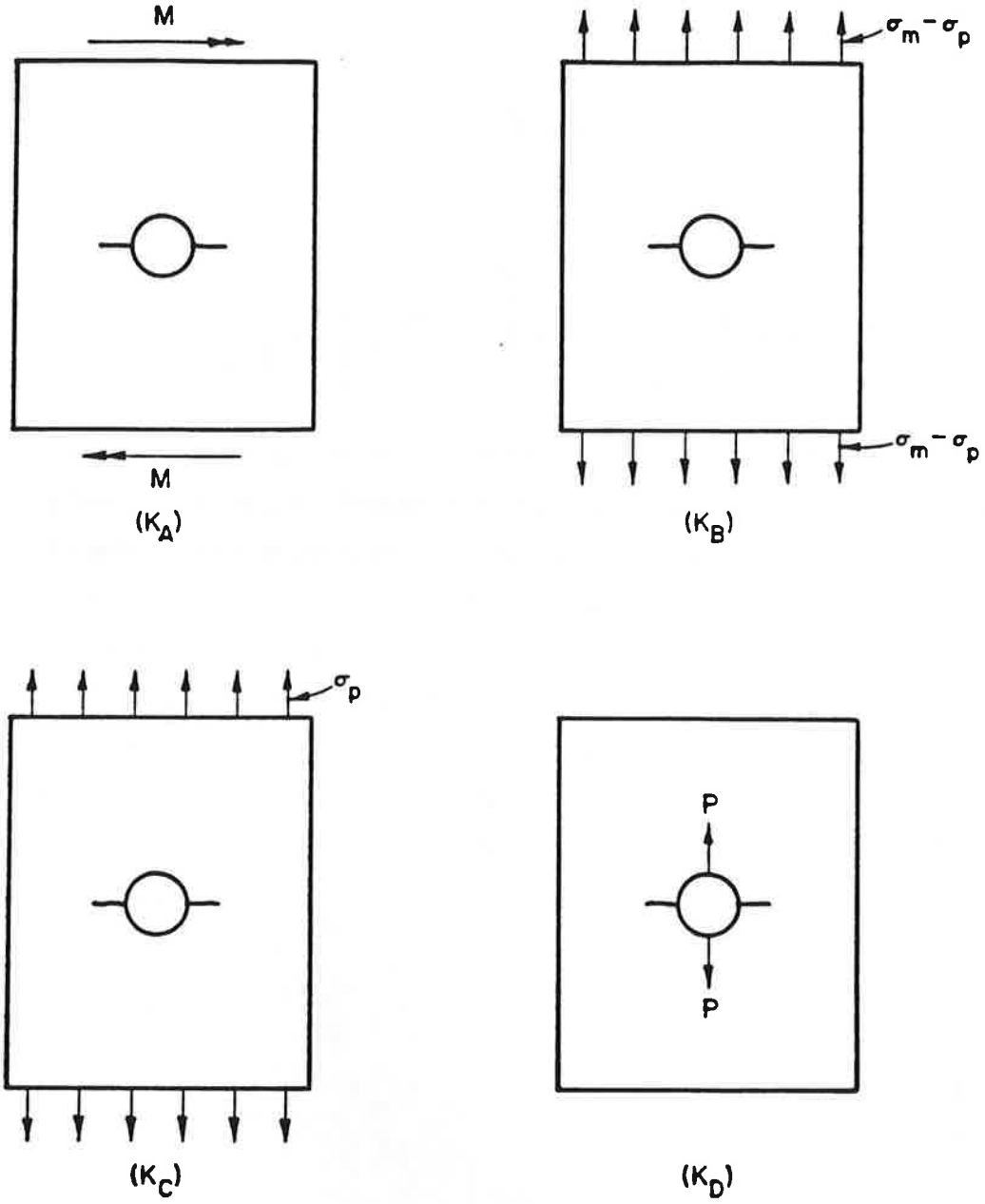

FIGURE 7-5. ADDITIVE DECOMPOSITION OF STRESS INTENSITY FACTOR

$$K_D = \frac{S}{\pi a_{eff}} \sigma_p \sqrt{\pi a_{eff}} \tag{7-10}$$

in which $\sigma_p = P/ts$, $a_{eff} = a + D/2$, D is the hole diameter, and W_{eff} is the effective width introduced to account for the effects of adjacent cracks[24]. These equations were taken directly from Reference [24]. From Equation (7-6), the total stress intensity factor K becomes

$$K = \bar{\beta}\ \sigma_m \sqrt{\pi a_{eff}} \tag{7-11}$$

where

$$\bar{\beta} = 0.39 \left[1 + 0.16 \left[\frac{a_{eff}}{W_{eff}}\right]^2\right] \frac{\sigma_b}{\sigma_m} + \sqrt{\sec\left[\frac{\pi a_{eff}}{W_{eff}}\right]} \left[1 - \frac{1}{2}\frac{\sigma_p}{\sigma_m}\right] + \frac{1}{2}\frac{s}{\pi a_{eff}}\frac{\sigma_p}{\sigma_m} . \tag{7-12}$$

Statistical Variability. Virkler, et al.[43-44] conducted a large replicate test program to identify the contribution of material inhomogeneity to the statistical variability observed in laboratory fatigue crack growth data (a vs. N). Crack growth data were generated from 68 identical 2.54 mm thick center-cracked panels cut from the same sheet of 2024-T3 aluminum. This alloy is still used in many aircraft fuselage structures. The replicate tests were performed under identical (within limits of experimental accuracy) constant amplitude loading conditions and with the same initial crack lengths. Under these carefully controlled conditions, the ensemble of crack growth curves exhibited in Figure 7-6 indicates a considerable amount of scatter. In order to achieve sample curves as those exhibited in Figure 7-6, the material constants C and m must be random variables for a given initial

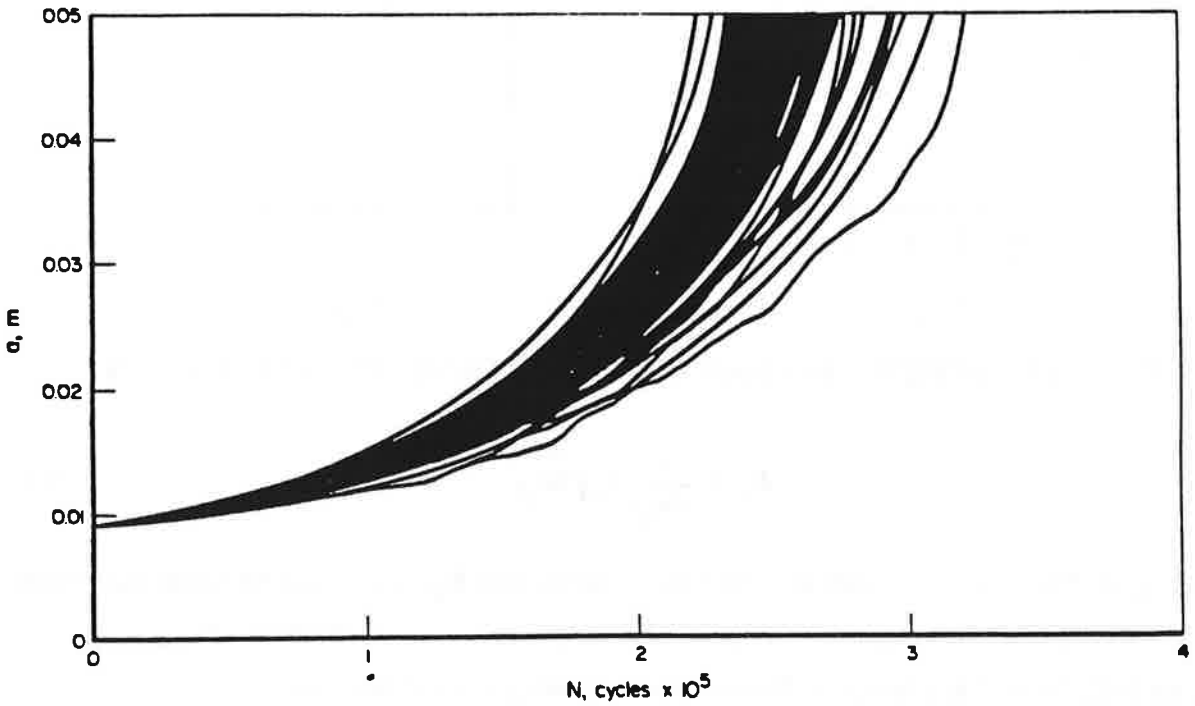

FIGURE 7-6. SCATTER IN CRACK GROWTH DATA FROM 68 REPLICATE TESTS (REFERENCE [33])

crack size and loading condition. Several options exist in modeling random crack growth behavior. Both C and m can be assumed to be jointly distributed random variables[32-33,45]. Other possible treatments include the use of C as a random variable and m as deterministic[24,46], and the use of C as a random variable and m as a function of C[47]. Here, it will be assumed that ln (C) and m are correlated random variables with jointly distributed bivariate Gaussian distribution functions. This was originally proposed in References [32] and [33]. More sophisticated models with random processes simulating intra-specimen variability of crack growth were also considered by Ortiz and Kiremidjian[32-33]. These approachs will not be addressed here. The statistical properties, such as mean, standard deviation, and the correlation coefficients of the random variables ln(C) and m can be obtained from analysis of the Virkler data and are readily available in References [32] and [33].

In order to obtain a particular solution of the differential equation for crack growth life based on the Paris model (Equation (7-4)), the initial condition specifying initial crack length a_0 must be characterized. The initial crack length a_0 is assumed to be realized following fatigue crack initiation. However, it has been found to be difficult to accurately quantify a_0 and currently, it is done rather empirically. Broek[24] has used a deterministic value of $a_0 = (D_h - D_s)/2$ with the argument that smaller crack sizes would not be detectable. This is indeed true and relevant when inspection intervals are based on cumulative probabilities of detection (CPOD), not the failure probability. In a reliability analysis, however, the probability of failure may be significantly dependent on a_0 and hence, a better deterministic and/or random description of a_0 is needed. In this study, a_0 will be treated as a uniform random variable with equal probability of occurrence between a judiciously chosen lower and upper bounds.

7.3.4 Structural Reliability Analysis

Structural reliability analysis requires a mathematical model derived from the principles of mechanics and experimental data which relates various input random parameters for a specific performance criterion of interest. For example, consider Equation (7-4) which when combined with Equation (7-11) becomes

$$\frac{da}{dN} = C\,\bar{\beta}^m\,\sigma_m(p)^m\left[\pi\left[a+\frac{D}{2}\right]\right]^{\frac{m}{2}} \tag{7-13}$$

in which it is noted that the stress ratio is zero due to the variation of fuselage pressure from zero to p. Following separation of variables and subsequent integration,

$$\int_{a_0}^{a} \frac{d\xi}{\bar{\beta}^m \left[\pi\left(\xi + \frac{D}{2}\right)\right]^{\frac{m}{2}}} = C\left[\sigma_m(p)\right]^m \int_{N_0}^{N} d\eta \tag{7-14}$$

where N_0 is the number of cycles to crack initiation. Define a damage function which when introduced in Equation (7-14) can be inverted to solve (implicitly) for the crack length as a function of number of cycles N. When material and geometric properties are specified, the crack length at any number of cycles N can then be obtained from Equation (7-16) for a given loading environment.

$$\psi(a;a_0) = \int_{a_0}^{a} \frac{d\xi}{\bar{\beta}^m \left[\pi\left(\xi + \frac{D}{2}\right)\right]^{\frac{m}{2}}} \tag{7-15}$$

$$a(N) = \psi^{-1}\left(C\left[\sigma_m(p)\right]^m (N - N_0) \; ; \; a_0\right) \tag{7-16}$$

Consider a simple failure criterion

$$a(N) > a_p \tag{7-17}$$

which is based on the exceedance of the crack length at N cycles beyond an allowable threshold, a_p. a_p is defined as a permissible crack size and can be evaluated following the net-section collapse criterion used in Reference [26]. Theoretically, a_p is a random variable. However, since the crack growth rate is very high near the permissible crack size, effects of a_p on the variability of fatigue failure threshold in rather small compared with other random variables involved in the system. This fail-safe condition can be conveniently expressed in the traditional form where the performance function

$$\begin{aligned} g(X) &< 0 \quad \text{(failure)} \\ g(X) &= 0 \quad \text{(limit state)} \\ g(X) &> 0 \quad \text{(survival)} \end{aligned} \tag{7-18}$$

$$\begin{aligned} g(X) &= a_p - a(N) \\ &= a_p - \psi^{-1}\left(C\left[\sigma_p(p)\right]^m (N - N_0) \; ; \; a_0\right) \end{aligned} \tag{7-19}$$

in which $X = \{N_0, a_0, C, m, p\}^T$ is a real vector of random parameters characterizing uncertainty in all load and system parameters, and the superscript T is a symbol for transpose of a vector. Note that the performance function g(X) itself is random, because it depends on the input random vector X. In the x space, the equation $g(x) = 0$ also known as limit state separates the domain $\mathfrak{D}$ of X into the safe set $\mathfrak{S} = \{x: g(x) > 0\}$ and failure set $\mathfrak{F} = \{x: g(x) < 0\}$. This result is shown schematically in Figure 7-7. The reliability P_S is the complement of the probability of failure P_F ($P_S = 1 - P_F$). P_F is

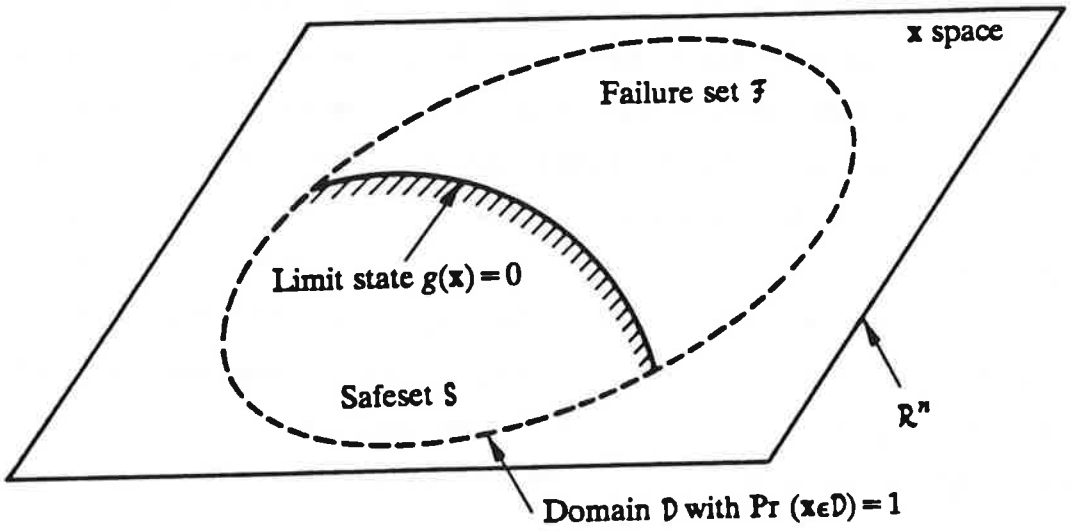

FIGURE 7-7. DEFINITION OF BINARY LIMIT STATE IN ORIGINAL SPACE

defined as the probability that the failure event represented by Inequality 37 is true, i.e.,

$$P_F \overset{\text{def}}{=} \Pr\left[g(X) < 0\right] \overset{\text{def}}{=} \int_{g(x)<0} f_X(x)\, dx \tag{7-20}$$

where $f_X(x)$ is the joint probability density function of input random vector $X = \{N_0, a_0, C, m, p\}^T$. which is assumed to be known. In general, the multi-dimensional integral in Equation (7-20) cannot be determined analytically. As an alternative, numerical integration can be performed, however, it becomes impractical and the computational effort becomes prohibitive when the dimension becomes greater than 2.

Several approximate methods exist for performing the multi-dimensional probability integration in Equation (7-20). Among them, First- and Second-Order Reliability Methods (FORM/SORM[48-53], Importance Sampling[48,54-58], Directional Simulation[59-61], MCS[48,62], and many others can be applied to estimate P_F in Equation (7-20). In this section, a few of them will be presented with regard to their potential for use in an approximate reliability analysis.

First- and Second-Order Reliability Methods (FORM/SORM). First- and Second-Order Reliability Methods (FORM/SORM) are general state-of-the-art structural reliability methods. The methods are based on linear (first-order) and quadratic (second-order) approximations of the limit state surface $g(x) = 0$ tangent to the closest point of the surface to the origin of the space. The determination of this point involves nonlinear programming (NLP) and is performed in the standard Gaussian image of the original space.

The FORM/SORM algorithms involve several steps. They will be described here briefly assuming a generic n-dimensional random vector $\boldsymbol{X}$. First, the space of uncertain parameters $\boldsymbol{x}$ is transformed into a new n-dimensional space $\boldsymbol{u}$ consisting of independent standard Gaussian variables. The original limit state $g(x) = 0$ then becomes mapped into the new limit state $g_U(u) = 0$ in the $\boldsymbol{u}$ space. Second, the point on the limit state $g_U(u) = 0$ having the shortest distance to the origin of the $\boldsymbol{u}$ space is determined by using an appropriate nonlinear optimization algorithm. This point is referred to as the design point or β-point, and has a distance β_{HL} to the origin of the $\boldsymbol{u}$ space. Third, the limit state $g_U(u) = 0$ is approximated by a surface tangent to it at the design point. Let such limit states be $g_L(u) = 0$ and $g_Q(u) = 0$, which correspond to approximating surfaces as hyperplane (linear or first-order) and hyperparaboloid (quadratic or second-order), respectively (Figure 7-8). The

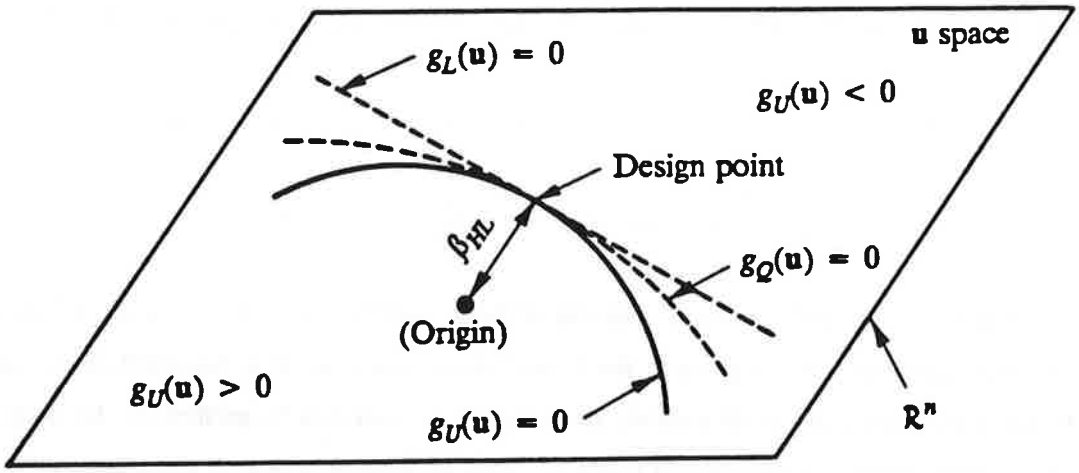

FIGURE 7-8. LINEAR AND QUADRATIC APPROXIMATIONS OF LIMIT STATE IN GAUSSIAN IMAGE

probability of failure P_F (Equation (7-20)) is thus approximated by $\Pr[g_L(u) < 0]$ in FORM and $\Pr[g_Q(u) < 0]$ in SORM. These first-order and second-order estimates $P_{F,1}$ and $P_{F,2}$ are given by[48-53]

$$P_{F,1} = \Phi(-\beta_{HL}) \tag{7-21}$$

and

$$P_{F,2} \simeq \Phi(-\beta_{HL}) \prod_{i=1}^{n-1} (1 - \kappa_i \beta_{HL})^{-\frac{1}{2}} \tag{7-22}$$

where

$$\Phi(u) = \frac{1}{\sqrt{2\pi}} \int_{-\infty}^{u} \exp\left(-\frac{1}{2} \xi^2\right) d\xi \tag{7-23}$$

is the cumulative distribution function of a univariate standard Gaussian random variate, and κ_i's are the principal curvatures of the limit state surface at the design point.

FORM/SORM are analytical probability computation methods. Each input random variable and the performance function $g(\cdot)$ must be continuous. Depending on the solver for nonlinear programming, an additional requirement regarding smoothness i.e., differentability of $g(\cdot)$ may be required.

Monte Carlo Simulation (MCS). Consider a generic n-dimensional random vector X which characterizes uncertainty in all load and system parameters with the known joint distribution function $F_X(x)$. Suppose, $x^{(1)}, x^{(2)},\ldots,x^{(L)}$ are L realizations of input random vector X which can be generated independently. Methods of generating samples of X can be obtained from standard texts on probability[62]. Let $g^{(1)}, g^{(2)},\ldots,g^{(L)}$ be the output samples of $g(X)$ corresponding to input $x^{(1)}$, $x^{(2)},\ldots,x^{(L)}$ that can be obtained by carrying out repeated deterministic evaluation of the performance function in Equation (7-19). Define l as the number of trials (analyses) which are associated with negative values of the performance function. Then, the estimate $P_{F,MCS}$ of the actual probability of failure P_F is given by

$$P_{F,MCS} = \frac{l}{L} \tag{7-24}$$

which approaches the exact failure probability P_F as L approaches infinity.

Practical experience with FORM/SORM algorithms indicate that their estimates usually provide satisfactory reliability measures. The SORM reliability is more accurate and may differ from FORM

reliability when the design conditions are highly nonlinear. Besides, the SORM reliability has the property of approaching the exact reliability P_S as P_S approaches 1 asymptotically. When the reliability is large (small probability of failure), FORM/SORM are extremely computationally efficient simulation methods. The Central Processing Unit (CPU) time for FORM is approximately linear in n (n = number of basic input variables) and the additional CPU time for SORM grows approximately with n^2. However, SORM based on the diagonal of the matrix of second-order derivatives at the β point (u space) has CPU time linear in n. Obviously, the absolute CPU time depends on the CPU time required to evaluate the performance function $g(\cdot)$. The CPU time may be invariant with the actual reliability level if the calculation of $g(\cdot)$ does not depend on different combinations of input variables. This means that when P_S approaches 1, the computational effort by FORM/SORM may remain relatively unchanged and hence become a superior method when compared with simulations.

Direct MCS is a general method based on repeated deterministic evaluation of the $g(\cdot)$ function due to random sampling of the input random vector **X** according to their joint distribution function. This method can be applied to any type of problem without requiring any continuity in the random variables or the limit state function. For a sample size L that approaches infinity, the estimated reliability converges to the exact result. For a finite sample size, uncertainty estimates on the results may need to be evaluated. As a rule of thumb, the CPU time grows linearly with n and $1/\text{Min}(P_F,P_S)$ for a given coefficient of variation on the estimator. The absolute value of the CPU time depends on the time necessary to evaluate the $g(\cdot)$ function. When P_S approaches 1 (P_F approaches 0), the MCS may be inefficient and expensive and hence, may become computationally prohibitive.

7.3.5 Inspection Planning and Repair Strategy. Aircraft in service are inspected at intervals to detect cracks before they become critical. When a maintenance action takes place after at a specified number of flights, there may be a change in the flaw size distribution. This change is obviously a function of inspection capability and the quality of repair. Inspection capability can be modeled by the probability of detection (POD) curve as a function of crack size a. The POD curve represents the cumulative distribution function $F_d(a)$ of the smallest detectable flaw size (a random variable). Repair quality can be expressed in terms of the equivalent repair crack size density function $f_R(a)$.

Consider a real line in Figure 7-9 which represents the number of load cycles in an aging aircraft. Following crack initiation after N_0 cycles, let N_1, N_2, N_3, $\cdots$ ($\cdots, > N_3 > N_2 > N_1$) be the successive number of cycles during which periodic inspections take place with a regular inspection interval $\Delta N_{ins} = N_2 - N_1 = N_3 - N_2 = \cdots$. Let $f_B(a)$ denote the probability density function of the

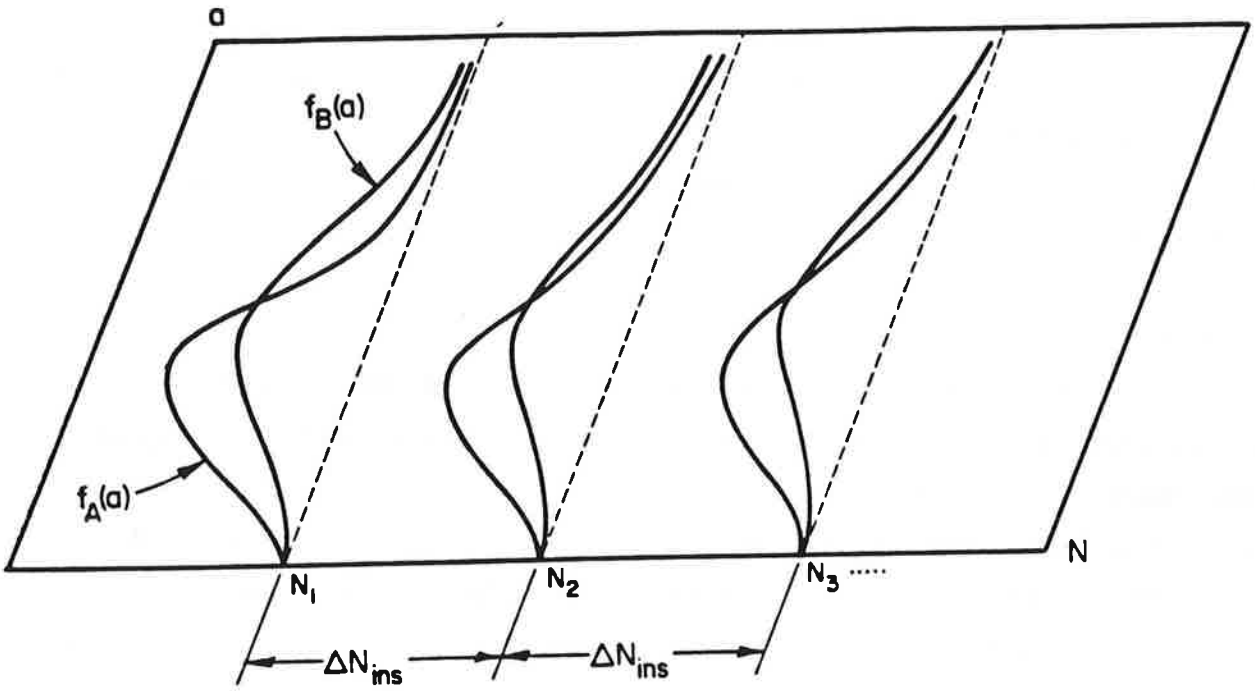

FIGURE 7-9. EFFECTS OF PERIODIC MAINTENANCE ACTION ON THE CRACK SIZE DENSITY FUNCTION

crack size at N_1 before inspection. $f_B(a)$ can be easily obtained following differentiation of the cumulative distribution function $F_B(a)$ ($f_B(a) = dF_B(a)/da$), which in turn can be calculated from

$$F_B(a) \overset{def}{=} Pr\left[a(N_1) < a\right] = 1 - Pr\left[a(N_1) > a\right]. \tag{7-25}$$

Methods of computing the probability $\Pr[a(N_1) > a]$ (*cf.* Inequality 37 and Equation (7-25)) are discussed in Section 7.3.4 (Equations (7-21), (7-22), and (7-24)). Let $f_A(a)$ represent the probability density function after inspection and repair at N_1 cycles. Due to this maintenance action, $f_A(a)$ can be obtained as[31]

$$f_A(a) = f_R(a) \int_0^{\infty} F_d(\xi)\, f_B(\xi)\, d\xi + \left[1 - F_d(a)\right] f_B(a)\ . \tag{7-26}$$

The post maintenance crack size density $f_A(a)$ is then projected forward for the next interval of uninspected usage, i.e., for $N_1 \le N \le N_2$. Thus, $f_A(a)$ can be treated as the initial crack size density at N_1 cycles replacing the density function of the original initial crack size. This process is continued for as many inspection intervals as desired. The methodology described above, however, implicitly

assumes that all the probabilistic characteristics of the basic input variables, such as C, m, p, etc., are unchanged due to maintenance actions. Appropriate performance function(s) similar to Equation (7-19) can be formulated which will allow evaluation of updated failure probabilities as a function of inspection and/or repair.

7.4 Numerical Example

7.4.1 Problem Description. Consider a fuselage lap joint with 100 fastener holes in a critical row. The model used for the FEM analysis shown in Figure 7-2 was obtained from the original References[24,27]. The geometrical parameters are assumed to be deterministic. They are as follows: fuselage radius $R = 1.905\ m$, skin thickness $t = 1.016 \times 10^{-3}\ m$, shank diameter $D_s = 4.572 \times 10^{-3}\ m$, fastener head diameter $D_h = 5.588 \times 10^{-3}\ m$, fastener hole diameter $D = 4.572 \times 10^{-3}\ m$, fastener spacing $s = 25.4 \times 10^{-3}\ m$, effective width $W_{eff} = 25.4 \times 10^{-3}\ m$, and permissible crack size $a_p = 5.207 \times 10^{-3}\ m$.

The random variables considered in this example are fuselage pressure p, initiation life N_0, initial crack length a_0, and Paris coefficients C and m. The fuselage pressure p is assumed to be lognormally distributed (arbitrary) with mean value $\mu_p = 0.0586\ MPa$, and a coefficient of variation V_p. Several values of V_p will be used to determine the sensitivity of results on V_p. It's probability density function is given by

$$f_p(x) = \begin{cases} \dfrac{1}{\sqrt{2\pi}\, x\tilde{\sigma}} \exp\left[-\dfrac{1}{2}\left[\dfrac{\ln x - \tilde{\mu}}{\tilde{\sigma}}\right]^2\right] & ;\quad x > 0 \\ 0 & ;\ \text{otherwise} \end{cases} \tag{7-27}$$

with

$$\begin{aligned} \tilde{\sigma} &= \sqrt{\ln(1+V_p^2)} \\ \tilde{\mu} &= \ln\mu_p - \frac{1}{2}\tilde{\sigma}^2 \end{aligned} \tag{7-28}$$

The initiation life N_0 normalized by its mean value $E[N_0]$ is assumed to be distributed with Weibull probability with the probability density function
with [25]

$$f_{N_0/E[N_0]}(x) = \begin{cases} \dfrac{k}{\nu-\alpha}\left(\dfrac{x-\alpha}{\nu-\alpha}\right)^{k-1} \exp\left[-\left(\dfrac{x-\alpha}{\nu-\alpha}\right)^{k}\right] & ; \quad x \geq \alpha \\ 0 & ; \text{ otherwise} \end{cases} \tag{7-29}$$

$$\begin{aligned} \alpha &= 0.50 \\ \nu &= 1.00 \\ k &= 2.00 \quad . \end{aligned} \tag{7-30}$$

The mean value $E[N_0]$ can be obtained for a given stress range, which in turn depends on the membrane stress $\sigma_m(p)$. An empirical equation originally proposed in Reference [26] is assumed here to determine $E[N_0]$ which is given by

$$E[N_0] = \exp\left[\frac{296.46-\sigma_m(p)}{18.89}\right] \tag{7-31}$$

where $\sigma_m(p)$ has to be expressed in *MPa*. Equation (7-31) predicts a lower value of mean crack initiation life when compared with the results of Hartman and Mayville shown in Figure 7-4. This is due to an adjustment made by the availability of actual data obtained from the Aloha Air incident[25]. Note that, due to the different system of units (System International) considered here, the constant parameters in Equation (7-31) are obtained by multiplying the parameters in Reference [25] with a conversion factor 6.8948 (1 *ksi* = 6.8948 *MPa*).

Equation (7-31) also indicates that the mean initiation life will be random if the fuselage pressure p is random ($V_p > 0$). This implies that N_0 and p may be correlated random variables. Hence, the probability density function of crack initiation life (N_0) will be conditionally Weibull only when the fuselage pressure is specified at a deterministic value.

Following crack initiation, the initial crack size a_0 is assumed to be uniformly distributed over the region (0 *m*, 0.000508 *m*). The associated density function is

$$f_{a_0}(x) = \begin{cases} \dfrac{1}{\alpha_2 - \alpha_1} & ; \ \alpha_1 \le x \le \alpha_2 \\ 0 & ; \quad \text{otherwise} \end{cases} \tag{7-32}$$

with

$$\begin{aligned} \alpha_1 &= 0.0 \\ \alpha_2 &= 0.000508 \end{aligned} \tag{7-33}$$

The vector $\{\ln C, m\}^T$ representing Paris coefficients is assumed to be a bivariate Gaussian random vector with the joint probability density function[32-33]

$$f_{\ln C,m}(x_1,x_2) = \frac{1}{2\pi\sigma_1\sigma_2\sqrt{1-\rho^2}} \exp\left[-\frac{\left(\frac{x_1-\mu_1}{\sigma_1}\right)^2 - 2\rho\left(\frac{x_1-\mu_1}{\sigma_1}\right)\left(\frac{x_2-\mu_2}{\sigma_2}\right) + \left(\frac{x_2-\mu_2}{\sigma_2}\right)^2}{2(1-\rho^2)} \right] \tag{7-34}$$

where

$$\begin{aligned} \mu_1 &= \text{mean value of } \ln C &&= -23.1 \\ \sigma_1 &= \text{standard deviation of } \ln C &&= 0.48 \\ \mu_2 &= \text{mean value of } m &&= 2.86 \\ \sigma_2 &= \text{standard deviation of } m &&= 0.20 \\ \rho &= \text{correlation coefficient} &&= -0.992 \end{aligned} \tag{7-35}$$

with the units in m and MPa. A linear elastic stress analysis by FEM was carried out in Reference [27] for the above geometrical parameters and a deterministic pressure of 0.0586 MPa. Reference [24] has a listing of all nominal stresses such as, membrane stress σ_m, fastener load P, and local bending stress σ_b computed for all the fastener holes. Using these values and Equations (7-21 to 7-23), the corresponding proportionality factors A_1, A_2, and A_3 can be easily calculated for each of the 100 fastener holes considered in this example. These factors are then used to calculate the stress distribution due to a new fuselage pressure, due to statistical variability from its expected value.

7.4.2 Reliability Analysis. Figure 7-10 shows several plots of probability of failure P_F versus number of cycles N obtained for one of the 100 fastener holes considered in the analysis. The associated proportionality factors for this hole (Equations (7-11 to 7-13)) are $A_1 = 0.928$, $A_2 = 3.427$

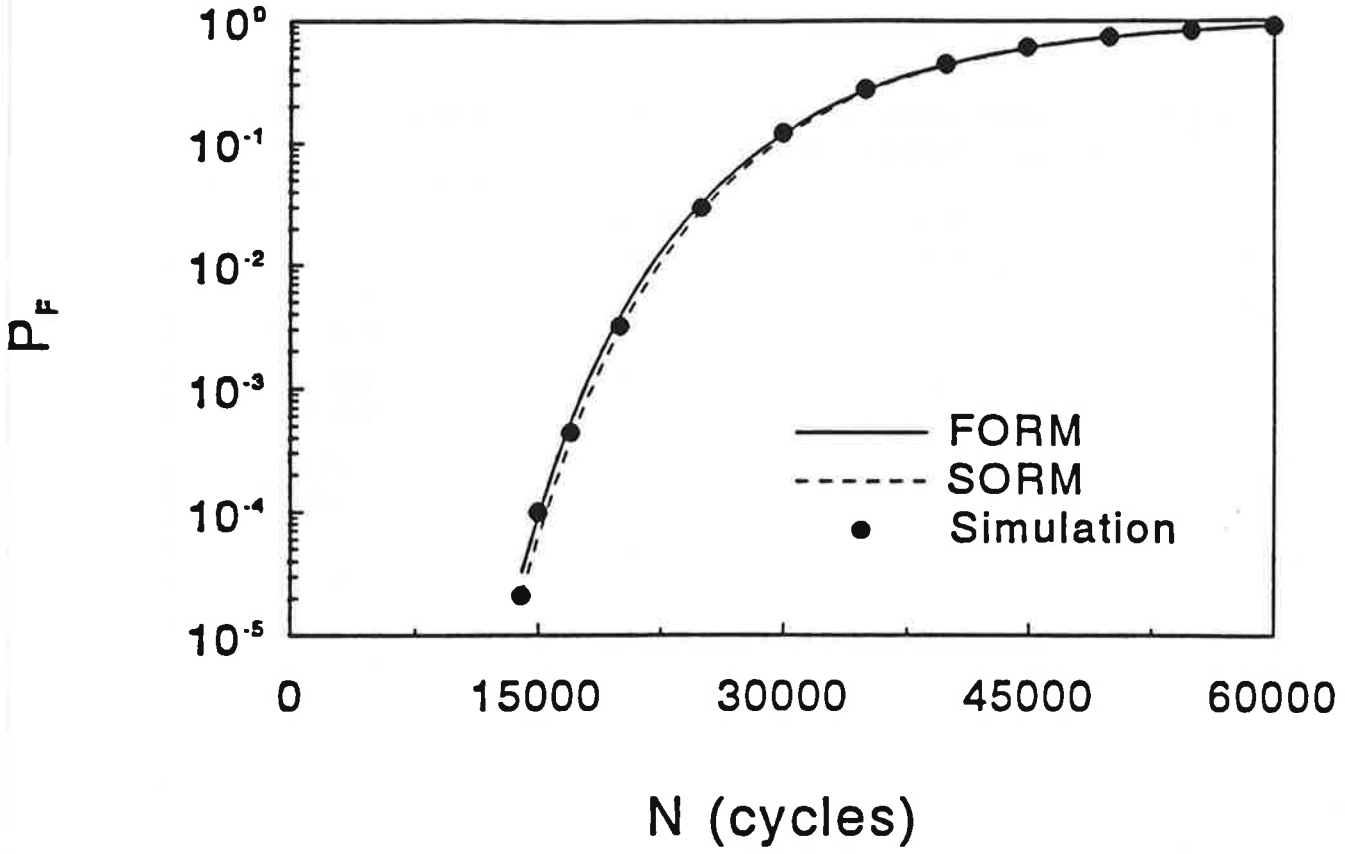

FIGURE 7-10. PROBABILITY OF FAILURE BY VARIOUS METHODS AS A FUNCTION OF NUMBER OF CYCLES

$\times 10^{-4}$ m, and $A_3 = 4.781 \times 10^{-4}$ m. The coefficient of variation V_p of the random fuselage pressure p was arbitrarily assumed to be 5 percent. Various reliability methods such as FORM, SORM, and MCS were applied to determine the failure probabilities. They all consistently indicated that P_F increases as N increases, and it approaches unity when N becomes large. Figure 7-10 also shows that the results obtained from the approximate methods, e.g., FORM and SORM provide satisfactory probability estimates when compared with results from MCS. The sample size (L) for the simulation was varied according to the level of probability being estimated. As a rule of thumb, the sample size has to be at least $10/P_F$ for obtaining a 30 percent coefficient of variation on the probability estimator[62]. All the plots in Figure 7-10 were obtained for uninterrupted usage of an aircraft.

Table 7-1 exhibits the relative effort and computational expenses required to determine the above solutions by analytical (FORM and SORM) and simulation methods. They were measured in terms of CPU seconds by executing computer programs for each of these methods in a 386-33 MHz

TABLE 7-1. COMPARISONS OF CPU TIME FOR CALCULATION OF FAILURE PROBABILITIES

N (cycles)	FORM (sec)	SORM (sec)	MCS (sec)
14000	14.43	15.01	10572.90 (500,000)
15000	14.33	14.77	2112.87 (100,000)
17000	14.12	14.70	528.38 (25,000)
20000	13.95	14.47	106.28 (5,000)
25000	1.86	2.41	12.45 (500)
30000	1.75	2.25	2.69 (100)

Values in parentheses denote corresponding number of sample size.

Personal Computer. Clearly, the FORM/SORM algorithms are more efficient than MCS and become superior particularly when the failure probabilities are in the lower range ("tail") of the distribution. For realistic structural systems, it is usually this lower range of probabilities which is of interest. This is certainly true for aging aircraft.

Figure 7-11 shows the sensitivity of the above failure probabilities as estimated by SORM as a function of randomness on the fuselage pressure p. It is apparent that the coefficient of variation V_p has a significant influence on the structural reliability. A small variation in V_p can make a large difference in the failure probability. Hence, considerable effort should be expended in accurately modeling the structural loads.

Figure 7-12 shows similar plots described by SORM and obtained for a deterministic fuselage pressure (i.e., $V_p = 0$) assigned to its mean value, and several deterministic realizations of crack initiation life. These plots were developed with the intent of showing the importance of simultaneous interaction of crack initiation and growth in a reliability analysis. In Figure 7-12, the probability of failure was obtained for three distinct deterministic values of crack initiation life which were characterized by their mean, and 10 and 25 percent lower fractiles. When the initiation life was assigned such deterministic values, it was assumed that the crack had already developed, and hence

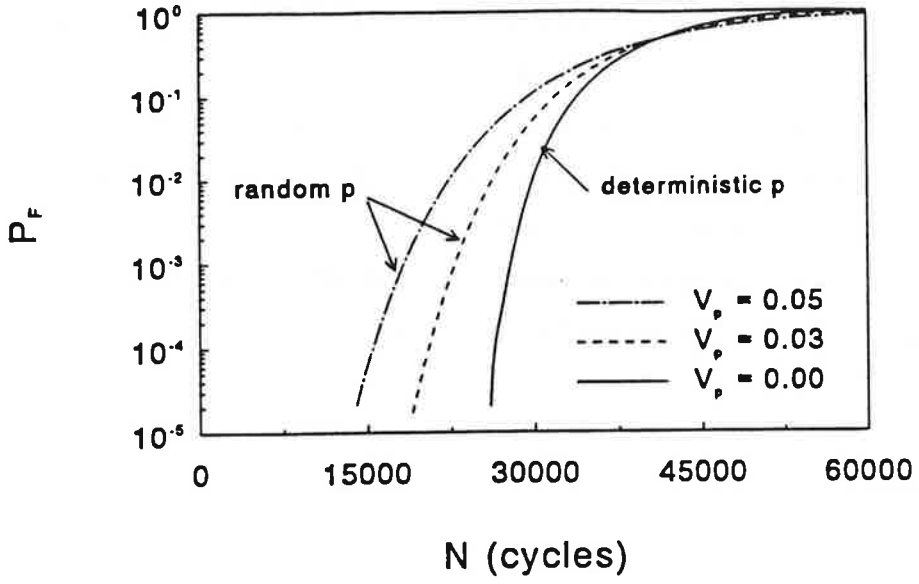

FIGURE 7-11. EFFECTS OF LOAD VARIABILITY ON FAILURE PROBABILITIES

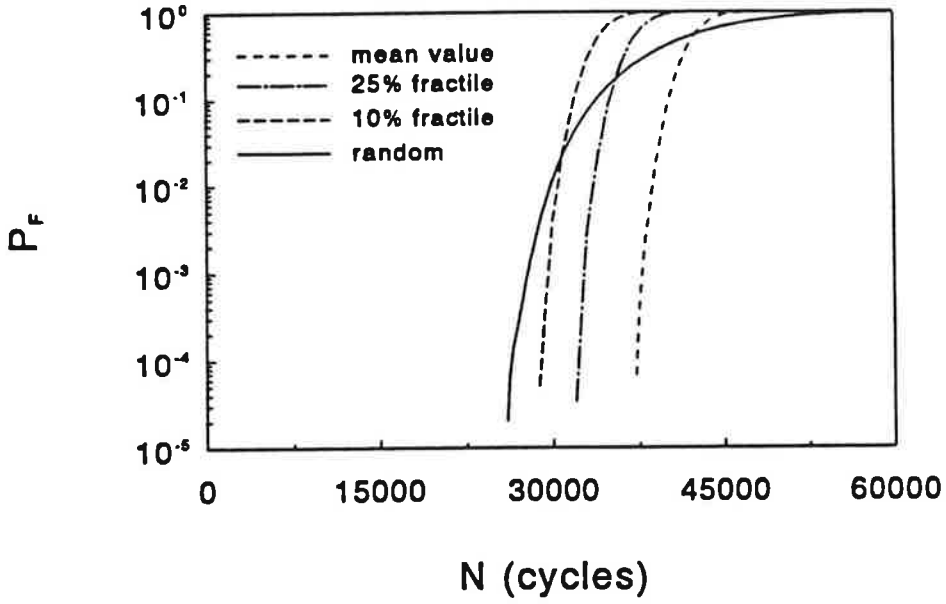

FIGURE 7-12. EFFECTS OF FRACTILES OF CRACK INITIATION LIFE OF FAILURE PROBABILITIES

the performance function was based solely on crack growth, without the possibility of no crack initiation. Comparison of results obtained from such considerations with those from fully random crack initiation lives suggests that there can be large differences in the calculated probability of failure.

Figures 7-10 to 7-12 can also be used to determine a threshold of first inspection. This can be performed based on reliability or probability of failure when a target reliability is known. This target value is usually decided by expert opinion and discussion in code committees. Using Figure 7-12, it is also possible to decide on a specific fractile of crack initiation life which may provide similar reliability estimates (in the region of interest) when compared with a fully random analysis. For example, in Figure 7-12, based on a 10 percent lower fractile and fully random analyses, an inspection threshold could be in the vicinity of 29000 cycles, with an associated failure probability of approximately 1.0×10^{-4}.

8.0 CONCLUSIONS AND RECOMMENDATIONS

Because of the distinct requirements of each of the technical tasks on this program, conclusions and recommendations are offered separately for each of them in the following paragraphs. In general, it is apparent that the structural integrity of repairs in aging aircraft is an important issue; the aircraft industry clearly is aware of this and is taking steps to improve the quality and reliability of aircraft repairs. Certainly, engineers at airlines and repair stations could substantially benefit from additional analytical tools that are simple to use, but effective for making intelligent repair design choices.

The analytical program, SKINFIX, could ultimately serve as one of these tools, or be embedded within an overall, user-friendly repair assessment software package. The techniques that were compiled for the estimation of fuselage stress spectra could also be incorporated into this package. If such an analytical tool is developed, it will be important to demonstrate the accuracy and range of applicability of it through a series of carefully controlled laboratory experiments. Even after this is done it would be prudent to expose the analysis software to a trial, "beta-test" period, in which interested repair stations and airlines could try out the software on a number of real repair problems.

8.1 Repair Database Assessment

The SDR database is more useful in providing global indications of trends than it is in allowing a detailed assessment of the problems associated with a particular type of repair. The SDR database, in combination with the Aircraft Utilisation Database, can show the relationship between aircraft age, flight hours and aircraft landings with the number of cracking or corrosion-related SDR's. Little SDR activity would be expected until an aircraft is at least 10 years old. After the aircraft reaches an age of about 20 years, the number of cracking and corrosion incidents could be expected to increase. The number of incidents of corrosion is less well correlated with flight hours and even more poorly correlated with aircraft landings. An examination of these trends versus specific airlines did not reveal significantly different trends.

In general, these results show an increase in the number of repairs as an aircraft's age exceeds 15 to 20 years. An obvious conclusion is that repairs to aging aircraft will likely increase in the U.S. commercial fleet unless a large percentage of these older aircraft are retired in the next few years.

Based on this brief study of the Service Difficulty Reporting System and the Aircraft Utilisation Database, the authors offer the following recommendations:

- Steps should be taken to ensure that enhancements to the SDR system are implemented. Results of this study and the efforts of the Data Analysis Subcommittee of the ATA should be given due consideration in defining the modifications.

- The Boeing **Structural Item Interim Advisory** system should be examined as a possible model for future SDR reports. These reports, several of which are included in Appendix H for the B727 aircraft, include detailed drawings of a trouble spot, along with a description of its specific location and exact SRM reference.

- Consider institution of a formal procedure for routing structurally significant SDR's through the OEM's (or other clearing house) to ensure consistency in nomenclature and completeness.

- In support of the FAA's ongoing aging aircraft research efforts, maintain a current version of the Aircraft Utilisation Database as a resource of information on service history and ownership of specific aircraft.

- Consider a pilot program to demonstrate the benefits of a more comprehensive aircraft damage and repair database in terms of tracking fleet trends and identifying the need for new airworthiness directives (AD's). Collaborate with the ATA on the specifics of such a program. Consider the merits of a fleet-leader tracking program in conjunction with this effort.

8.2 Compatible Displacement Analysis

A linear elastic compatible displacement analysis methodology has been developed and used to analyze a repair configuration. The methodology is a biaxial extension of the Swift analysis. The hypothetical repair was of sufficient complexity to simulate an actual repair and to be analytically challenging. The results of the analyses were compared with strain and displacement data obtained from laboratory tests performed on a representative specimen at two different load levels. The analysis was found to be in good agreement with the test data in terms of general load distribution patterns and bypass stresses at many specific locations in the repair assembly. The analysis exhibited errors in some areas; the probable sources of error are local bending and locally high bearing-to-bypass stress ratios. A nonlinear analysis would be required to achieve the correct results, regardless of the calculation method employed. The necessary corrections for bending and local concentrated loadings are technically feasible, as is the nonlinear analysis. These would add to the size and complexity of the computer program, of course. Also, the computer program is presently in a low stage of automation, requiring significant manual effort and engineering judgement up front to perform an appropriate analysis. However, the analysis process can be automated to reduce the level

of user effort and technical proficiency required. This would require some type of CAD-like software to facilitate model generation.

The authors make the following recommendations for improvement of the compatible displacement analysis:

(1) Adapt an out-of-core matrix solution algorithm from existing software to facilitate PC-based use.

(2) Improve the model-generating package or adapt such a procedure from existing software to facilitate analysis of arbitrary repair configurations.

(3) Perform analyses on other benchmark configurations which have been analyzed by competing methods and/or physically tested for purposes of comparison.

(4) Incorporate the effects of local bending.

(5) Incorporate the effects of concentrated loading.

8.3 Standardized Load Spectra

A simplified procedure for the development of stress histories for use in the analysis of aircraft repairs was presented in Section 5 of this report. Although repairs of all components of the airframe are of interest, this analysis concentrated on stress histories for fuselage skin repairs. A description of typical fuselge loadings was provided, and basic fuselage stress histories were described. A method for development of an exceedance diagram for analysis of fuselage skin repairs was detailed. Subsequently, a methodology for generating detailed stress histories was reviewed. Some of the key features are (1) the inclusion of a range of flights of different severities, (2) the inclusion of deterministic loads where they occur, e.g. ground-air-ground cycles, (3) the use of a near-optimum number of stress levels (10-16 positive and negative), (4) the combination of positive and negative excursions of equal frequency, and (5) matching of the total number of flights and cycles with the total exceedance diagram. Two methods of estimating fuselage skin stresses were presented, the first based on static equilibrium requirements and the second based on a limit load analysis.

A comparison of the proposed history generation scheme with that of an airframe manufacturer for the KC-135 was also presented. The predicted fatigue crack growth patterns for a hypothetical through-crack at a fastener hole were compared for the two history generation schemes at three areas within a fuselage. Predicted crack growth lives were within a factor of 1.5 for two of the three cases. For the third case (which was predicted to be the least severe by both techniques) the proposed

scheme resulted in substantially longer crack growth life predictions. The probable reasons for these differences were discussed.

Overall, we conclude that the procedures that were developed for estimation of fuselage stress histories compare favorably with common industry practice. In general, when generating an aircraft stress history it is important to:

- Apply flights of different severity in accordance with their historical or predicted frequency of occurence. Randomly apply stress excursions within flights, with the following exception.
- Apply deterministic loads at the point where they occur, e.g. GAG cycles must occur *between* flights.
- Select a reasonable number of stress levels (10-16 positive and negative are recommended). More levels will complicate the procedure without improving the results and make the generation of different flight types much more cumbersome.
- Combine positive and negative excursions of equal frequency. Random combination of positive and negative excursions will require subsequent recounting.
- Match the total number of flights and cycles with the overall exceedance diagram.

As followup to this study it is recommended that these procedures for estimating fuselage stress histories be distributed to the aircraft industry for further comment and consideration.

8.4 Repaired Panel Testing

It is important to ascertain whether SKINFIX or other candidate repair analysis procedures will provide sufficient accuracy, simplicity and adaptability to be used by designated engineering representatives (DER's) and small aircraft repair stations to assess the suitability of various candidate fuselage repairs.

With SKINFIX it was found that predictions of fastener displacements and skin stresses were in error by as much as 20 percent when compared with detailed laboratory data on a simple Type III fuselage skin repair. In particular, the stresses in the Type III repair involving the highest load transfer between the sheet and doubler were predicted with the least accuracy. By inference, if SKINFIX provides poor correlations with these detailed laboratory measurements of repair stresses and displacements, then other finite element procedures which provide predictions similar to SKINFIX will also provide poor correlations. This line of reasoning suggests that any stress analysis model that is being considered for use in analyzing fuselage skin repairs should be validated in

comparison with a series of carefully documented laboratory experiments on common repair configurations. The experimental work that was done in this program represents only a beginning.

To increase the credibility of these experiments, it is recommended that a major aircraft manufacturer be invited to participate in the design and fabrication of these flat panel repairs. At least the following basic issues should be resolved through further laboratory experimentation:

- Fatigue crack initiation and growth behavior of the three basic types of fuselage repairs can be accuratelly predicted by SKINFIX or other currently available analytical tools that can readily be used by DER's and others required to design fuselage repairs. Detailed data suitable for such an assessment are available on only one Type III temporary doubler repair sample. Type I and II doubler designs must also be evaluated.

- Replicate test data for each of these doubler designs should be developed to fully assess the variability caused by specimen to specimen fabrication differences, as well as uncertainties caused by scatter in laboratory measurements of rivet displacements and skin and doubler strains. No replicate data of the type required for model validation exists at the present time.

- A wider range of cutout to doubler size ratios and doubler to skin thickness ratios should be explored to better demonstrate the suitability of available analytical procedures in predicting the impact of these variables on the location and duration of crack initiation, as well as the rate of crack growth. Only one cutout size, one doubler size, and two doubler/skin thickness ratios have been explored to date.

8.5 Reliability Assessment

This work included completion of a state of the art review, development of a probabilistic model, and initial model validations.

State-of-the-Art Review. A state-of-the-art review was conducted to determine the adequacy of current methods for performance evaluation of aging aircraft subjected to in-service environmental loads. Both deterministic and probabilistic approaches were reviewed. Based on this literature survey, it was concluded that novel probabilistic model(s) are required to determine structural reliability under the potential adverse effects of multiple site damage (MSD) and periodic repairs.

Development of Probabilistic Model. An analytical model was developed to evaluate stochastic performance (reliability) of aircraft components subject to MSD and periodic repairs. The model is based on (*i*) phenomenological models of fatigue crack initiation and fatigue crack growth, (*ii*) linear elastic fracture mechanics (LEFM), and (*iii*) First- and Second-Order Reliability Methods (FORM/SORM) of modern structural reliability theory. It incorporates various uncertainties in

structural loads, properties governing fatigue crack initiation, properties governing fatigue crack propagation, and initial conditions characterizing flaw sizes at "crack initiation". The proposed model is versatile and can be easily adapted when additional uncertainty parameters are required to describe the relevant performance criteria. Based on this model, optimal inspection and repair strategies for an aging aircraft could be determined.

Model Evaluation. The proposed analytic model was evaluated by comparing its failure probability estimates with those obtained from reference solutions. The method of MCS was used for comparison purposes. A numerical example based on a fuselage lap-joint subjected to MSD was considered. Preliminary results suggest that the approximate methods, such as FORM and SORM can provide accurate estimates of failure probability with much less computational effort than those obtained from MCS.

Based on these positive initial results, the authors recommend the following work be undertaken: various existing databases be explored to accurately characterize input variables (deterministic and random). Then, the model would be used for a significant number of specific (real world) cases. The proposed theoretical formulation should be coded as a complete computer program. The effect of additional sources of damage and variability, including repair location and size, should be assessed. Finally, the resulting software should be integrated in a framework that would provide a tool for assessing the reliability of aircraft as a function of relevant parameters, such as age, probability of damage detection, inspection interval, flight load distribution, and others.

REFERENCES

[1] Rice, R. C., "Repair Database Assessment", Summary Report on Subtask 2 to the Volpe National Transportation Systems Center, Contract No. DTRS-57-89-C-00006, Project No. VA-0013, (March 6, 1991).

[2] Rice, R. C., and Rosenfeld, M., "Compatible Displacement Analysis", Progress Report to the Volpe National Transportation Systems Center, Contract No. DTRS-57-89-C-00006, Project No. VA-0013, (March 7, 1991).

[3] Vlieger, H. and Sanderse, A., User's Manual of ARREST, A Computer Routine for Prediction of Residual Strength of Cracked Stiffened Panels, National Aerospace Laboratory (1976).

[4] Swift, T., "Repairs to Damage Tolerant Aircraft", International Symposium on Structural Integrity of Aging Airplanes (1990).

[5] Swift, T., "Development of the Fail-Safe Design Features of the DC-10", Damage Tolerance in Aircraft Structures, ASTM STP 486 (1971).

[6] Hussein, R. M., Computer Aided Engineering: Advanced Structural Analysis (1988).

[7] Gallagher, R. H., Finite-Element Analysis Fundamentals (1975).

[8] Poe, C. C., Jr., "The Effect of Riveted and Uniformly Spaced Stringers on the Stress Intensity Factor of a Cracked Sheet", MS Thesis, Virginia Polytechnic Institute (1969).

[9] "I-DEAS Finite Element Modeling User's Guide", Structural Dynamics Research Corporation, Milford, Ohio (1990).

[10] "ABAQUS Finite Element Analysis User's Guide", Version 4.7, Hibbitt, Karlsson & Sorenson Inc., Providence, R.I. (1988).

[11] Broek, D., *The Practical Use of Fracture Mechanics*, Kluwer Academic Publishers, (1988).

[12] Crabill, N. L., "The NASA Gigital VGH Program-Exploration of Methods and Final Results, Volume I-Development of Methods, Volume II-L 1011 Data 1978-1979: 1619 Hours, Volume III-B727 Data 1978-1980: 1765 Hours, Volume IV-B747 Data 1978-1980: 1689 Hours, Volume V- DC10 Data 1981-1982: 129 Hours," NASA Contractor Report 181909, NASW 4430, Eagle Engineering Inc., (December 1989).

[13] De Jonge, J. B., et al., "A Standardized Load Sequence for Flight Simulation Tests on Transport Aircraft Wing Structures (TWIST)", LBF-FB-106, NLR TR 73029U, (1973).

[14] Schijve, J., "The Analysis of Random Load-Time Histories With Relation to Fatigue Test and Life Calculations, Fatigue of Aircraft Structure", p. 115, Pergamon, (1963).

[15] Broek, D., and Smith, S. H., "Fatigue Crack Growth Prediction Under Aircraft Spectrum Loading", *Engineering Fracture Mech.*, **11**, pp. 122-142, (1979).

[16] Bullen, N. I., "The Chance of a Rough Flight", RAE TR 65039 (1965).

[17] Anon., "Fuselage Load Spectrum for Modification Design per Damage Tolerance Criteria", Enclosure to BMAC letter, No. 3-KC-135-6183-1130, (1986).

[18] Fowler, K. R., and Watanabe, R. T., "Development of Jet Transport Airframe Test Spectra", Boeing paper without date or number.

[19] Hoggard, A., "Aircraft Repairs Program Review", Manufacturer's/FAA Meeting, Douglas Aircraft Company, (May 8, 1990).

[20] Smith, I., Howard, D. M., and Smith, F. C., "Cumulative Fatigue Damage of Axially Loaded Alclad 75S-T6 and Alclad 24S-T3 Aluminum Alloy Sheet", National Advisory Committee for Aeronautics, NACA Technical Note 3293, (September, 1955).

[21] Rice, R. C., Davies, K. B., Jaske, C. E., and Feddersen, C. E., "Consolidation of Fatigue and Fatigue-Crack Propagation Data for Design Use", NASA Contractor Report, National Aeronautics and Space Administration, NASA CR-2586, (October, 1975).

[22] Orringer, O., "Significance of Multiple Site Damage (MSD) on Damage Tolerance of Aircraft", Presented at the Airworthiness Assurance Task Force, (January 1991).

[23] Mayville, R., "Influence of Joint Design Variables on MSD Formation and Crack Growth", Presented at the Airworthiness Assurance Task Force, (January 1991).

[24] Broek, D., "The Inspection Interval for Multi-Site Damage in Fuselage Lap-Joints", Final Report, TR-9002, USDOT/VNTSC, (April 1990).

[25] Broek, D., "Analysis Concerning the Inspection Threshold for Multi-Site Damage", Final Report, TR-9104, USDOT/VNTSC, (June 1991).

[26] Broek, D., "Outline of Risk Analysis to Establish Requirements for Inspection Interval", Preliminary Discussion Document, Galaxy Scientific Corporation, (July 1991).

[27] Patil, S., "Finite Element Analysis of Lap-Joint", Foster Miller Inc., (1991).

[28] Broek, D., "The Feasibility of Proof Testing", Report TR 8916, FractuREsearch Inc., Galena, Ohio, (1989).

[29] Lincoln, J., "Life Management Approach for USAF Aircraft", Paper presented at AGARD meeting, Bath, United Kingdom, (April 1991).

[30] Lincoln, J., "Risk Assessment of an Aging Military Aircraft", *Journal of Aircraft*, 22 (8), pp. 687-691, (August 1985).

[31] Berens, A., "Risk Analysis for Aging Aircraft Fleets — Demonstration Report", University of Dayton Research Institute, (February 1991).

[32] Ortiz, K., and Kiremidjian, A., "Stochastic Modeling of Fatigue Crack Growth", Engineering *Fracture Mechanics*, **29** (3), pp. 317-334, (1988).

[33] Ortiz, K., and Kiremidjian, A., "Time Series Analysis of Fatigue Crack Growth Rate Data", *Engineering Fracture Mechanics*, **24** (5), pp. 657-675, (1986).

[34] Hartman, A., "Fatigue Tests on Three-Row Lap-Joints in Clad 2024-T3 Manufactured by Riveting and Adhesive Bonding", Report TN M-2170, National Aerospace Laboratory, NLR, Amsterdam, (1967).

[35] Schijve, J., "The Endurance Under Program Fatigue Testing", *Full Scale Testing of Aircraft Structures*, pp. 41-59, Permagon Press, (1961).

[36] Jarfall, L., "Review of Some Swedish Work on Fatigue of Aircraft Structures During 1975-1977", Report TN HE-1918, Institute for Aviation Research, FFA, Stockholm.

[37] Haas, T., "Spectrum Fatigue Tests on Typical Wing Joints", *Materialprufung*, **2**, pp. 1-17, (1961).

[38] "Causative Factors Relating to Multi-Site Damage in Aircraft Structures", ADL Report-63053, (1990).

[39] Grover, H. J., "Fatigue of Aircraft Structures", NAVAIR 01-1A-13, (1966).

[40] Paris, P., and Erdogan, F., "A Critical Analysis of Crack Propagation Laws", *Journal of Basic Engineering, ASME*, **85**, pp. 528-534, (1963).

[41] Broek, D., "The Practical Use of Fracture Mechanics", Kluwer Academic Publishers, (1988).

[42] Broek, D., "Elementary Engineering Fracture Mechanics", Kluwer Academic Publishers, (1986).

[43] Virkler, D. A., Hillberry, B. M., and Goel, P. K., "The Statistical Nature of Fatigue Crack Propagation", AFFDL-TR-43-78, Air Force Flight Dynamics Laboratory, (April 1978).

[44] Virkler, D. A., Hillberry, B. M., and Goel, P. K., "The Statistical Nature of Fatigue Crack Propagation", *J. Engng. Mater. Technol.*, **101**, pp. 148-153, (1979).

[45] Varanasi, S. R., and Whittaker, I. C., "Structural Reliability Prediction Method Considering Crack Growth and Residual Strength", Symposium on Fatigue Crack Growth Under Spectrum Loads, 78th Annual Meeting of ASTM, ASTM STP 595, pp. 292-305, Montreal, Quebec, Canada, (June 1975).

[46] Lidiard, A. B., "Probabilistic Fracture Mechanics", *Fracture Mechanics, Current Status, Future Prospects*, Permagon Press, Oxford, (1979).

[47] Engesvik, K. M., "Analysis of Uncertainties in the Fatigue Capacity of Welded Joints," Division of Marine Structures", The University of Trondheim, The Norwegian Institute of Technology, Trondheim, Norway, (December 1981).

[48] Rahman, S., "A Markov Model for Local and Global Damage Indices in Seismic Analysis", Doctoral Dissertation presented at the Graduate School, Cornell University, Ithaca, NY, (May 1991).

[49] Fiessler, B., Neumann, H. J., and Rackwitz, R. "Quadratic Limit States in Structural Reliability", *Journal of Engineering Mechanics, ASCE*, **105(EM4)**, pp. 661-676.

[50] Rackwitz, R. and Fiessler, B., "Structural Reliability under Combined Random Load Sequences", *Computer and Structures*, **9**, pp. 484-494, (1978).

[51] Madsen, H. O., Krenk, S., and Lind, N. C., *Methods of Structural Safety*, Prentice-Hall, Inc., Englewood Cliffs, New Jersey, (1986).

[52] Hohenbichler, M., "New Light on First- and Second-Order Reliability Methods", *Structural Safety*, **4**, pp. 267-284, (1987).

[53] Breitung, K., "Asymptotic Approximation for Multinormal Integrals", *Journal of Engineering Mechanics, ASCE*, **110** (3), pp. 357-366, (March 1984).

[54] Fu, G., and Moses, F., "A Sampling Distribution for System Reliability Applications", Proceedings of the First IFIP WG 7.5 Working Conference on Reliability and Optimization of Structural Systems, Aalborg, Denmark, pp. 141-155, (May 1987).

[55] Harbitz, A., "An Efficient Sampling Method for Probability of Failure Calculation", *Structural Safety*, **3** (1), pp. 109-115, (October 1986).

[56] Harbitz, A., "Efficient and Accurate Probability of Failure Calculation by Use of the Importance Sampling Technique", Proceedings of the 4th International Conference on Applications of Statistics and Probability in Soil and Structural Engineering, Florence, Italy, (1983).

[57] Ibrahim, Y. and Rahman, S., "Reliability Analysis of Uncertain Dynamic Systems Using Importance Sampling", Proceedings of the Sixth International Conference on Applications of Statistics and Probability in Civil Engineering, Mexico City, Mexico, (1991).

[58] Melchers, R. E., "Efficient Monte Carlo Probability Integration", Report No. 7, Dept. of Civil Engineering, Monash University, Australia, (1984).

[59] Bjerager, P., "Probability Integration by Directional Simulation", *Journal of Engineering Mechanics, ASCE*, **114** (8), pp. 1285-1302, (August 1988).

[60] Deak I., "Three Digit Accurate Multiple Normal Probabilities", *Numerische Mathematik*, **35**, pp. 369-380, (1980).

[61] Ditlevson, O., Olesen, R., and Mohr, G., "Solution of a Class of Load Combination Problems by Directional Simulation", *Structural Safety*, **4**, pp. 95-109, (1986).

[62] Rubinstein, R. Y., *Simulation and the Monte Carlo Method*, John Wiley & Sons, New York, New York, (1981).